ONR Report No. NR319-110

1976 NAVY STUDY ON SUPERCONDUCTIVE ELECTRONICS

sponsored by

Office of Naval Research

and

Naval Electronic Systems Command

FINAL REPORT

Edited by Arnold H. Silver

August 2-13, 1976

Naval Postgraduate School, Monterey, California

Copies of this Report can be obtained by writing to:
Mr. E. A. Edelsack (Code 427)
Office of Naval Research
Arlington, Virginia 22217

NAVY STUDY GROUP ON SUPERCONDUCTIVE ELECTRONICS

Participating Members

Dr. Arnold Silver, Chairman

Dr. Fernand Bedard
Dr. Richard Brandt
Dr. James Carpenter
Mr. Edgar Edelsack
Dr. Robert Hansen
Mr. Verne Hildebrand
Prof. Donald Langenberg
Dr. Martin Nisenoff
Prof. Paul Richards
Dr. David Scott
Dr. Robert Terhune
Prof. Michael Tinkham
Prof. Theodore Van Duzer
Dr. Nancy Welker
Mr. Max Yoder
Dr. James Zimmerman

Technical Consultants

Dr. Kenneth Allen
Prof. Raymond Chiao
Prof. John Clarke
Dr. Thomas Finnegan
Prof. Robin Giffard
Dr. Dennis Herrell
Prof. James Lukens
Dr. Malcolm McColl
Dr. Donald McDonald
Mr. David McIntyre
Mr. James Franson
Mr. Elliot Ressler
Dr. Merrill Skolnik
Dr. John Turneaure
Dr. Frank Vernon
Dr. Virgil Wall

1976 NAVY STUDY ON SUPERCONDUCTIVE ELECTRONICS

EXECUTIVE SUMMARY

This report presents the findings of a two-week study which convened to assess the impact of superconductive electronics (SCE) on future Navy and other DoD electronic systems. No attempt was made to conduct a complete study of any single area. System areas which were considered included radar, communications, computers, electronic warfare, and navigation; areas in which the Navy has already clearly expressed its recognition of the potential impact of SCE, such as magnetic anomaly detection, have been largely excluded from this Study except as points of reference. The conclusions identify a number of relevant functional technology items which are of potential interest to the Navy and DoD. Specific recommendations are made for development and exploitation of SCE in the most promising system areas; important areas for further research are suggested.

More than a decade of research has largely concentrated on the properties of elementary devices. The most extensively studied class of devices is the Josephson junction; however, the superconducting Schottky diode and superconducting cavity have received attention in recent years. While the accomplishments to date are indeed impressive and can be used to project the potential for this field, much of this work should be viewed as "cat whisker" technology. Significant improvements in performance as well as in reliability and reproducibility are expected as more sophisticated fabrication techniques are utilized.

Few programs have been devoted to the development of integrated SCE systems as distinct from single-element devices. For example, "SQUID (Superconducting Quantum Interference Device) systems" which are commercially marketed and widely used as magnetometers consist of an elementary SQUID in a conventional electronic system. Exceptions to this situation include the Josephson junction digital processor program at IBM and, to a lesser extent, the superconducting low noise millimeter-wave receiver program at The Aerospace Corporation. This approach to the utilization of SCE is inadequate. Full exploitation will require the development of integrated superconducting and cryogenic circuitry. An expanded level of support will be required to apply microelectronic fabrication and interfacing techniques in order to achieve the higher level of performance possible in integrated SCE receiver, amplifier, and digital signal processing circuits.

The advantages of SCE are high speed, large bandwidth, high sensitivity, low device power, and small attenuation. As requirements and goals for DoD electronic systems are set higher, the relevant capabilities of current and projected conventional (room temperature) technologies will be surpassed and serious consideration must be given to the application of superconductive electronics. This Study finds clearly defined examples which warrant near-term investment in the development and application of SCE systems. These are digital processor technology, millimeter-wave electronics, and low-frequency communications. In addition a number of promising areas require further investigation before a meaningful projection of potential applications can be made. Specific recommendations are included in each case.

High-Speed Digital Processing

We stand on the threshold of a major breakthrough in computer technology based on SCE. Logic, memory, and analog-to-digital conversion significantly beyond the projected limits of semiconductor technology are predicted because of the greater intrinsic speed at lower power and consequently higher packing density possible with Josephson junctions. The present effort at IBM has made significant technological advances which promise greater than a hundred-fold improvement in computing capability over projected conventional technology. This program by no means approaches the theoretical limits and should be viewed as a first-order approach to it. Digital SCE can play an important role in existing and future DoD systems, such as radar, electronic warfare, and space systems. The Study finds the current U.S. technical base for SCE is inadequate to meet the projected system needs, particularly in digital SCE systems.

> It is recommended that the DoD seek to broaden this technical base and expand the industrial capability in digital SCE in order to conceive and develop the optimum product to meet DoD needs in the 10 to 20 year time frame.

Existing and potential DoD systems suffer from inadequate A/D converter speed. With the possible introduction of SCE digtal computers, this inadequacy will be further emphasized. It is projected that SCE A/D will be superior to conventional technology.

The Study recommends the development of a viable SCE A/D technology with the goal of achieving sampling rates of 10 GHz and 4-bit resolution in the near term, and significantly greater resolution in the next decade.

Microwave/Millimeter Wave Electronics

SCE receivers promise the lowest noise figure and simultaneously largest bandwidth from X-band to the far infrared. Elementary SCE detectors will be used for radio astronomy within the next three years. However, development of sensitive, wideband intercept and communication receivers into the millimeter-wave region is important for many DoD applications.

The Study recommends the development of compatible SCE circuit components such as low loss striplines, phase shifters, mixers, and amplifiers for the 15 to 100 GHz spectrum.

In order to achieve the advantages offered by SCE it is necessary to integrate the individual components into a functional system.

The Study recommends development of a superconducting low-noise 35 GHz intercept receiver within five years.

Low Frequency Communications and Surveillance

SCE offers the most sensitive, compact detectors of electromagnetic signals at all frequencies from DC through HF (0—30 MHz) which are important for communications and surveillance. Utilizing five-year-old SQUID technology, currently available systems are undergoing field test outside the low temperature physics laboratory in a variety of applications from magnetic anomaly detection and geothermal prospecting to biomedical research. The full potential of SCE systems in this frequency range cannot be achieved until optimum use of cryogenic components has been implemented.

The Study recommends a coordinated program to develop integrated SCE SQUID receivers and to expand the existing Navy programs in order to demonstrate their application to surveillance and communication systems.

Ultra-Stable Oscillators

Research with very high Q superconducting cavities has demonstrated the potential for very stable, low phase-noise microwave oscillators. These presently exceed the best short-term frequency standards and may surpass the long-term stability of the hydrogen maser. This provides a technology which could be brought to fruition in the next five to ten year period.

> The Study recommends an exploratory program to establish the limits of long-term stability of superconducting cavity stabilized oscillators and evaluate their potential application, particularly for military satellite navigation systems.

Refrigeration

It is abundantly clear that SCE will not become a universal component in military systems. The opportunities for which it is suited are special high performance problems which require the speed or bandwidth, high sensitivity or low device power, or unique low-loss features of SCE. Even in these areas, acceptance will be slowed by the lack of attention focused on cryogenic cooling technology and by the natural reluctance of military planners to employ "exotic" solutions. While most low temperature researchers use liquid helium as a consumable, it is necessary to provide reliable, low power, closed cycle refrigerators if SCE systems are to be fully utilized in DoD.

> The Study recommends the development of exemplary cryogenic refrigeration systems as follows:
>
> — efficient closed cycle refrigerator systems with one-watt refrigeration capacity at 4 Kelvin for SCE digital computers; and
>
> — efficient closed cycle refrigerator systems with 10-milliwatt refrigeration capacity at 4 Kelvin for SCE sensors.

Research

The above recommendations are specific development programs for which both the technology and system opportunities were clearly demonstrated. However, many other unique technical features were identified as were many technical uncertainties which are not adequately understood and thus could not be evaluated for application.

The Study recommends continuation of a strong research program to establish the fundamental limits and expand the basis for further applications of SCE. This program should emphasize:

- development of reproducible fabrication techniques for Josephson junctions especially for high frequency and digital applications;
- experimental clarification of the fundamental properties of various types of Josephson weak links;
- investigation of non-equilibrium effects to determine the physical limitations which they impose and the new applications which they imply;
- investigation of coherence mechanisms in Josephson junctions, arrays, and traveling wave structures; and
- development of techniques to improve the electromagnetic coupling to Josephson junctions and superconducting Schottky diodes.

The Study itself has redirected the thinking of panel members and consultants towards the relevant capabilities of SCE and the nature of the system demands which the technology will be required to meet.

The Study recommends that a follow-up review be conducted in not less than one year to reassess the status of the technology and to evaluate the impact of this study upon it.

ONR Report No. NR 319-110

Edited by Arnold H. Silver

Copies of the complete report can be obtained by writing to:

Mr. E. A. Edelsack (Code 427)
Office of Naval Research
Arlington, VA 22217

Preface

The past decade has seen a marked change in the nature of superconductive electronics (SCE) from the discovery and elucidation of the Josephson "effect" as a unique example of quantum physics to the development and utilization of the voltage standard, ultrasensitive low frequency magnetometers, and cryogenic thermometers utilizing superconducting electronic devices. A massive amount of literature and numerous reviews have appeared; more recently technicians in the field are projecting further development and application of Josephson and other superconductive devices to a wide spectrum of uses from microwave/millimeter wave detectors to high speed computers to frequency synthesizers and spectrum analysers. At the same time new superconductive phenomena are under investigation.

Funding in the U.S. for these developments has come from only a few corporations and the U.S. Government, principally DOD. The U.S. Navy has assumed the lead position in research and development of superconductivity applicable to military systems. This is an appropriate time to conduct a critical review of the potential for applications of superconductive electronics to the Navy and DOD in a 5 to 10 year period, and beyond. Such a review can provide R&D planners with an assessment of the current state-of-the-art, with those applications which are now ripe for exploratory and advancement development, with the expectation for developments in the 5 to 10 year period, and with promising new research areas which are now on the horizon.

This review was jointly sponsored by the Office of Naval Research and the Naval Electronic Systems Command. It was conducted as a two-week Study at the U.S. Naval Postgraduate School at Monterey. The Study Group, drawn from the academic community, government, and industry, represented both specialists in superconductive electronics and generalists knowledgeable in electronics and DOD systems. The participants, listed in the Appendix, were divided into the permanent panel, which is responsible for the contents and recommendations of this report, and the technical specialists who contributed background information on DOD system opportunities and the state-of-the-art of SCE. No attempt was made to conduct a complete study of any one area. Rather this was a broad brush survey of the technology and its potential applications. In-depth studies to define the specific programs are left to the appropriate funding agencies.

This study was conducted on three levels, reflecting: (1) the manner in which the technology has developed to date, (2) the systems approach, and (3) the transition required to effect a meaningful connection between them. The first half of the Study, devoted to the formal Agenda printed in the Appendix, presented an overview of system opportunities in radar, communications, computers, and electronic warfare as well as a review of SCE. Superconductive electronics was defined to include Josephson and other weak link junctions, superconducting-semiconducting devices, superconducting cavities, transmission lines, and other circuit elements designed for low power operation. Therefore the presentation of the state-of-the-art in SCE was conducted in the areas of low frequency SQUIDs, coupled junctions and arrays, high frequency devices, and digital devices. The assessment of the technology sought to emphasize issues which may impact applications to DOD missions.

Whenever possible we sought to develop functional technology items and evaluate these against competitive technologies with respect to system requirements. As a result a number of systems opportunities for SCE have been identified. In addition, functional technology items of possible future interest were discussed, i.e., solutions in search of a problem. The Study formulated specific recommendations for near term action at the levels of applications, technology, and research.

The participants in this study wish to express their appreciation for use of the facilities at the Naval Postgraduate School, made available by RAdm. Isham Linder, Superintendent, and for the able assistance provided by Dr. Robert Fossum, Dean of Research, and his staff. Special thanks are due Mrs. Ruth Guthrie and Mr. Charles Wagner for their expert help with administrative details and to Mrs. Nancy Schottler for her cheerful and capable secretarial assistance in the preparation of this report.

The Editor wishes to express his appreciation to all the participants for their cooperation during the study and in the preparation of this report, to The Aerospace Corporation for its support during the editing of this report, and to Joanne Kari for typing the final report.

1976 NAVY STUDY ON SUPERCONDUCTIVE ELECTRONICS

CONTENTS

LIST OF FIGURES

LIST OF TABLES

STATE OF THE TECHNOLOGY

1. INTRODUCTION

Superconductive electronics arise from the unique electrodynamic properties of superconducting materials. In this part we review the relevant phenomenology of superconductivity, Josephson junctions, Superconducting Quantum Interference Devices (SQUIDS), and superconducting-Schottky diodes. Emphasis is placed on current and projected properties and performance, attempts to establish fundamental limits, and define the major unsolved problems. Since systems designers are interested in functions rather than devices, we carry out a corresponding assessment of superconducting electronics at the functional technology level, and make appropriate comparisons with competitive technology at this level. Thus the review focuses on such items as LF receivers, digital electronics, analog-digital converters, microwave receivers, and oscillators. Because of the importance of a cryogenic environment we also discuss the problem of cryorefrigeration.

The elementary devices are:

Josephson weak link diodes which come in several forms including tunnel junctions and microbridges,

SQUIDs,

semiconductor-superconductor diodes such as the super-Schottky diode,

thin film bolometers, and

superconducting cavities, filters and transmission lines.

The advantages of using these devices derive from some combination of the low loss and device power dissipation, large bandwidth and sensitivity, and unique properties such as the small superconducting energy gap and Josephson relations. Currently, the disadvantages are low power handling capability, large impedance mismatch between the active (nonlinear) devices and conventional electronics, the "cat whisker" nature of much of the technology, and the need for cryogenic cooling temperatures near that of liquid helium.

As a result of the study it is recommended that the Department of Defense continue to conduct a strong research program in SCE in order to provide a technology base for military applications. This program should emphasize, but not be restricted to:

improved methods of fabricating reproducible Josephson weak links which can be applied to high frequency and digital systems,

experimental clarification of the fundamental properties of various types of Josephson weak links, particularly those which are amenable to modern fabrication methods,

investigation of non-equilibrium effects in order to determine the physical limitations which they place on devices and any possible new applications,

investigation of coherence mechanisms in Josephson junctions which may lead to the development of coherent arrays and traveling wave structures, and

techniques to improve the electromagnetic coupling of Josephson junctions and super-Schottky diodes and will lead to integrated superconducting microcircuits.

2. SUPERCONDUCTIVITY

2.1 Electrodynamics of Superconductors

Superconductors are metals which undergo a phase transition on cooling through a critical temperature T_c ($\lesssim 23$K for all presently known materials) to a state in which a fraction n_s/n of the electrons pair up and condense into a macroscopic quantum state described by a complex wavefunction $|\psi(\vec{r})| \exp i\phi(\vec{r})$. In terms of this form, the density of superconducting pairs is $n_s^* = n_s/2 = |\psi|^2$, which goes to zero as $(1-T/T_c)$ at T_c, and the supercurrent density is

$$\vec{J}_s = n_s^* e^* \vec{v}_s = |\psi|^2 (e^* \hbar/m^*)(\nabla\phi - 2\pi\vec{A}/\Phi_o) \qquad (2.1)$$

where $e^*=2e$ is the charge of a pair, $\vec{v}_s$ is the velocity of the pairs, m^* is the effective mass of a pair, $\hbar = h/2\pi$ where h is Planck's constant, $\vec{A}$ is the vector potential describing the magnetic field $\vec{B} = \text{curl}\,\vec{A}$, and $\Phi_o = h/2e = 2.07 \times 10^{-15}$ Webers is called the flux quantum.

In weak fields we can take the phase ϕ equal to a constant, so that

$$\vec{J}_s = \frac{-(e^*)^2}{m^*} |\psi|^2 \vec{A} \qquad (2.2)$$

for singly-connected superconductors (the London gauge) and the two London equations describing the electrodynamics of superconductors are

$$\vec{E} = \frac{\partial}{\partial t}(\mu_o \lambda^2 \vec{J}_s) \qquad \vec{B} = -\text{curl}\,(\mu_o \lambda^2 \vec{J}_s)\,. \qquad (2.3)$$

The first describes the fact that a superconductor has zero DC resistance: an electric field induces an ever-accelerating current rather than sustaining a steady Ohm's law current against dissipation. Lossless current densities as large as 10^8 amps/cm^2 can be obtained before this breaks down, and their lifetime can be estimated to be greater than the age of the universe. The second equation describes the perfect diamagnetism of bulk superconductors in weak fields, with an exponential cut off of the field penetration governed by the frequency-independent London penetration depth,

$$\lambda(T) = \left(\frac{m}{n_s e^2 \mu_o}\right)^{\frac{1}{2}} \propto \frac{1}{|\psi|} \propto (1-\frac{T}{T_c})^{\frac{1}{2}} \qquad (2.4)$$

which is typically in the range 50-100 nanometers well below T_c.

Another important property of superconductors is found by calculating $\oint \vec{J}_s \cdot \vec{ds}$ Noting that $\oint \vec{A} \cdot \vec{ds} = \Phi$, the flux enclosed by the path, and that ψ must be single-valued, we obtain

$$\Phi + \frac{m^*}{e^{*2}} \oint \frac{\vec{J}_s \cdot \vec{ds}}{|\psi|^2} = b\Phi_o, \qquad (b = \text{integer}). \qquad (2.5)$$

That is, the quantity on the left (which is called the fluxoid of the circuit) is quantized in units of the flux quantum Φ_o. If the integration circuit is taken where $\vec{J}_s = 0$ (as in the interior of a ring of type I superconductor), this implies that the enclosed flux itself is quantized. On the other hand if the circuit contains weak links, Φ need not be $b\Phi_o$, and although Eq. (2.1) is not rigorously applicable, the line integral term in Eq. (2.5) reflects the finite phase difference $\Delta\phi$ across the link.

A strong magnetic field tends to reduce $|\psi|^2$ at the surface so as to reduce the diamagnetic energy by increasing λ. This tendency is resisted by an energy term proportional to $|\nabla \psi|^2$, characterized by the Ginzburg-Landau coherence length

$$\xi(T) \approx \xi(0)\,(1-\frac{T}{T_c})^{-\frac{1}{2}},$$

where $\xi(0) \approx \xi_o$ for pure metals and $\xi(0) \approx \sqrt{\xi_o \ell}$ when the electronic mean free path $\ell < \xi_o$. Here $\xi_o = \hbar v_F/\pi\Delta(0) = 0.18\,\hbar v_F/kT_c$ is the Pippard coherence length, v_F the Fermi velocity, $\Delta(0) = 1.76\,kT_c$ the zero-temperature energy gap of the BCS theory, and k = Boltzmann's constant. Unlike λ, ξ_o varies greatly with the material ranging from $\sim$3 nm for Nb_3Sn to $\sim$30 nm for Nb to $\sim$300 nm for Sn to $\sim 10^3$ nm for Al, because of the large range of v_F and T_c. The classic type I materials, (Pb, Sn, Al) have $\kappa \equiv \lambda/\xi < 1/\sqrt{2}$ and exclude flux until superconductivity is destroyed discontinuously at a critical field H_c (typically $\leq$1000 gauss). Materials with $\kappa > 1/\sqrt{2}$ (such as Nb and

Nb_3Sn) are called type II superconductors; for them the gradient energy term is small enough to allow ψ to be depressed locally so that flux can enter the bulk of the material (for fields $H > H_{c_1} \approx H_c/\sqrt{2}\kappa$) in quantized vortices each carrying one quantum of flux, Φ_o. In this case,[1] it is usually convenient to abandon our choice of ϕ = const in Eq. (2.1) and use a gauge for the vector potential such that the phase ϕ increases by 2π in a circuit surrounding the nodal line of $|\psi|$ at each vortex center.

Although type I superconductors have zero DC resistance until a critical current is reached, type II superconductors containing penetrated flux have finite DC resistance because of flux motion driven by the current. This resistance is almost negligible, however, until an effective critical current (determined by flux pinning strength) is reached. These critical currents may be as large as 10^5-10^6 amps/cm^2 in commercial material, depending on the flux density. In addition, substantial hysteretic loss can occur if type II materials are cycled in field (or current) in AC applications. This loss is minimized by use of twisted multifilamentary conductors.

Even type I superconductors show some AC loss because the electric field required by Eq. (2.3) to accelerate and decelerate the supercurrent in the skin layer also acts on the normal electrons. As long as the supercurrent dominates (as will usually be the case up to millimeter wavelengths), the resulting dissipation can be described by an effective resistivity

$$\rho_{eff} = \rho_n (f_n/f_s^2)\omega^2\tau^2 \qquad (2.6)$$

where $f_n \approx \exp\left[-\Delta(T)/kT\right] \approx \exp\left[-1.76T_c/T\right]$ is the normal state fraction, $f_s \approx (1-f_n) \approx 1$ is the superconductive fraction, ρ_n is the normal state resistivity, and τ is the normal electron scattering time $\sim 10^{-13}$ sec. Above the energy gap frequency the electrical properties in the superconducting and normal states are almost the same.

Electronic applications of superconductivity which were under review arise from three principal sources:

(1) low electrical loss which is intrinsic to all superconductors,

(2) finite phase differences which can be created across superconducting weak links, and

(3) the tunneling of electrons into energy levels in the vicinity of the superconducting energy gap.

2.2 Critical Materials

None of the important elements in superconducting materials (Nb, Pb, Sn, In, Al, Ti, V, Ge, Si) are in short supply relative to any conceivable applications in electronics. Helium could become a problem if no conservation program is maintained.

3. JOSEPHSON JUNCTIONS AND OTHER WEAK LINKS

3.1 Resistively Shunted Junction Model

Electronic applications of superconductivity arise from the unique properties of localized weak couplings between two relatively massive superconductive electrodes. Josephson [1965] originally envisioned weak coupling by superconducting electron pair tunneling through an insulating barrier between two superconductors, but similar properties are obtained if the weak coupling is configured from a point contact, a constriction or microbridge in a thin film ("Dayem Bridge"), an S-N-S junction (in which pairs move through a "normal" metal layer), a proximity-effect bridge (similar to S-N-S, but where the "normal" metal may be a superconductor above its T_c), or an S-Se-S bridge (where a semiconductor is used to give a lower tunnel barrier) [Clarke, 1973; Silver and Zimmerman, 1975]. The weak link can even be induced in a homogeneous superconducting thin film strip by creation of a localized excess quasiparticle population by tunnel injection or optical irradiation, in principle allowing the strength of the link to be modulated at frequencies up to the reciprocal of the recombination time [Wong, et al., 1976]. All these diodes can be described for circuit purposes by the generalized Resistively-Shunted Josephson Junction (RSJ) model (Fig. 3.1) in which the device current is

$$I = I_c \sin\phi + \frac{V}{R} + C\frac{dV}{dt} \tag{3.1}$$

where ϕ is now and henceforth the phase difference across the link, I_c is the maximum DC supercurrent, R is the shunt resistance representing the normal current flow, C is the capacitance across the junction, and V is the voltage across the junction. The phase difference ϕ evolves in time at an instantaneous frequency

$$\omega = \frac{d\phi}{dt} = \frac{2eV}{\hbar} \tag{3.2}$$

which implies a voltage-tuneable frequency which is strictly linear. (For completeness, an additional term $\alpha VR^{-1}\cos\phi$ with $|\alpha| \lesssim 1$ should be added to Eq. (3.1), but we omit it here since for most purposes it is unimportant.) The maximum supercurrent I_c varies as $(T_c - T)$ near T_c, reaching a limiting value $I_c(0)$ at low temperatures.

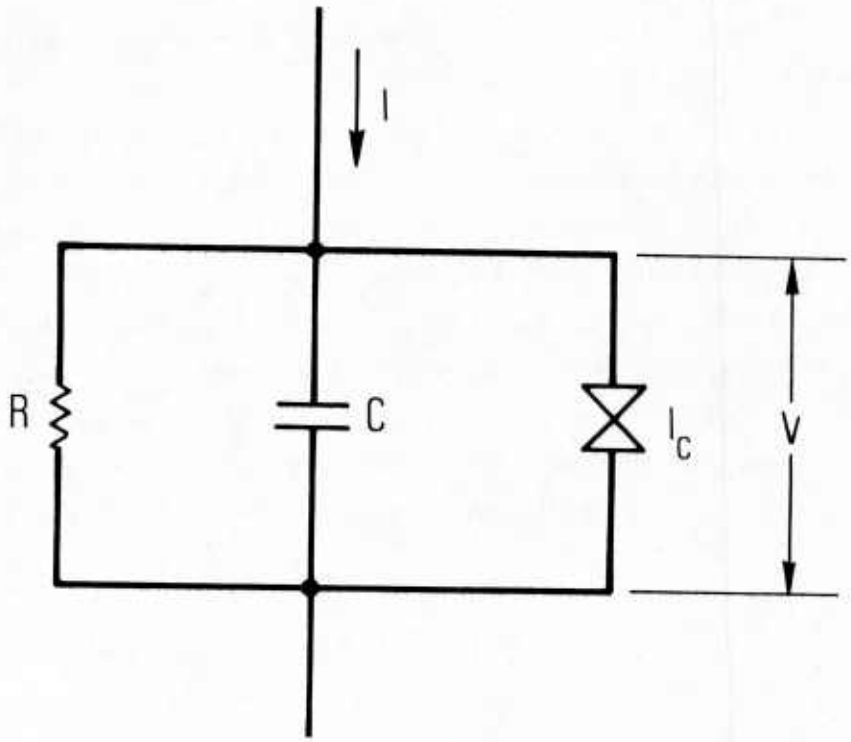

Figure 3.1

Equivalent circuit of the resistively-shunted Josephson junction (RSJ) model.

In ideal junctions, whether tunnel or point contact, $I_c(0)$ is inversely proportional to R, so that to a good approximation

$$RI_c(0) = \frac{\pi\Delta(0)}{2e} = \frac{1.76\pi kT_c}{2e} = 0.24T_c(\text{in mV}) \qquad (3.3)$$

Thus high T_c materials allow larger characteristic signal voltages, typical values being in the mV range. Because of the relation (3.2), this also implies higher characteristic frequencies, and it is useful to define a characteristic frequency $\omega_c \equiv 2eRI_c/\hbar$ and a normalized frequency

$$\Omega = \frac{\omega}{\omega_c} = \frac{\hbar\omega}{2eRI_c} \approx \frac{\hbar\omega}{\pi\Delta(0)} \approx \frac{\hbar\omega}{1.76\pi kT_c} . \qquad (3.4)$$

The latter forms apply only if the RI_c product has the ideal value (3.3), but since this value is achievable in good tunnel, point contact, and microbridge geometries, we shall use them to illuminate the basic material dependences. For $\Omega < 1$, the supercurrent dominates; for $\Omega > 1$, the normal shunt current dominates. Thus, high T_c materials have an advantage.

3.1.1 Capacitive limits

The RC time constant defines a second characteristic frequency $\omega_{RC} \equiv (RC)^{-1}$. To avoid effects of capacitive shunting, ω_{RC} must exceed ω_c. This yields the Stewart-McCumber criterion [Stewart, 1968; McCumber, 1968]

$$C \lesssim \frac{\Phi_o}{2\pi(RI_c)R} \approx \frac{1\ \text{pF}}{T_c(\text{K})\ R\ (\text{ohms})} \qquad (3.5)$$

for non-hysteretic operation. It is also the requirement for avoiding high-frequency shunting effects. Whereas $\hbar\omega_c \sim kT_c$ is set by the material, ω_{RC} depends critically on the specific junction configuration. C is the major variable, since for most applications R

should lie in the range 0.1 - 100 ohms. Since the Josephson coupling is $\Phi_o I_c/2\pi = \Phi_o \pi \Delta(0)/2eR$, R cannot exceed about 10^3 ohms before thermal fluctuations destroy the junction coherence. On the other hand coupling becomes increasingly difficult below $\sim$1 ohm. From (3.5) we see that when T_c = 10K and R = 10 ohms, C should be less than 10^{-14}F, which requires very small size. For a tunnel junction of area A(cm^2) and thickness d(cm), where

$$C \approx \frac{0.09 \varepsilon A}{d} \qquad \text{(in pF)} \tag{3.6}$$

and $I_c = J_c A$ (so long as the transverse dimensions are less than λ_J, the Josephson penetration depth), the condition (3.5) can be expressed in terms of the required current density

$$J_c \gtrsim 2 \times 10^{-5} \frac{\varepsilon}{d} T_c^2 \approx 3 \times 10^4 \text{ amp/cm}^2 \tag{3.7}$$

taking representative values d = 2 nm, ε = 3, and T_c = 10K. (Since J_c depends exponentially on d, useful values of d lie in a narrow range.) Although this is an immense tunnel current density, values up to 3×10^4 amps/cm^2 have been obtained by the IBM-Zurich group [Broom, et al., 1975] and values up to 2×10^5 amps/cm^2 were reported for PbIn junctions [Niemeyer and Kose, 1976] . With J_c from (3.7), the junction area is

$$A = \frac{(RI_c)}{(RJ_c)} \approx \frac{10^{-6} \text{cm}^2}{T_c R} \tag{3.8}$$

which is $(1 \mu m)^2$ for T_c = 10K and R = 10 ohms. Thus, to avoid capacitive problems, a tunnel junction must simultaneously have a very small area and a high current density, approaching the point contact or Dayem bridge regime. Alternatively, an external shunt can be used to deliberately reduce the RI_c product below the intrinsic value, as is done in the tunnel SQUIDs of Clarke, et al. [1975a]. However this degrades performance below that intrinsically possible. The same effect is obtained in an S-N-S junction, where tunneling through the normal metal gives a very small RI_c product except at low temperatures (small T/T_c).

Turning to the microcontact configuration, the capacitance (in pF) is of the order of the radius (in cm) of the base of the conical tip. If this is held below $\sim 100\mu$ m, the capacitance criterion will be met for the $T_c = 10K$, R = 10 ohms example treated above. Thus, capacitance limits are seldom a problem with point contacts and small bridges, in contrast with tunnel junctions.

3.1.2 Heating Limits

The third major limitation on the operation of weak links is the disequilibrium (crudely speaking, "heating"), caused by finite voltage dissipative operation. This cannot be avoided in high frequency applications, since the applied voltage V, at frequency ω, must be of order $\hbar\omega/2e$ in order to obtain phase modulation $\Delta\phi \gtrsim 1$ required for useful non-linear properties. In any case, the power dissipated in the junction will be $P=\overline{V^2}/R$, where $\overline{V^2}$ is the mean squared voltage, including DC and AC components, and the junction "temperature" will rise until energy is removed at an equal rate by diffusion of the "hot" electrons.

Thermal diffusion is most efficient in the case of "3-dimensional" cooling, as in a point contact or a "variable thickness bridge" (VTB), in which the electrodes are much thicker than the (short) bridge. Variable thickness bridges have been made successfully by the simple mechanical means of carefully controlled cutting and/or scratching, and with more precise control by a combination of electron-beam lithography and ion milling as reported by Jillie, et al. [1975]. In these geometries, the excess temperature (or density of hot electrons) falls as 1/r, and hence is halved as soon as the diameter of the constriction has doubled; this will be only ~ 100 nm for a 100 nm diameter contact. In planar microbridges with "2-dimensional" cooling, the excess temperature falls only logarithmically with distance, and depends on heat transfer from electrons to phonons and then through the surface thermal resistance to the substrate (or He bath) to avoid unlimited temperature rise at the bridge. The distance the heat must travel in the film before escaping is the thermal healing length $\eta = (Kd/\alpha)^{\frac{1}{2}}$, where K is the thermal conductivity and d is the thickness of the film, while α is the heat transfer coefficient across the interface. Typically, $\eta \sim 5\mu$m for a 100 nm film. Finally, in "1-dimensional" situations, where the heat flow is along a strip of uniform width, there must be a constant temperature gradient until the heat is removed through the surface.

These three cases were analyzed [Skocpol, et al., 1974] assuming that coherence is lost when there is a region above T_c in the middle of the link whose length exceeds some $\bar{\xi}$. The conclusion was that planar microbridges could be used up to the gap $V \approx 2\Delta/e$, whereas 3-dimensional cooling geometries should allow V up to $\approx (2\Delta/e)(\bar{\xi}/r)^{\frac{1}{2}}$, where r is the neck radius.

Tinkham, et al. [1977] have recently given a more quantitative treatment of the 3-dimensional case which shows that for $T \ll T_c$ the maximum supercurrent becomes a function of the power dissipated in the weak link such that

$$I_c(P) = I_c(0)\exp\ (-P/P_o)$$

where

$$P_o \approx \frac{2}{3\gamma^2}\left(\frac{kT_c}{e}\right)^2 \frac{\xi(0)}{\rho_o}\Omega_s \approx 2\Omega_s\left[\frac{T_c^2\ \xi(0)(\mu m)}{\rho_o(\mu\Omega\text{-cm})}\right] \quad (\text{in } \mu W). \qquad (3.9)$$

In this, Ω_s is the solid angle of the cone on either side of the junction through which the hot electrons can diffuse away, typically, $\leq \pi$. The quantity in square brackets is a material-dependent figure of merit, which should be as large as possible. Actually, its value is approximately 2 for Nb, Pb, Sn and Al, assuming a residual resistance ratio of 20 in all cases, so that P_o is typically $10\mu W$. That is, the higher electronic diffusivity in the better metals such as Sn and Al roughly compensates for their lower T_c. This formula seems to account for data of Octavio, et al. [1977] on a 1/3 ohm tin VTB, which showed $\sim$180 X-band microwave steps up to 3.7mV, at which point the center of the bridge is estimated to be at $\sim$20K. It also accounts for the observation by McDonald, et al. [1969] of a limit of 17 mV in a Nb point contact, if the junction resistance was $\sim$10 ohms. The above figure of merit is much lower (worse) for the high T_c material Nb_3Sn because the very poor electronic properties outweigh the high T_c, but this result may not be relevant since our approximation is based on a neck diameter much less than ξ, which is $\sim$3 nm for Nb_3Sn. Of course, the higher RI_c products for the high T_c materials remain an advantage, for any application in which heat removal causes no problem.

The heating analysis above relies on the Wiedemann-Franz proportionality of the electrical and thermal conductivities in a metal. With a tunnel junction there is an additional degree of freedom, since the electrical conductance (1/R) determining the dissipation $\bar{V}^2/R$ is the low tunnel conductance while the thermal conductance removing the heat reflects the higher conductivity of the metal electrodes. Thus the temperature rise is reduced by the ratio of the tunnel resistance to the electrical spreading resistance in the electrodes out to the point where the heat is transferred to the substrate. This heating reduction factor can readily be made as large as 10^2 by using thick films and relatively high ($\sim$100 ohms) tunnel resistance. Therefore, heating is much less of a problem in tunnel junctions than in constriction weak links; this is just the reverse of the situation with the capacitive limitation.

3.2 Coupling Between Junctions

When junctions operate in very close proximity, as in an array structure, there may be mutual coupling through the localized electronic disequilibrium they generate, in addition to macroscopic coupling such as that enforced by current conservation in a series array or that determined by electromagnetic radiative coupling. The length scale is set by the appropriate diffusion length

$$\Lambda = \sqrt{D\tau} \tag{3.10}$$

where $D = (1/3)\, v_F \ell \approx 300\ cm^2/sec$ is the electronic diffusion constant, and τ is the appropriate time. For DC phenomena, the quasiparticle diffusion length is $\Lambda_2 = \sqrt{D\tau_2}$, where τ_2 is the inelastic scattering time for the nonequilibrium electrons. Since $\tau_2 \approx \left(\frac{\Theta}{T}\right)^3$ where Θ is the Debye temperature, it varies widely with materials, with typical values of 10^{-7}, 10^{-10}, 10^{-11} sec. for Al, Sn, and Pb, respectively. Thus, Λ_2 is typically several microns. If the characteristic time is that for "branch-mixing" relaxation [Tinkham and Clarke, 1972; Tinkham, 1972]

$$\tau_Q \approx \tau_2 \Big/ \left(1 - \frac{T}{T_c}\right)^{\frac{1}{2}} \tag{3.11}$$

the length is even longer near T_c. These lengths measure the distance over which differences between pair and quasiparticle electrochemical potentials, μ_p, μ_n relax. If one is interested in the response of the pairs to nonequilibrium quasiparticles, Aslamazov and Larkin (preprint) argue that the time is the gap time $\hbar/\Delta(T)$, in which case

$$\Lambda \approx \xi(0) / \left(1 - \frac{T}{T_c}\right)^{\frac{1}{4}} \tag{3.12}$$

which normally is about 0.1 μm, and hence less than junction separations in practical array structures.

If the device is operating at a finite frequency ω, then the disequilibrium will fall off with an additional decrement factor $\exp -[(1+i)r/\delta]$, where

$$\delta = (2D/\omega)^{\frac{1}{2}} \approx \xi(0)\,(\omega_g/\omega)^{\frac{1}{2}} \tag{3.13}$$

where ω_g corresponds to the energy gap, $\hbar\omega_g = 2$. At X-band, δ is typically 1 μm.

Experimentally, both the Stonybrook [Jillie, et al., 1976] and Cal Tech [Palmer and Mercereau, 1975] groups reported synchronization between microbridges at 2 μm separation but not at 10 μm separations. Moreover the strength of the coupling decreased sharply with increased operating voltage (hence Josephson frequency) and junction spacing in at least qualitative agreement with (3.13). Lukens at Stonybrook used pairs of microbridges and found synchronization only when the bias currents in the two bridges were in opposite directions. The Cal Tech experiments involved a series array of many bridges in which the currents were necessarily in the same direction. This unexplained discrepancy may not be significant because of the very different geometries in the two experiments. In any case, the investigation of interjunction electronic coupling is still in its infancy, and many questions remain open to future investigation.

3.3 Bolometric Mixing

McDonald, et al. [1974] have shown that 31 THz signals from two CO_2 lasers can be mixed in a Nb point contact detector, with strong IF response at 60 MHz and useable response up to $\sim$100 GHz. However, they were not able to determine definitively

whether this mixing occurred through the Josephson non-linearity or by a heating effect. One can estimate the latter effects by combining the ideas leading up to Eqs. (3.9) and (3.13). The instantaneous power at the center of the junction is modulated at the beat frequency ω_b, changing the temperature over a length

$$\delta = (2D/\omega_b)^{\frac{1}{2}} \approx \xi(0)\,(\omega_g/\omega_b)^{\frac{1}{2}}.$$

To be fully effective, this temperature change must propagate over the entire region whose temperature is above T_c. Under typical local oscillator conditions, this will have a thickness $\beta\xi(0)$, where $\beta \approx 2$-3, corresponding to substantial depression of the zero-voltage step. Thus, one might expect a rolloff as

$$\left[1+(\beta^2\omega_g/\omega)^2\right]^{-\frac{1}{2}}$$

which sets in at $\omega_b \sim \omega_g/\beta^2 \sim \omega_g/10$. This would be roughly consistent with the reported observations.

To compare the bolometric with the true Josephson response, we note that at low beat frequencies the mixing efficiencies are inverse to the power levels required to reduce the zero-voltage current. Thus, the ratio of bolometric to true Josephson mixing should be of order

$$\frac{1}{R}\left(\frac{\hbar\omega}{2e}\right)^2 \Big/ P_o$$

where P_o is defined in Eq. (3.9) and is typically only $\sim 10\ \mu$W. Accordingly, we estimate that the bolometric effect is an order of magnitude greater than the true Josephson effects for low frequency beats of CO_2 laser carriers, but true Josephson effects should dominate for carriers 30 THz as long as the junction has effective 3-dimensional cooling.

3.4 Noise

Within the framework of the RSJ model the noise source is the Johnson noise of the shunting normal resistance. Although this is an adequate approximation in most applications, in SQUIDs it is important to note the work of Kurkijärvi and Webb [1972] on

noise due to fluctuations in the transition point between fluxiod states, which was confirmed experimentally by Jackel, et al. [1974]. It is also important to note the existence of excess 1/f noise which is typically important below ~1Hz [Clarke and Hawkins, 1976]. The impact of these noise effects on state-of-the-art performance will be discussed in the section on low-frequency devices.

3.5 High T_c Materials

The highest T_c of an elemental metal is ~9K for niobium. Higher T_c's have been obtained with binary and ternary compounds such as NbN (16K), Nb_3Sn (18K), Nb_3Ge (~22K). All these materials are type II superconductors with short coherence length ($\lesssim$ 10 nm) and long penetration depth ($\gtrsim$ 200 nm). These properties are responsible for the high H_{c2} values which makes them useful for high-field magnets, etc., despite their brittle mechanical properties.

The high T_c makes them interesting for electonic applications as well because of the simplified cryogenics and the higher RI_c product that one would expect with higher T_c. However, what little is known empirically about their performance as weak links in SQUIDs suggests that their performance is inferior (noisy, with poorer signal patterns) to devices using high conductivity metals. More work in this direction is required to discover whether this is a result of fundamental differences or only material fabrication problems.

On the theoretical side, one needs a different model for the operation of a point contact or constriction weak link when $\xi < a < \lambda$ as will presumably be the case, since the neck radius a can hardly be less than 10 nm , but can be less than ~300 nm . Instead of gradients in ψ set by the constriction, one now has vortex rings shrinking and annihilating at the center. The time t for this to occur can be estimated to scale as a^2 and to be $\sim 10^{-9}$ sec for a = 100 nm. This implies that for $\omega t > 1$ or $2eVt/\hbar > 1$, a more complex phase-slip process must be occurring than in a conventional weak link.

Whatever the detailed nature of the phase-slip process, there will be heating at finite voltage operation, and as noted earlier, the very poor thermal diffusivity of these materials would be expected to make their maximum operating power lower than that for the better metals with lower T_c. These considerations suggest that the most promising applications of these high T_c materials as constriction weak link devices may be in

relatively low-frequency, low-dissipation applications. For S-I-S tunnel junctions their advantage over lower T_c materials will likely depend on the ability to produce reliable junctions. This technology is not at hand.

3.6 Russian Work

The properties of various kinds of superconductive weak links are the subject of a large Russian scientific literature, involving leading theorists such as Aslamazov, Larkin, and Eliashberg, much phenomenological work by Likharev, as well as extensive experimental work. They seem to be concentrating on the variable-thickness-bridge concept, which we have noted combines the integrity of a continuous metallic microbridge with the efficient 3-dimensional cooling of a point contact. Less is known about their work on computer applications.

3.7 Summary

Josephson effect properties can be obtained with many types of weak links, including S-I-S tunnel junctions, point contacts, planar microbridges, variable thickness microbridges, S-N-S junctions, S-Se-S junctions, and proximity effect junctions, the categories not always being entirely distinct. The theoretical limit for the RI_c product $[\sim 0.24\ T_c(mV)]$ has been achieved at least in tunnel junctions, variable thickness bridges, and point contacts. This RI_c product sets the characteristic voltage scale, and, through the Josephson frequency relation, the characteristic frequency scale $\omega_c = 2eRI_c/\hbar$. In addition, both junction capacitance and heating effects limit high frequency/high voltage performance, and also can cause hysteresis or "latching." Capacitance is a major consideration with tunnel junctions, but not with point contacts and microbridges, whereas the reverse is true of heating. However, the current state of the art allows fabrication of tunnel junctions with current densities of $\sim 10^5$ amps/cm^2 over $\sim 1\ \mu m^2$ areas, which accordingly have little hysteresis. Also, in 1976 it has been shown that variable thickness tin microbridges can show microwave-induced steps up to 3.7 mV (corresponding to 1.8 THz) before heating destroys the Josephson effects. This approaches the reported high voltage performance ($\sim$6 mV) of tunnel junctions, but still falls short of that of Nb point contacts (17 mV). Because of the mechanical instability of point contacts, it appears that small high-current-density tunnel junctions and variable thickness microbridges are the most promising configurations for further development for

military applications requiring high speed or high voltage operation. Published Soviet work seems to center on the variable thickness bridge configuration.

In addition to setting a limit to the high-voltage operation of a weak link, heating provides an alternative non-linear process which can be used for square-law detection and mixing. On the basis of a recent analysis Octavio, et al. [1977] estimate that this "bolometric mixing" mechanism typically dominates over the true Josephson effect in point contacts and variable thickness bridges of $\sim 10\Omega$ resistance for carrier frequencies above $\sim$30 THz and beat frequencies up to $\sim \omega_g/10$, where ω_g is the gap frequency. These estimates are consistent with the 31 THz data reported by McDonald et al. in 1974.

High T_c intermetallic compounds such as Nb_3Sn play a major role in superconducting magnet technology primarily because their short coherence lengths ($\xi \approx 4$ nm) give them high critical fields H_{c2}; unfortunately their poor thermal conductivities require use of massive copper cladding to provide thermal stability. These same properties appear to limit their usefulness in Josephson junction electronics to low frequency/low voltage applications since junctions cannot be made small compared to ξ, and since the poor thermal conductivity makes heating more of a problem than it is in Nb. However, because of their potential importance in simplifying the cryogenic requirements, further experimental and theoretical work should be carried out to define their performance limits more reliably.

Recent (1975) experiments at Cal Tech and SUNY-Stonybrook have demonstrated the mutual coupling of junctions several micrometers apart as evidenced by their synchronous Josephson oscillation. The dependence of the coupling strength on frequency and distance suggests that the coupling mechanism is the diffusion of nonequilibrium electrons from one junction to the other. Because of the potential importance of this coupling for the construction of phase-locked arrays, further research should be undertaken to elucidate these nonequilibrium effects.

4. SQUIDs

4.1 General Properties

There are at least two applications in which the future of superconductive electronics is assured: the SQUID magnetometer and the standard of voltage. The SQUID (Superconducting Quantum Interference Device) is the simplest superconducting circuit incorporating Josephson junctions; it consists of one or more Josephson junctions connected with small superconducting elements (inductors) to form a closed circuit. In a SQUID Eq. (2.5) can be expressed simply by

$$\Phi + \frac{\Phi_o}{2\pi} \sum_{n=1}^{N} \phi_n = b\Phi_o \qquad (4.1)$$

where ϕ_n are the quantum phases across each of the N junctions in the circuit.

The two types of SQUIDs in common use are the DC SQUID [Zimmerman and Silver, 1966] and the RF SQUID [Silver and Zimmerman, 1967]. Many reviews of the construction and operation of SQUIDs have appeared [e.g., Clarke, 1973; Silver and Zimmerman, 1975] and several commercial versions have been marketed. We present here only a brief review of their salient operating characteristics.

Operational SQUIDs of either type use non-hysteretic Josephson junctions. In the DC SQUID two (nearly) identical junctions are placed in a superconducting ring and connected as shown in Fig. 4.1. Since the currents in the ring, and hence in the two junctions, result from both the current source (I) and the shielding current in response to an external magnetic field, the V-I characteristics will vary with applied magnetic field as shown in Fig. 4.1. For convenience we express the magnetic field in terms of the flux intercepted by the circuit, Φ_x. Because of the phase-dependent interaction between the junction current and the quantum condition (4.1), the maximum supercurrent varies periodically with applied flux with period Φ_o. The amplitude of this current oscillation ΔI is limited to the lesser of I_c or $\Phi_o/2L$, where I_c is the critical current of each junction and L is the inductance of SQUID circuit [deWaele and deBruyn Ouboter, 1969]. As a result the impedance of the SQUID varies approximately as $\cos(2\pi\Phi_x/\Phi_o)$, and the voltage measured across the SQUID (which can be considered the SQUID "output") is a similar periodic function of the applied flux (which is considered the "input").

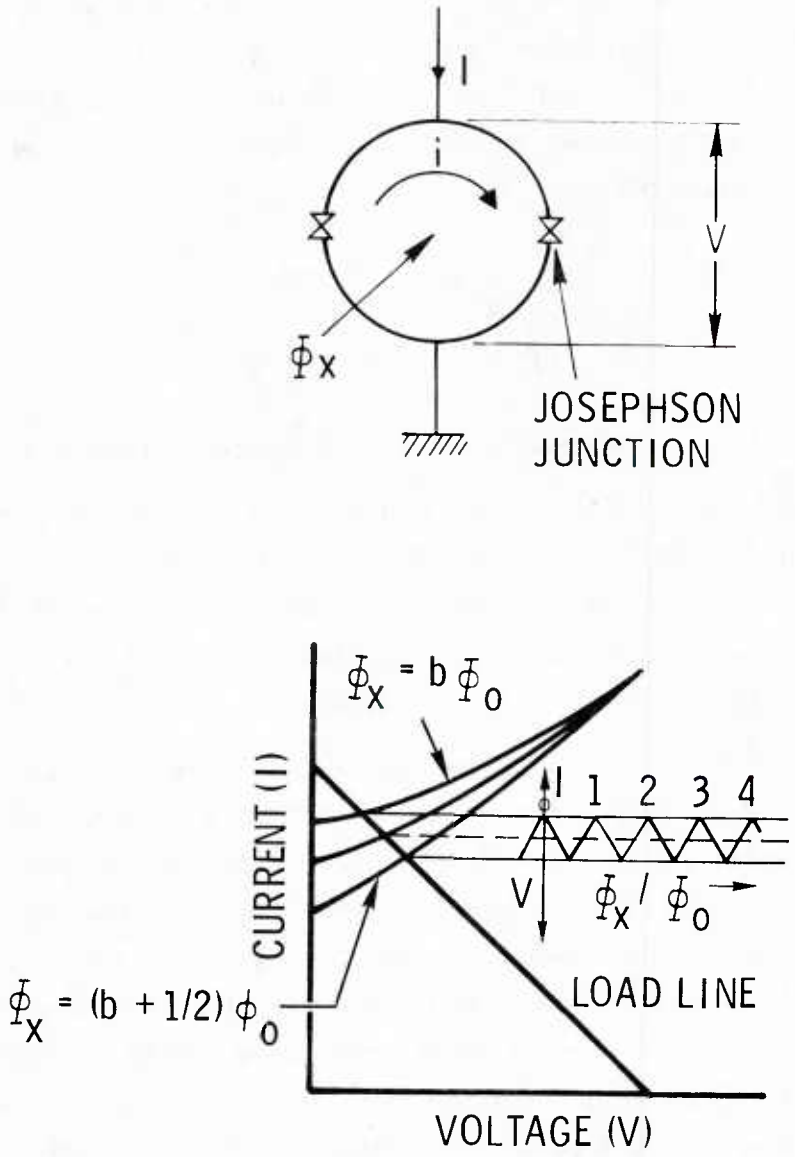

Figure 4.1

Configuration (top) and I-V characteristics (bottom) of the DC SQUID. Each Josephson junction has a maximum supercurrent I_c and the total ring inductance is L. The inset in the bottom graph shows the magnetic dependence of I(V).

The RF SQUID is a circuit containing only one Josephson junction and is represented by an inductance in parallel with the junction as shown in Fig. (4.2). When this circuit is driven by an oscillating magnetic field $\Phi_x^1 \cos \omega t$, such that $\Phi_x^1 \gtrsim LI_c/2$, the impedance at ω becomes a periodic function of both the average applied flux, Φ_x^o, and the amplitude of the oscillating flux Φ_x^1. In both cases the period is Φ_o. Therefore at sufficiently large frequencies ω, in the RF region or above, one can measure an RF voltage periodic in Φ_x/Φ_o by means of the circuit shown in Fig. 4.2.

The periodic variation in the SQUID impedance and the associated output voltage is the basis of SQUID applications. The SQUID has an intrinsic fundamental calibration unit, $\Phi_o = 2.07 \times 10^{-15}$ Webers, in units of which any input signal can be measured. For magnetometry and related applications where the signal can be converted to a low frequency magnetic field, this only requires the magnetic field corresponding to the flux quantum to be determined once. One flux quantum for a typical SQUID corresponds to a few microgauss.

4.2 Fabrication

SQUIDs can be produced in a variety of forms using any of the junction types listed in Section 3.1. In one form of SQUID two bulk half-cylinders of superconducting material are assembled with a thin sheet of mylar (or other insulator) electrically separating the two halves (Fig. 4.3). A small finely pointed niobium (or other superconductive) screw is then inserted into a tapped hole until its point just penetrates through the mylar sheet making a small area contact between the two halves of the cylinder. A similar contact can then be made across the other gap for a double point contact device, or DC SQUID. The insulating mylar can be removed from the other gap for a single contact or RF SQUID (see Fig. 4.3). The critical current of the junction(s) can be adjusted by varying the contact pressure and area. Other forms of bulk devices which have been widely used as RF SQUIDS are toroidal, two-hole, and multi-hole as shown in Fig. 4.4. These forms offer advantages in sensitivity, coupling efficiency, or rejection of background field noise.

SQUIDS can be made by thin film technology in two typical configurations. In one case a planar thin film is deposited and then covered with a thick insulating layer (for example, formvar) and one or two "windows" are cut into this layer exposing the film

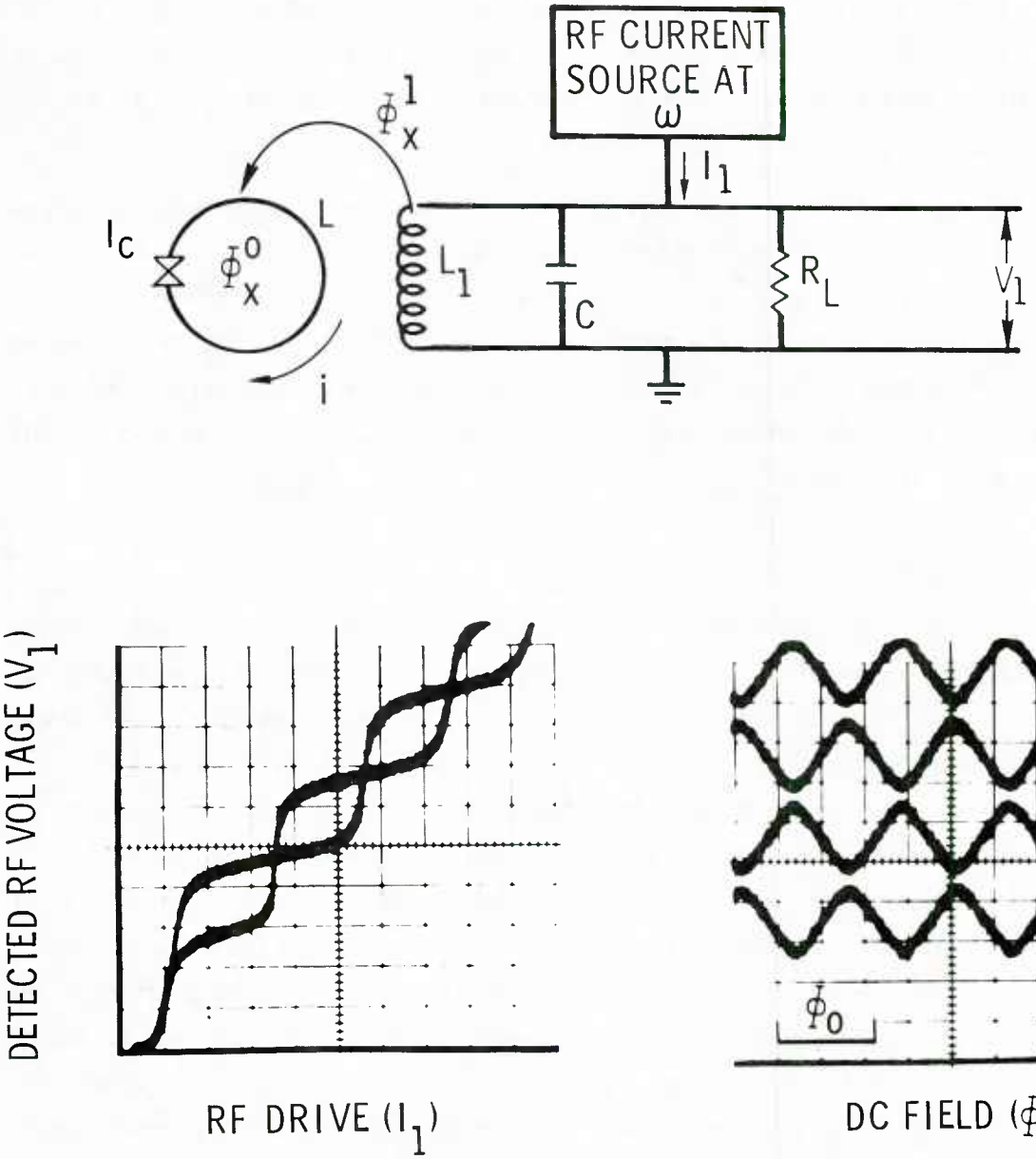

Figure 4.2

The RF SQUID and its associated circuitry (top), and the operating characteristics (bottom).

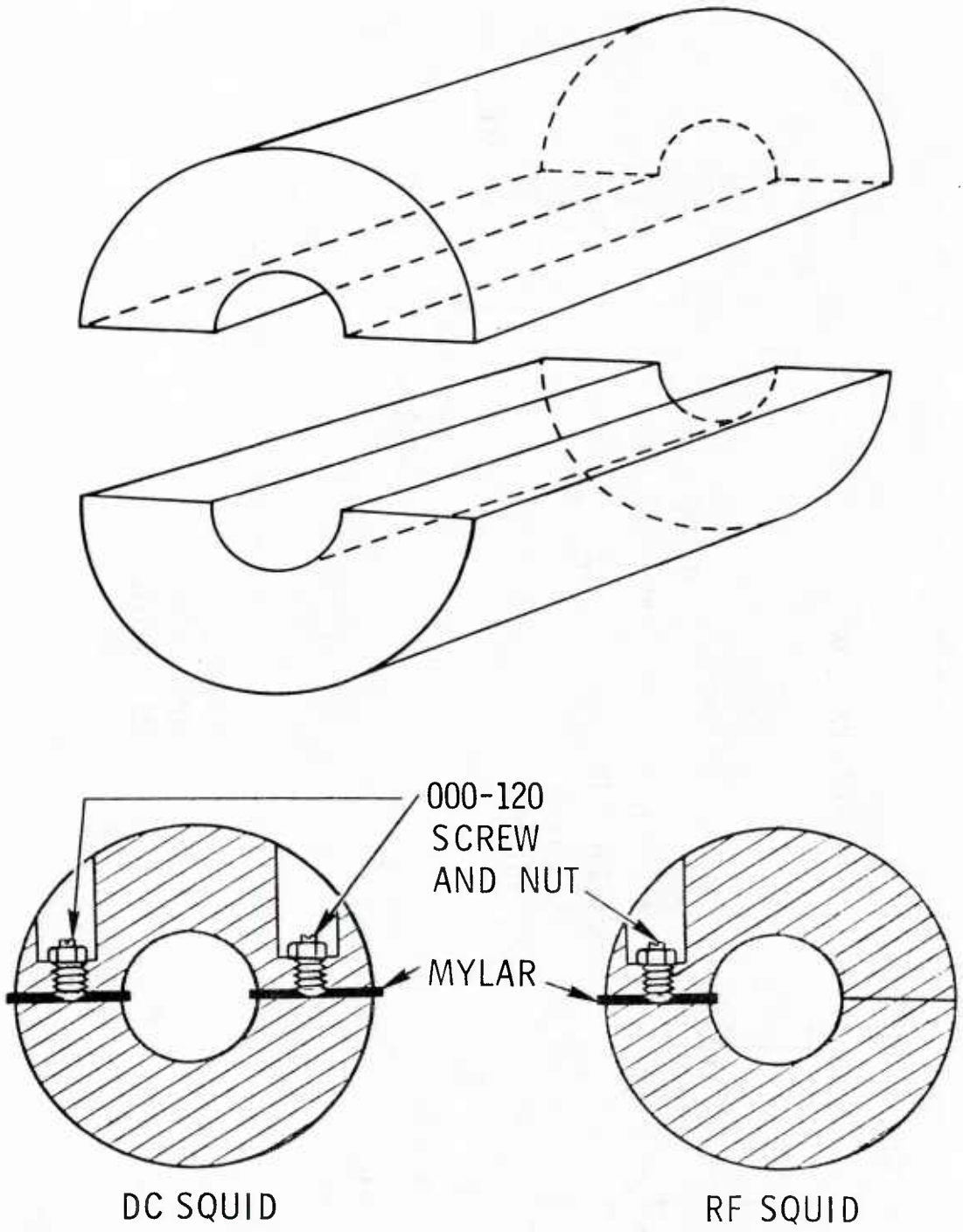

Figure 4.3

Bulk point contact SQUID formed by dividing a superconducting cylinder into two half cylinders (top) and then reassembling into a DC SQUID (left) or an RF SQUID (right).

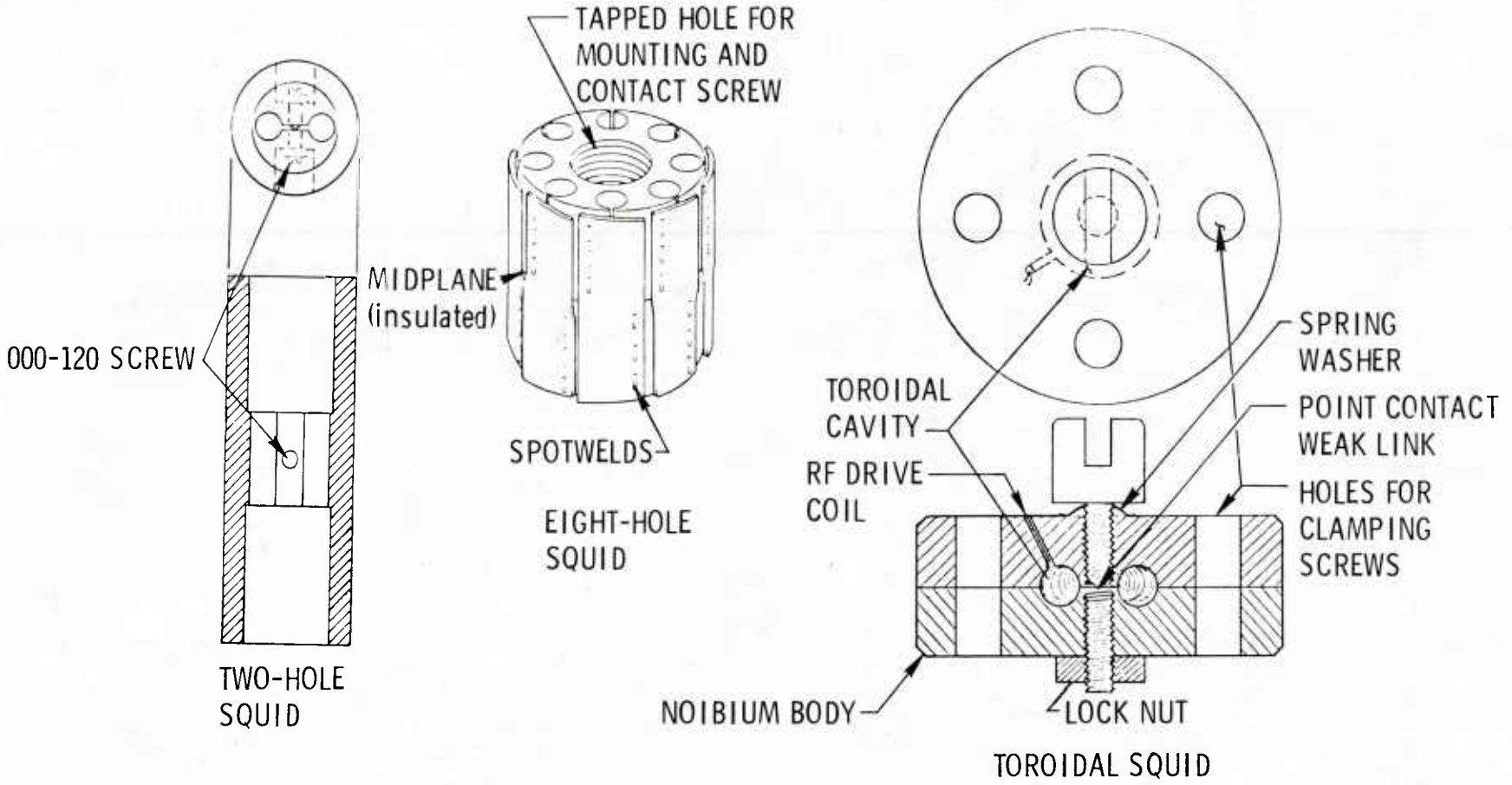

Figure 4.4

Other forms of bulk, multi-hole RF SQUIDs.

underneath. Through these windows a tunneling oxide layer may be grown onto the bottom film or a semiconducting or normal conducting film of desired thickness can be deposited. A covering film of superconductor is then deposited forming a one (or two) junction device shown schematically in Fig. 4.5. The thick insulating layer, enclosed by the two superconducting films and the two tunneling barriers, defines the area of the SQUID. In the other thin film configuration a superconducting film is deposited on a cylinder of dielectric material. At one or two positions along the circumference of the film Dayem microbridges are fabricated. In this case the enclosed area of the SQUID is defined by the cross section of the cylindrical substrate rod. (See Fig. 4.5).

4.3 Sensitivity

It would appear that increasing the SQUID area, and hence the intercepted flux for any given applied magnetic field, would enhance the sensitivity. However, L increases as the area, and the signal voltage for both types of SQUIDs varies inversely as L. This arises because the amplitude of the currents which give rise to the output signals varies as Φ_o/L. Furthermore the energy difference between maximum and minimum signal voltage is approximately $\Phi_o^2/8L = 5 \times 10^{-31}/L$ joule. Since $kT = 6 \times 10^{-23}$ joules at 4K, L must be less than 10^{-8} henries to prevent thermal washout of the periodic SQUID response.

As indicated earlier, for certain values of current through a SQUID the voltage across the SQUID will be periodically modulated by an applied magnetic flux. In order to use this characterstic, the SQUID is placed in a constant current circuit and the voltage across the device monitored. The device is connected to a resonant circuit operating at the drive frequency ω. The use of the resonant circuit facilitates impedance matching of the low impedance SQUID into the electronic detection system. The output of the resonant circuit is amplified and then detected in order to remove the "carrier" or drive frequency component and thus the amplitude of the voltage across the tank circuit is made available for processing.

However the periodic variation of output vs input implies an enormous ambiguity in interpreting a particular output level. In practical terms, if the input field is changing at a manageable rate a fast input noise transient can oscillate the output too rapidly for the readout circuit to follow, resulting in an unknown offset $x\Phi_o$ (x unknown)

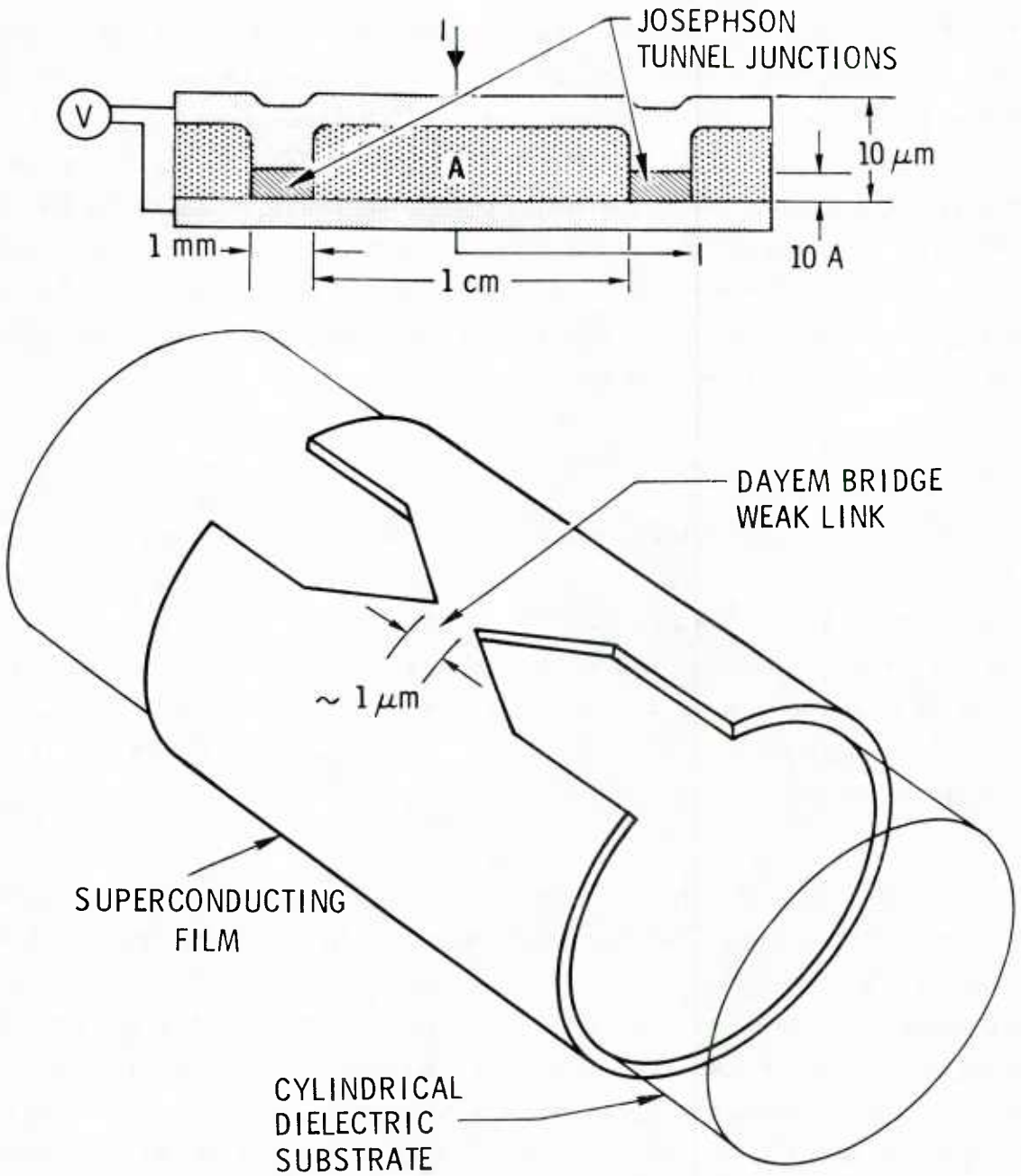

Figure 4.5

Schematic drawing of thin film SQUID configurations. (Top) a planar device consisting of two thick superconducting films whose width (into plane of figure) is $\sim$ 1 mm. The magnetic flux is applied normal to the plane of the figure. (Bottom) cylindrical thin film SQUID configuration with a single Dayem weak link.

introduced into the record. Fast transients are no problem in certain controlled environments, but may be a serious problem in others such as geophysics (lightning strokes) and military uses. There is no intrinsic way that existing single SQUID instruments can recover the lost information, but a separate, relatively-insensitive device could in principle be incorporated to keep track of the field variations to within one flux quantum and correct the SQUID output. Other methods of coping with the problem have been proposed.

Two modes of operation, digital and analog, are used in SQUID instrumentation. In the digital mode, the output oscillations are electronically counted such that the input can only be measured to within one flux quantum. In the analog (or "lock-on") mode, a low-frequency modulation of the order of $\Phi_0/2$ is applied to the SQUID input. The output is synchronously detected and fed back to the input so that the flux in the SQUID is "locked" to a fixed value. The feedback current is then the analog output signal whose magnitude is now linearly related to the input signal. The sensitivity of a SQUID in the analog mode is generally $<10^{-4}\Phi_0/\sqrt{\text{Hz}}$, depending on the noise level of the associated electronics. The intrinsic limit of sensitivity may be $10^{-6}\,\Phi_0/\sqrt{\text{Hz}}$, or 10^{-21} Webers/$\sqrt{\text{Hz}}$.

4.4 SQUID Magnetometry

SQUIDs are either used or under development for a variety of applications including geophysics, biophysics, magnetic anomaly detection and tracking, and some special uses in connection with DC and AC standards of voltage, current, and power, and RF attenuation. A great deal of operational experience has been gained in these applications, some of which is summarized below.

4.4.1 Magnetotellurics

Frederick, et al.[1974] and Clarke [private communication] have reported on the use of SQUID magnetometers for measuring earth conductivity within a few kilometers of the surface. The term denoting the basic phenomenon is "magnetotellurics." To date the main impetus for this work is geothermal prospecting, mapping regions of anomalously high conductivity indicative of hot subterranean rock masses. Since rock is a semiconductor the conductivity is a rapid function of temperature, particularly if it is permeated with water. The method uses natural magnetic field fluctuations below 1 Hz (micropulsations) as an incident signal applied to the earth's surface,

and measures the electric field in the surface associated with the current induced by the magnetic field. From this measurement the earth conductivity within the field penetration depth can be derived. Briefly, it is just the classical skin effect problem of a plane wave incident on the surface of a conducting medium, with the solution given by

$$\text{conductivity } \sigma = (B(\omega)/E(\omega))^2 \omega/2\mu_o \tag{4.2}$$

$$\text{penetration depth } \delta = \sqrt{2/\omega\mu_o\sigma}. \tag{4.3}$$

The micropulsations, $B(\omega)$, are typically of the order of 1 to 10 μG from 10^{-1} to 1 Hz, although this depends strongly on latitude and time of day [Campbell, 1967]. Thus, for good accuracy a sensitivity $\gtrsim 10^{-8}$ G/$\sqrt{\text{Hz}}$, which a SQUID magnetometer easily provides, is required. The electric field $E(\omega)$ orthogonal to B is measured by means of a pair of metal electrodes attached to the surface a hundred meters apart. This technique requires operation under inhospitable field conditions and demonstrates the potential for conductivity anomaly detection.

4.4.2 Biomagnetism

The use of SQUID magnetometers to measure magnetic signals from the heart (MCG), brain (MEG), eyes (MOG), blood, injured tissue, fetuses in utero, lung contamination, muscles, and other organic sources has probably created more interest in and out of the scientific community than all other small-scale SCE applications combined. This work is summarized here because the techniques and experience may be relevant to other low-field measurements.

The signal levels vary from 10^{-7}G down to 10^{-10}G or less at frequencies between 1 and 100 Hz. Research is currently going on at Stanford (MCG and blood flow), MIT (all the above), NYU (MEG), and Helsinki U. of Technology (MCG, MOG, etc.), and significant work has been done at NBS, Boulder (MEG instrumentation) and at TRW (MCG). Three different techniques have evolved, all with comparable results but with somewhat different projections for future uses. Cohen, et al. [1970] at MIT pioneered the use of a SQUID magnetometer in these applications. The system employed there is a magnetometer in a highly-sophisticated multi-layer relatively-expensive

magnetically-shielded enclosure about $2\frac{1}{2}$ m across inside. The system sensitivity approached 10^{-10}G/$\sqrt{\text{Hz}}$ sensitivity. NBS uses both first and second-derivative gradiometers in an inexpensive aluminum enclosure which provides considerable AC shielding above 1 Hz. This sytem also approached 10^{-10}G/$\sqrt{\text{Hz.}}$ NYU uses a second-derivative gradiometer with no shielding and have done some remarkably good studies of brain fields in the range of 10^{-9}G or less. Stanford uses a gradiometer in a magnetic shield that is probably inferior, and less expensive, than Cohen's, and Helsinki uses a gradiometer, with no shielding, in a very favorable location.

The peak magnetic field of the human heart a few cm from the chest is 10^{-7}G, and the brain field just outside the scalp is 10^{-9}G except for a few individuals with large α-rhythm currents. It is a fact of nature that these and all other magnetic fields decrease at least as the cube of the distance from the source; gradients decrease as the fourth power and second-derivatives as the fifth power of the distance. It is for this reason that a second-derivative gradiometer can measure the very weak fields of the brain without any shielding, as long as potential sources of interference (e.g., electric motors) are at least several meters away. For the same reason the instrument must be as close as possible to the source it is intended to detect. Within the framework of present or projected SQUID sensitivities and interference-rejection techniques, there is no conceivable way that brain fields will be measured at distances greater than a few cm, or heart fields at distances greater than a meter or two.

4.4.3 SQUID Low Frequency Technology

The Navy's interest in the frequency region below about 1 MHz is primarily directed toward underwater surveillance and communications. The motivation for communication to submarines at these low frequencies is that seawater is a conducting medium with a conductivity of approximately 4 mhos per meter and the skin depth is approximately 250 $f^{-\frac{1}{2}}$ meters. Thus for a submarine to receive signals while at operating depth, an extremely low carrier frequency must be used. In the area of underwater surveillance the signal from an anomaly as seen by a sensor on a moving platform is also in this frequency range.

The detection problem in this frequency range is complicated by several factors. First the magnetic background noise is variable with season, latitude, naturally occurring magnetic disturbances, etc. (See Figs. 4.6 and 4.7). Second the

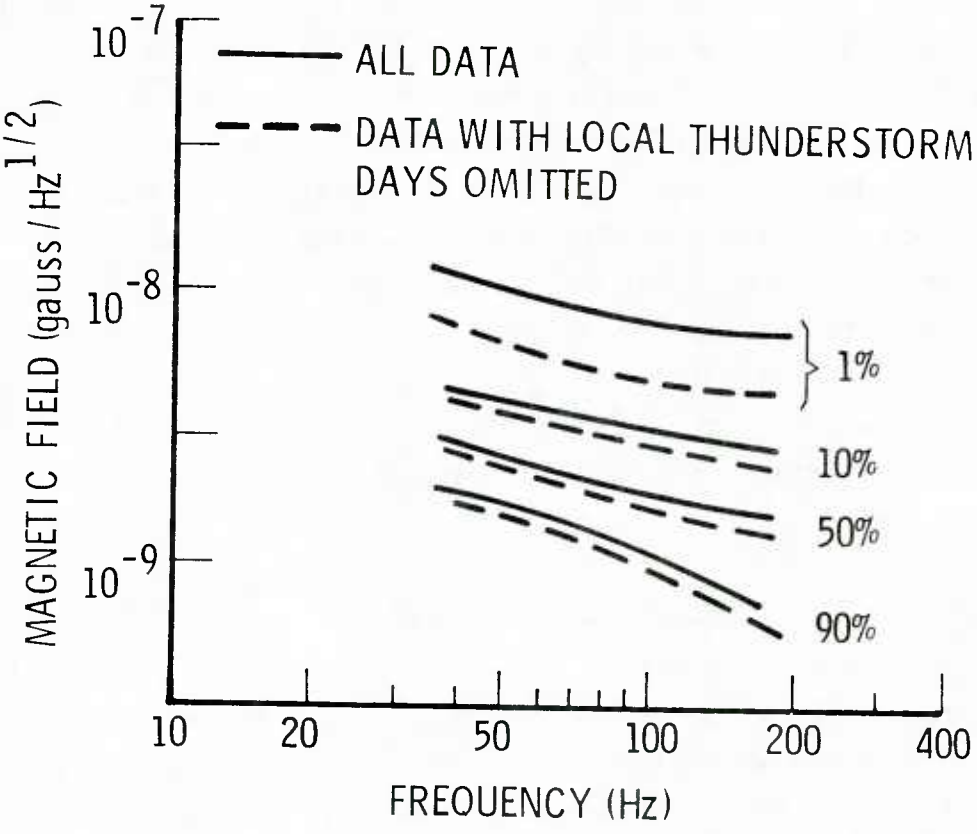

Figure 4.6

ELF geomagnetic noise measured at Malta during Autumn 1969. The several curves are labeled with the amplitude probability that noise at the given frequency will exceed the indicated value. Note that the effect of local thunderstorms, which tend to be very "spikey", is very pronounced on the 1% data and less on the higher probability curves.

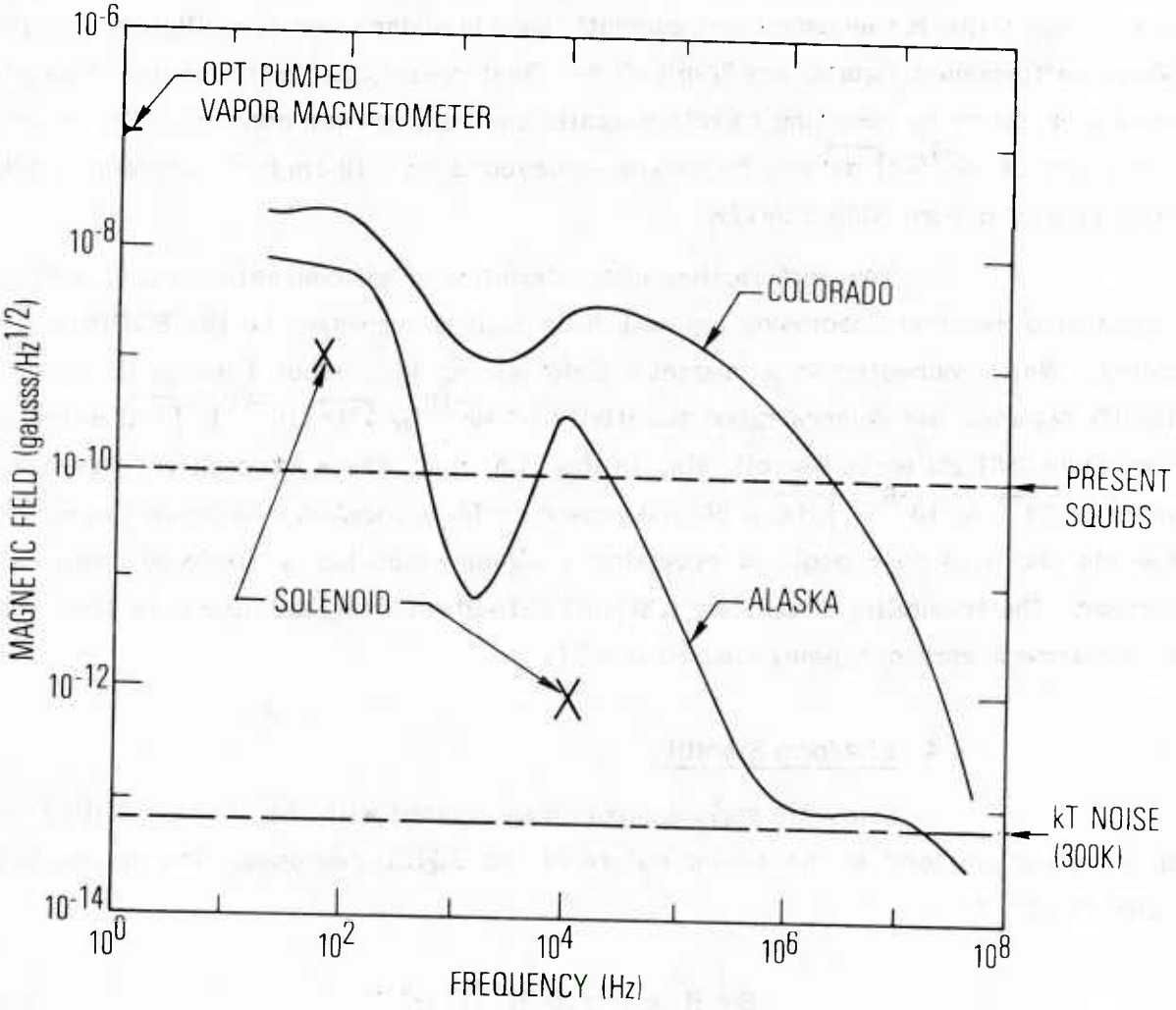

Figure 4.7

Examples of ELF receiver sensitivity compared to variations in geomagnetic noise.

magnetic detection system most commonly used is the induction loop whose sensitivity varies inversely with frequency. (See data points on Fig. 4.7.) Furthermore, induction type detection systems, especially at frequencies less than 10^2 Hz tend to be physically quite large. In Figure 4.7 the performance of the optically pumped vapor magnetometer is also shown as this is the instrument currently used in underwater surveillance operations. These performance figures are "typical" for fleet operational instruments. One can do somewhat better by resorting to rather exotic and cumbersome concepts. For example, a sensitivity of 10^{-8}G/$\sqrt{\text{Hz}}$ at 1 Hz can be achieved using a 10 cm by 10 cm loop of 500,000 turns of copper wire cooled to 77K.

The performance characteristics of all conventional (i.e., non-superconducting) receivers operating below 100 Hz can be surpassed by the SQUID magnetometer. When connected to a magnetic field sensing loop about 3 inches in diameter, a SQUID detector has demonstrated sensitivity of 10^{-10}G/$\sqrt{\text{Hz}}$ (10^{-14}T/$\sqrt{\text{Hz}}$) in the signal band from 0.01 Hz up to several kHz. In the ELF band, where atmospheric noise is of the order of 10^{-8} to 10^{-9}G/$\sqrt{\text{Hz}}$, a SQUID sensor could be located well below the surface of the sea and still be capable of receiving a signal which has a usable S/N ratio at the surface. The feasibility of building a SQUID H-field receiving antenna to be towed behind a submarine is currently being studied at NRL.

4.4.4 Platform Stability

One very serious problem associated with the use of a SQUID system on a mobile platform is the vector nature of the SQUID response. The motion induced signal has the form

$$S = H_e \cos\Theta \approx H_e (1 - \Theta^2/2) \tag{4.4}$$

if the sensor axis is parallel to the earth's magnetic field, H_e, and

$$S = H_e \sin\Theta \approx H_e\Theta \tag{4.5}$$

if the sensor axis is not parallel to the earth's magnetic field. Hence even in the most favorable situation, with the sensor parallel to the earth's field, the orientation must be

maintained to better than 10^{-5} radians to avoid an induced signal comparable to the noise. This level of platform orientation stability is probably beyond the state-of-the-art of magnetically quiet servosystems. Thus the approach of both NCSL and NRL is to employ a multi-sensor array (all superconducting or a mix of superconducting and conventional sensors) and to compensate for the motion induced signal by some adaptive data processing technique. In the NRL system for ELF communications, the output signals of three nominally orthogonal sensors (triaxial) are squared and suitably added to produce an output signal proportional to the square of the earth's field and thus insensitive to rotation of the sensor array in the earth's field. In the NCSL system, signals from vector component magnetometers are used to correct for motion induced signals from the gradiometer array. The level of sophistication for the compensation of motion induced noise, of course, depends on several contributions to the total noise of the system and the desired level of sensitivity required relative to the various noise sources.

4.4.5 Present SQUID System Performance

The NRL triaxial SQUID system probably represents the present day state-of-the-art of such systems. The following is a list of system characteristics:

SQUID bias frequency	19 MHz
Magnetic flux noise in frequency band from 0.01 to 2,000 Hz	$2 \times 10^{-4} \Phi_o / \sqrt{\text{Hz}}$
Magnetic field sensitivity with 3 inch diameter field coil	1×10^{-10} gauss/$\sqrt{\text{Hz}}$
Analog dynamic range (referred to instrument noise)	10^7 from DC to 65 Hz 3×10^6 at 130 Hz
Small signal response (100 x instrument noise)	DC to 10 kHz
Slewing rate	$8 \times 10^5 \Phi_o / \sqrt{\text{Hz}}$

These characteristics are probably adequate to demonstrate the feasibility of using SQUIDs in the systems under consideration, and to identify problem areas associated with the use of superconductive electronics in operational situations.

To construct a SQUID gradiometer, two field sensing coils wound in series opposition are connected to the SQUID sensor. The degree of "perfection" of the gradiometer depends on the ability to "balance" the gradiometer, that is, the degree to which the two loops can be matched in effective area and angular orientation. A perfectly balanced gradiometer will have zero response to a uniform magnetic field applied in any direction. At the present time one can achieve a mechanical balance (i.e., the balance after careful fabrication) of the order of 1 part in 10^4 which will remain unchanged after repeated temperature cycling between room temperature and cryogenic temperatures. Greater than 1 part in 10^6 can be achieved by magnetic trimming, i.e., by suitably distorting the loops or by suitably locating superconducting tabs in the vicinity of the loops. However, this level of gradiometer balance usually has to be adjusted after each temperature cycle.

4.5 Directions for SQUID System Improvement

Areas of useful improvements in SQUID systems, both magnetometers and gradiometers, are listed below, with near term needs listed first and ultimate needs listed later.

(1) Dynamic Range and Slewing Rate -

Improvement in the dynamic range and slewing rate would be beneficial since it would relax the requirement on platform stability that is imposed in order to prevent SQUID reset or "flux jump". In addition the increased slewing rate would allow the SQUID feedback system to cope with a larger signal bandwidth.

(2) Gradiometer Balance -

Improved design and fabrication of gradiometer coils could lead to a greater degree of balance that can be retained during temperature cycling and would decrease the necessity of requiring highly skilled personnel to operate and maintain

superconductive sytems. This problem area includes such topics as mechanical properties of construction materials at low temperatures (linear expansion, flexing, etc.,), weak magnetic properties of construction materials, and dimensional stability of structures built with dissimilar materials at room temperature and then cooled to cryogenic temperatures.

(3) Higher Sensitivity SQUIDs -

As system engineers learn to work with SQUIDs with equivalent flux noise of $10^{-4}\,\Phi_o/\sqrt{\text{Hz}}$, the increased gain available by operating at higher RF excitation frequency should be utilized to increase system sensitivity. The effective reduction in electronic instrument noise will uncover new operating problems with regard to dynamic range and slewing rate, noise arising from magnetic inclusions in the construction materials located close to the sensor, mechanical instabilities, etc. After each improvement in sensor performance, solutions to these problems must be found before the increase in sensitivity can be usefully employed.

(4) Cryogenics -

In the early feasibility studies liquid helium storage dewars will be used to provide the necessary cyrogenic environment. Once overall SQUID system feasibility has been demonstrated, a careful investigation of closed-cycle refrigeration systems and the possibility of SQUIDS made from high T_c material should be undertaken to establish desirable thermal configurations for a system whose performance and convenience of operation would be acceptable to typical fleet personnel.

5. SUPERCONDUCTING DIGITAL ELECTRONICS

5.1 Logic and Memory

A Josephson junction, when provided with some means of control, becomes a gate or switching element which can be utilized for simple binary logic and/or memory. Junctions which are hysteretic in their I-V characteristics can be switched between the pair tunneling (V=O) and quasiparticle tunneling ($V \approx 2\Delta/e$) states to form a latching logic system. Non-latching logic can also be developed in which the voltage resets rapidly to zero after a voltage transient which is less than the gap voltage. The problems in developing a viable SC digital technology can be broken down into two principal areas: development of reliable, reproducible, high-yield junctions of the proper characteristics, and development of logic and integrated superconducting circuitry which makes optimum use of the junction characteristics. To date the major efforts in these two areas have been at the IBM Research Laboratories at Yorktown Heights, New York, and Zurich, Switzerland.

In the areas of digital signal and data processing, Josephson junction technology offers a number of performance features which are neither found nor predicted to occur simultaneously in any competing semiconductor technologies. The greatest impact arises from the combination of two features--high speed and low power dissipation. For 5μm line-width technology, switching times on the order of 10 picoseconds have been measured, and fully loaded logic delays of 100 picoseconds are achievable. For latching devices (those which switch to the energy gap voltage and remain there until the supply current is lowered) power dissipation of the present devices is on the order of 1 microwatt/device when switching at maximum speed. In non-latching devices, which set to a voltage well below the gap and require no resetting, dissipation three orders of magnitude lower can be achieved. Therefore the low power dissipation allows the high speed feature to be fully exploited. When switching speeds are measured in 10's of picoseconds, signal transmission delays become the limiting factors. Time delays are $\approx$100 picoseconds for each cm of transmission lines. These delays can be kept low only with high packing density. This in turn requires the low power dissipation levels exhibited by Josephson junction

devices which, for latching logic at packing densities of 10^5 gates/cm^2 will produce power dissipation densities on the order of 10 milliwatts/cm^2. Fast (e.g., $>$ 0.5 GHz) semiconductor devices, both demonstrated and predicted, have power dissipation of 10's of milliwatts/gate, or power densities of hundreds of watts/cm^2 when packed at 10^5 gates/cm^2. This is well beyond the capability of conventional refrigeration techniques including circulating fluorocarbons. Therefore, it is only through the combination of low power with high speed that the requirements of high performance LSI can be met, a combination found only in Josephson junction technology.

The technique required to fabricate individual Josephson junctions and multiple junction circuits is now well developed at the IBM Research Laboratory, Yorktown Heights, New York. This technique involves a self-limiting RF oxidation process in which the surface is sputter cleaned on one half-cycle and oxidized on the other, with the two competing processes balancing to produce a critically controlled oxide thickness which is independent of oxidation time. Beyond this crucial step the fabrication process consists of routine deposition and patterning of thin film insulation and metal layers. The cost per device in this technology, when fully developed, can be estimated to be no greater than that for competing semiconductor techniques. In a related area, the ability to tailor critical currents to requirements and to reproduce them from device to device and from chip to chip has increased commensurate with circuit complexity to produce acceptable tolerance margins. In some cases the margin requirements will determine which circuit designs are implemented. A problem not shared by conventional semiconductor technologies is that of cycling from helium to room temperature. This problem has been alleviated by development of a superconducting alloy to the point where it does not appear to limit the usefulness of the technology. Since the fabrication process is still in the development stage, realistic yield numbers are not yet available.

When used in digital circuits, Josephson junctions are switched between their pair and quasiparticle tunneling states to produce current steering for the execution of logic and memory functions. Switching between the pair and quasiparticle states is accomplished in the IBM logic by using the single junction quantum interference characteristics. Thus for junctions small compared to the Josephson penetration length the maximum supercurrent I_M is depressed by an applied magnetic field such that

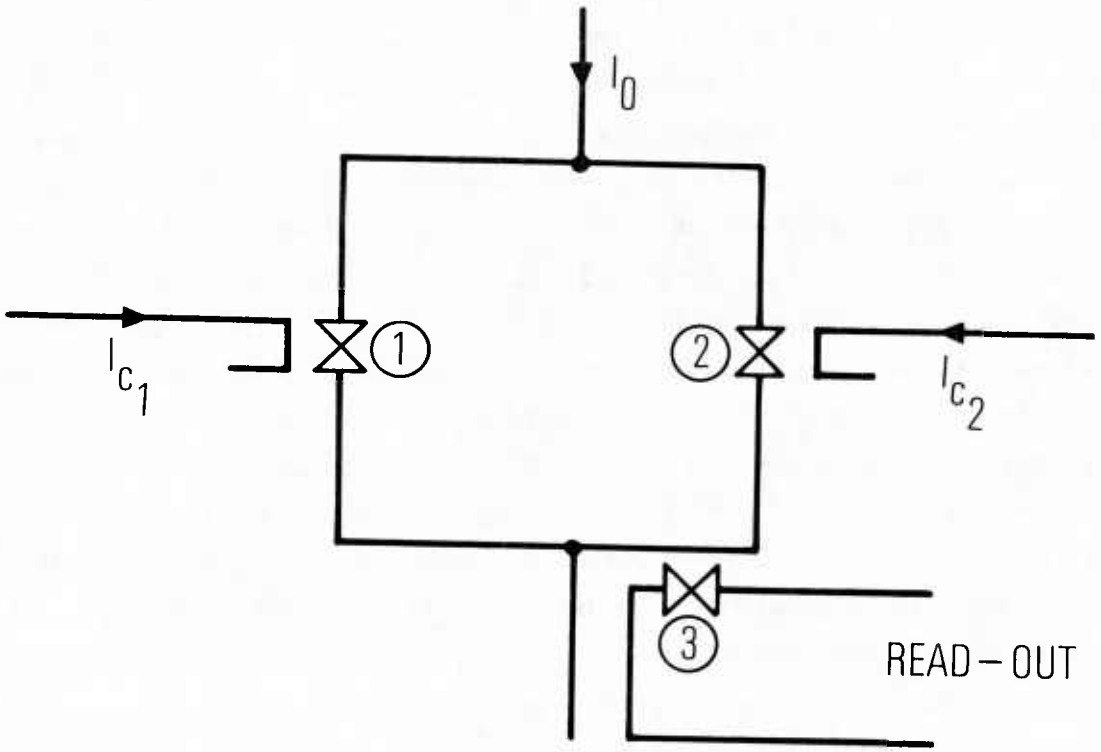

Figure 5.1

Schematic diagram of a Josephson junction memory cell. ① and ② represent input gates and ③ is the output gate.

$$I_M = 2J_c Wd \left| \frac{\sin(\pi \bar{\Phi} / \bar{\Phi}_o)}{\pi \bar{\Phi} / \bar{\Phi}_o} \right| \quad . \qquad (5.1)$$

J_c is the critical current density and W and d are respectively the width and thickness of the junction orthogonal to the magnetic field. The actual storage of information is achieved by means of circulating currents in superconducting loops, a method which contributes to the overall low system power levels since there is no dissipation in the standby state. If desired, three level memory can be implemented using circulating clockwise and counterclockwise currents and the absence of current for the three states.

Figure 5.1 shows one version of a memory cell where 1 and 2 represent Josephson junction gates, I_o is the supply current, I_{c_1} and I_{c_2} are the control currents for gates 1 and 2, and the third junction provides for read-out. Initially I_o will split equally between gates 1 and 2. If now control I_{c_1} is driven, gate 1 will be forced into its quasiparticle tunneling state, and all of I_o will be diverted through gate 2. When I_{c_1} is removed the current will remain through gate 2 such that when the supply current is dropped a clockwise circulating current will be stored in the now completely superconducting loop. The lower right branch of the loop forms the control for the read-out junction. When the loop is interrogated by driving the supply current, I_o will split equally, adding to the stored current in the clockwise direction and subtracting in the opposite direction. The clockwise current will now be sufficient to switch the read-out junction, indicating the state of the loop. Clearly, to store a counterclockwise current, the same procedure would be repeated driving I_{c_2}.

Representative logic and memory circuits in this technology have been built and tested. The logic circuits consist of one or more junctions across a matched superconducting transmission line. Because of the small dispersion in these low loss transmission lines they can be matched over a wide bandwidth and no reflections will occur to upset the driving logic.

Figure 5.2a represents a three input gate whose operation can be understood by examination of the gate current versus control current (I_g-I_c) characteristic shown in Figure 5.2b. When the control currents I_{c_1}, I_{c_2} and I_{c_3} are

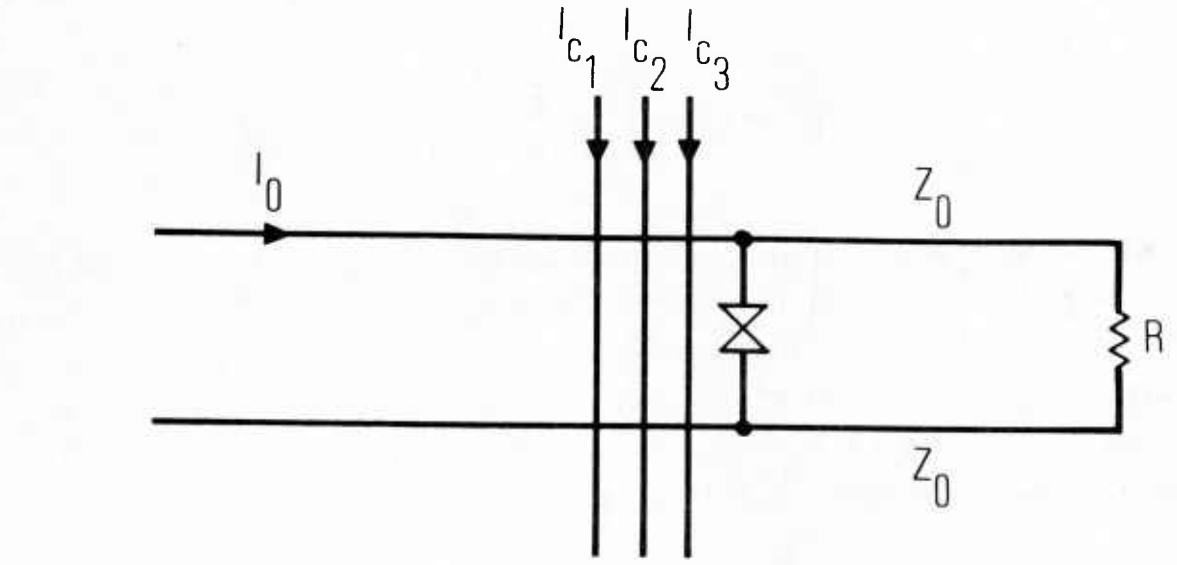

(a)

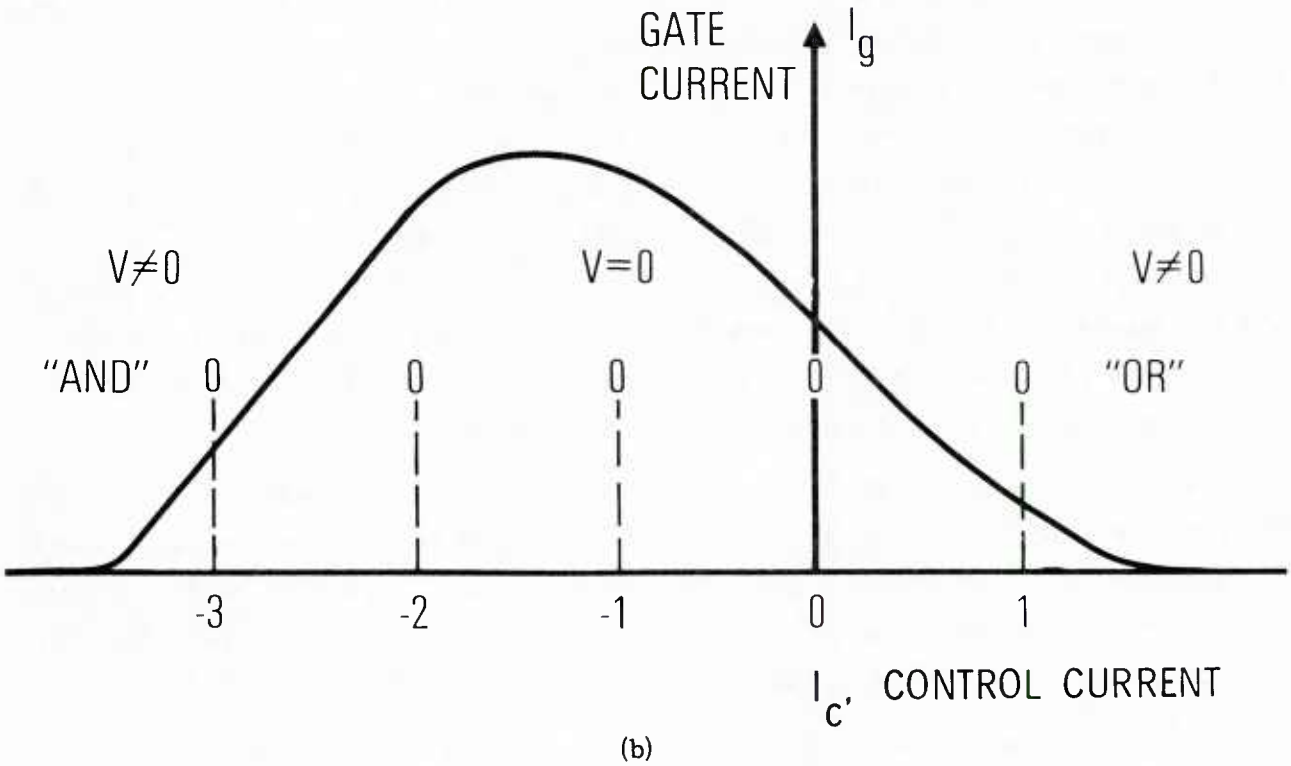

(b)

Figure 5.2

Three-input Josephson junction gate (a) and gate characteristics (b).

parallel to the gate current, I_g, this represents an "OR" gate in which only one control need be driven to force the gate into the $V \neq O$ state. If the control currents are antiparallel to the gate current, all three control currents must be driven to put the gate into the $V \neq O$ state, and the gate now performs an "AND" function. The asymmetric shape of the I_g-I_c characteristic arises from having the control in-line with the gate and makes this type of logic possible. Thus only the basic switching time, which is determined by the junction capacitance and is on the order of 10 picoseconds, is required to perform elementary logic. In the case of the memory cells an L/R time constant on the order of 100 picoseconds for present devices must be included to provide for current transfer. Of course, in all cases clock periods are longer than the basic switching times. The circuits tested to date by IBM include a complete logic family, an eight bit shift register, a four bit multiplier, a three bit cross-section of an eight bit analog-to-digital converter (A/D), and a fully decoded eight by eight bit memory. Since all of these circuits were built using 25 and 50 μm line width technology, their performance specifications are of limited significance now that 5 μm line widths are achievable. For example, the A/D converter study indicates an analog bandwidth of 37 MHz using a successive approximation technique and a single comparator.

A number of more complex circuits are presently being studied at IBM to investigate such problems as on-chip power regulation, clocking, and signal propagation delays. They are also testing an alternative, destructive read out memory configuration known as the Single Flux Quantum (SFQ) memory. These cells are extremely small and low power ($\sim$15 nanowatts/gate at a 100 MHz clock rate, fully decoded) and are thus ideal for bulk memory applications.

5.2 Analog-to-Digital Converters

Analog-to-digital (A/D) converters which are used to quantize analog electrical signals are of vital interest in DoD applications. Their critical characteristics are sensitivity, number of bits, sample rate, and aperture time. Although there are a large number of approaches, the two in general use for high speeds are the successive approximation and the parallel threshold types. The successive approximation type is capable of both high resolution (16 bits) and comparatively high speed ($>$1M bit throughput rate) as currently implemented in non-superconducting technologies. On the other hand, parallel threshold types have an intrinsic speed advantage

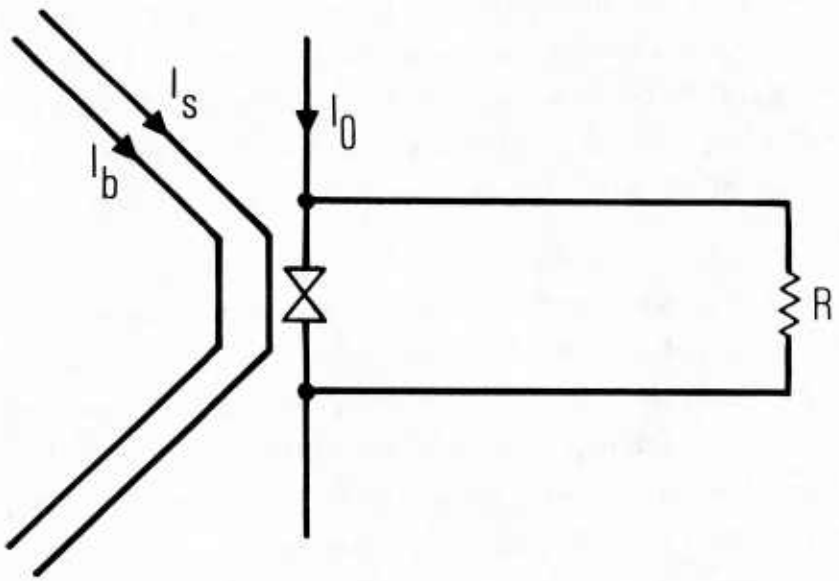

Figure 5.3

Josephson junction current comparator.

since the speed is limited only by the switching time of the input comparators and the subsequent gates used for conversion to binary. Unfortunately, the number of comparator elements increases geometrically with the required resolution. For 4 bits, 15 comparators and seven 8-input gates are required; for 5 bits, 31 comparators and nine 16-input gates are necessary. To exploit this extremely high speed configuration, spatial time delay between comparators must be reduced to a small fraction of the significant time resolution of the corresponding signal. Heat dissipation in semiconductors has prevented the ultimate exploitation of the intrinsic high speed of the parallel approach. Its relative complexity and cost has made it largely non-competitive at the slower speeds achievable by other approaches.

In either approach the heart of a high speed A/D converter is a current comparator. A Josephson junction based current-comparator is shown in Figure 5.3. Such a comparator can be made to act as a threshold device for any chosen signal current, I_s, simply by adjusting the bias current, I_b. It is the combination of I_s and I_b which switches the Josephson junction and drives the supply current, I_o, into the matched transmission line. The speed of operation of this comparator depends on the rise time of the Josephson junction, but the clock rate for the entire A/D process may include many other considerations such as the set-up time of a sample-and-hold circuit to feed the comparator and propagation delays.

McDonald [private communication] at NBS, Boulder, has proposed a fully parallel Josephson junction circuit to perform A/D conversion at a 20 GHz rate. This high speed performance has not yet been demonstrated, but it is important to assess and test as soon as possible the highest performance that can be achieved with manufacturable devices.

5.3 Comparison of A/D Technologies

The speed and power characteristics of Josephson junction devices were previously compared with those of individual semiconductor devices. It is also useful to make such comparisons for functional units such as A/D converters. Silicon technology switching speeds of 2 GHz may eventually be achieved but only at low densities because of high power levels. Because of the propagation delays at low density, practical clock speeds of 850 MHz with 4 bit resolution will probably be the limit for silicon technology.

TABLE 5-1

APERTURE TIME (IN PICOSECONDS) AT VARIOUS BIT RATES
(WORST CASE ANALYSIS)

Sample rate (Hz) / # Bits	10^8	10^9	10^{10}	10^{11}
2	397	39.7	4.0	.4
4	99.4	9.9	.99	.1
6	24.8	2.5	.25	.025
8	6.2	.62	.06	.006

Gallium arsenide based transferred electron logic devices (TELDs), field effect transistors (FETs) and combinations thereof offer the potential of 10 GHz clock speeds for A/D converters at 4 bit resolution.

The limiting factor in many A/D converter designs is the aperture time defined as the finite interval required for the input analog signal amplitude to be sampled. Aperture time represents the effective jitter during the analog sampling process. In a worst case analysis, the aperture time τ must be

$$\tau \leq \frac{1}{2^N 2\pi f} \tag{5.2}$$

where N is the number of bits resolution and f is the highest frequency to be sampled. It can be argued (but remains to be demonstrated) that for other than unmodulated monochromatic analog signals, the aperture time may be relaxed by a small but significant factor without encountering objectional error or loss of dynamic range. Table 5-1 gives the aperture time (in picoseconds) for various bit rates (sample rate times bits resolution) as calculated from Eq. (5.2).

The hybrid technology of electron beam semiconductor (EBS) A/D converters consumes greater than 100 times the weight, space, and power of semiconductor A/D converters, but has achieved the best bit rates to date. For EBS converters the aperture time can be independently controlled but must bear some synchronous relationship to the clock frequency. There are, however, factors which weigh against the eventual dominance of the field by EBS converters. They exhibit poor sensitivity and their bit rates will probably not exeed 2×10^{10}. EBS A/D converters are currently limited by two factors. First, it is difficult to form the required thin sheet electron beam and, second, it is difficult to handle the high data rate of the semiconductor diode output. By integrating GaAs FET or TELD devices with the silicon diode outputs, it may be possible to achieve 8 bit parallel output resolution at clock speeds of 4 GHz or higher if the electron gun problems can be overcome.

Figure 5.4 compares the clock frequency and number of bits for various A/D approaches which are either predicted or under development. Table 5-2 gives a more expanded comparison of various A/D converter technologies including sensitivity. The high sensitivity of the Josephson junction converters allows the possibility of digitization without amplification directly off an antenna.

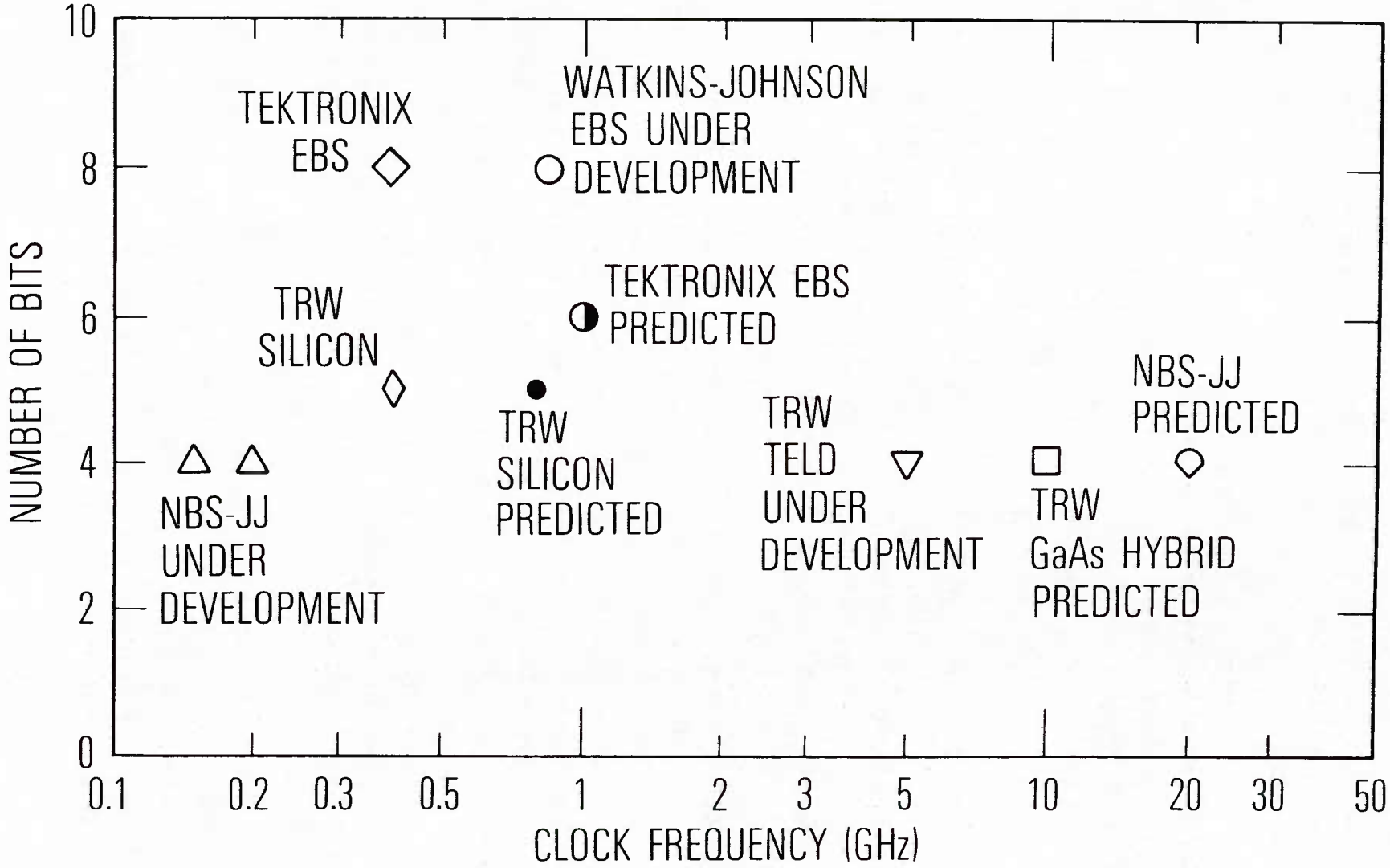

Figure 5.4

Comparison of various A/D converter technologies.

Table 5-2

COMPARISON OF HIGH SPEED A/D TECHNOLOGIES

DEVICE	NUMBER OF BITS	CLOCK FREQUENCY GHz	BIT RATE GBPS	REQUIRED APERTURE TIME+ (PICOSECONDS)	DEVICE APERTURE TIME++ (PICOSECONDS)	SENSITIVITY (VOLTS)
TRW SILICON	5	0.4	2.0	12.4	18.0	1.0
TEKTRONIX EBS	8	0.4	3.2	1.6	500.0	1.0
IBM JJ	8	0.075	0.6	8.3	<20.0	0.004
WATKINS-JOHNSON EBS*	8	0.085	6.8	7.3	30.0	5.0
TRW TELD*	4	5.0	20.0	2.0	20.0	2.0
TEKTRONIX EBS*	6	1.0	6.0	2.5	100.0	0.25
TRW SILICON*	5	0.85	4.25	5.8	17.0	1.0
NBS JJ*	4	0.2	0.8	49.7	<1.0	0.004
TRW GaAs#	4	10.0	40.0	1.0	2.0	2.0
TERNARY#	4	30.0	120.0	0.3	2.0	1.0
EBS HYBRID#	8	4.0	32.0	0.2	20.0	5.0
NBS JJ#	4	20.0	80.0	0.5	<1.0	0.004

*UNDER DEVELOPMENT

#PREDICTED

+WORST CASE ANALYSIS

++MEASURED OR PREDICTED PERFORMANCE.

As previously stated for single Josephson junctions, the significant advantage of Josephson circuits is the low power level. While semiconductor based A/D converters require about 50 mW per gate or comparator function at GHz sample rates, current latching Josephson junction gates require only about one microwatt. Predictions for non-latching gates are in the nanowatt range. (An optimistic prediction for future TELD devices is in the 20 mW range.) For high speed operation, no single dimension should exceed the wavelength in the microstripline, which for 10 GHz operation is $\sim$ 9 mm. This produces a maximum chip area of 81 mm^2. For a 4 bit parallel converter in semiconductor technology, this leads to a power density of 37 milliwatts/mm^2, a tractable number. However, for 5 bits and 8 bits, the power densities are 74 milliwatts/mm^2, and .67 watts/mm^2, respectively. Therefore, for converters requiring more than 6 bits of resolution, semiconductor technology will be power density limited. Josephson junction technology is clearly unique for high density, high speed applications.

5.4 System Problems

In spite of the great progress which has been made in SC digital technology, there remain a number of problems yet to be solved. Perhaps the greatest of these is packaging. One of the significant advantages of Josephson technology is that the devices can be connected by low loss superconducting transmission lines. This advantage will be reduced if the interconnections between various packaging levels produce significant discontinuities in the transmission lines. Further, the packaging scheme must provide for relative ease in making engineering changes. This attribute is desirable in any technology but is essential for the production of one of a kind special purpose processors. It can be anticipated that a large portion of the DoD needs will lie in this area. These problems are currently under study and will certainly require significant further effort.

The question of testing and maintenance of Josephson technology systems must be carefully assessed. In this respect Josephson technology shares the same reqirements and restrictions as any other LSI technology. Just as room temperature LSI circuits cannot readily be probed, neither can Josephson circuits easily be tested. Therefore, it is essential to build in adequate test and diagnostic circuitry in the design

stage to alleviate this problem. The added complexity of a liquid helium environment is a small perturbation on the general problem of LSI testing.

The performance figures given here are those achievable using photolithographic fabrication methods identical with those currently employed in the semiconductor industry. For general purpose machines and many special purpose processors, these switching speeds are completely adequate since the overall system clock will have to be slowed to accommodate long signal propagation paths. However, certain pipe-lined processors can be designed which can benefit from even greater switching speeds, and the aperture time requirements in fast A/D converters may also require greater speeds. This can be achieved by resorting to electron beam lithography to further reduce the area and, therefore, the capacitance of the junctions. It is estimated that for 1 μm junctions, the switching time will be on the order of 1 picosecond and the propagation delay will be proportionately reduced. The usefulness of this increased switching speed will be highly dependent on the circuit design. Because of the intrinsic high speed of the devices, the added complexity of electron beam fabrication will be required only for very specialized applications.

6. MICROWAVE/MILLIMETER WAVE RECEIVERS

Receivers in the microwave/millimeter wave spectral region are of the following two types: (1) Superheterodyne with mixer front end followed by an intermediate frequency (IF) amplifier; and (2) RF amplifier front end using low noise traveling wave tube amplifier (TWTA), parametric amplifier such as a varactor or a maser, or solid state amplifier such as a GaAs FET. SCE devices are under development which will increase the sensitivity of both classes of receivers, although at a reduction in dynamic range.

Josephson junctions are highly nonlinear devices with frequency response which extends well into the far infrared. A wide variety of high frequency applications has been explored. In addition, several high frequency superconducting devices are being developed which do not use the Josephson effect. These include a superconducting version of the Schottky barrier diode for use as a high frequency heterodyne mixer and a video detector, and also a composite superconducting bolometer. In this section, we discuss the state of development of superconducting mixers, detectors, and parametric amplifiers at microwave, millimeter and submillimeter wavelengths and compare them to conventional systems.

6.1 Mixers

A useful figure of merit for a voltage-controlled fundamental mixer or square-law detector is the current responsivity, $R_I \equiv dI/dP$ in amps/watt. In general the responsivity of a non linear element is $(d^2I/dV^2)/(2dI/dV)$. For an exponential device, $R_I = S/2$ where S is the logrithmic derivative, $S = d(\ln I)/dV$.

In the classical Shottky diode, $S = e/kT$ in the high temperature region. As the temperature is reduced, there are practical limits to the S-values which can be obtained. There is a fundamental quantum upper limit $S = 2e/\hbar\omega$ which can be approached if the temperature is low compared with the operating frequency, i.e., $kT \ll \hbar\omega$. Low temperatures are thus required to obtain the quantum limited S for frequencies below the infrared range.

An efficient mixer is driven hard enough by the local oscillator (LO) so that the conversion loss L_c (defined as the ratio of the available signal power P_S to the single sideband power P_{IF} coupled out into the intermediate frequency (IF) amplifier) approaches a limiting value $L_c \gtrsim 2$ which depends on how the mixer is terminated at harmonic

frequencies. The mixer is capable of efficient conversion only if the curvature S exists over a wide enough voltage range ΔV. The limiting value of L_c is approached when $S\Delta V \gtrsim 8$. The local oscillator power required to reach this limit is $P_{LO} \gtrsim 4/R_D S^2$, where $R_D = dV/dI$. If the usable P_{LO} is limited by availability or by a small value of the product $S\Delta V$, then the minimum detectable power of a coherent heterodyne mixer is

$$NEP \approx \frac{2\,\overline{i_N^2}}{P_{LO} S^2} \text{ (Watts/Hz)}, \tag{6.1}$$

where $\overline{i_N^2}$ is the mean square noise current in R_D in a bandwidth B. For an incoherent power detector the corresponding relation is

$$NEP = \frac{2(\overline{i_N^2})^{\frac{1}{2}}}{S} \text{ (Watts/}\sqrt{\text{Hz}}\text{)}. \tag{6.2}$$

From (6.1) and (6.2) it is evident that the sensitivity is increased by increasing $R_D S^2$ if the noise is thermal (that is, if $\overline{i_N^2} = 4\,kTB/R_D$) and by increasing S^2 if it is not.

The signal power at which mixer saturation begins is a fraction of the P_{LO} applied up to $P_{LO} \approx 4/R_D S^2$. Large S values are therefore generally associated with small saturation levels. However, since the noise level can be very low in large S-value, low temperature mixers, the dynamic range can still have useful values. A cooled attenuator at the front end can be used to sacrifice low noise in favor of an increased saturation level for the system.

In the following discussion we characterize heterodyne mixers with a single sideband receiver noise temperature T_R referred to the mixer input, which contains contributions T_m from the mixer itself, and $L_c T_{IF}$ from the intermediate frequency amplifier. The conversion loss L_c which can be tolerated depends on the noise temperature of the available IF amplifier.

6.1.1 Super-Schottky Mixer

An ordinary Schottky barrier diode is biased with a voltage comparable to the barrier height, so that thermally excited carriers give $S = e/kT$ at room temperature. When such diodes are cooled, the S value usually saturates at a few times

the 300 K value and non-thermal noise is seen. Although not understood in detail, these effects are usually attributed to leakage currents. A superconducting version of the Schottky diode has been developed to obtain large S-values at low temperatures. It operates in the tunneling dominated regime, and is nonlinear because of the sharp energy gap structure in the superconducting density of states near the Fermi surface. The effect is essentially the same as quasi-particle tunneling in a superconductor-insulator-normal metal junction. A conventional diode I-V characteristic is obtained with S=e/kT over a wide voltage range at LHe temperatures.

The best super-Schottky performance demonstrated thus far [McColl, et al. 1976, 1977] has been with 5 μm diameter Pb contacts on high conductivity p-type GaAs. Values of $S \approx 10^4\ V^{-1}$ have been obtained which are essentially equal to e/kT for the ambient pumped ^{4}He temperature. The range of voltage Δ V over which S is constant can be sufficiently wide to obtain an intrinsic conversion loss $L_o < 5$ dB. Parasitic loss due to the junction capacitance and the spreading resistance into the semiconductor contributes additional conversion loss. In order to effect a proper impedance match, compromises may have to be made between the intrinsic and parasitic losses. For example in experiments at 9 GHz, this additional loss was less than $L_p \approx 1.5$ dB, although the intrinsic conversion loss was increased to 6 dB. Since the parasitic loss will increase as ω^2, it is a serious problem for higher frequency operation. It can be reduced by increasing the conductivity of the semiconductor, or by changing the conduction geometry. Improvement is possible by using a large number of smaller diodes connected in parallel. Alternatively, a very thin semiconducting barrier, such as the etched single crystal Si barrier could be used [Huang and Van Duzer, 1976].

Experiments at 9 GHz on a 1.1 K super-Schottky diode have given a mixer noise temperature $T_m = 6$ K and a conversion loss of 7.5 dB. This is the lowest microwave mixer noise temperature ever reported [McColl, et al. 1976, 1977]. It demonstrates the high potential of these devices for low noise applications.

The saturation level of this mixer has not been measured but it can be estimated from given values of $P_{LO} = -46$dBm and $S \approx 10^4$. This mixer should saturate severely at $P_S = P_{LO} \approx 2\times10^{-8}$W. This corresponds to a dynamic range of $\sim 10^5$ for $T_m =$ 6 K and a bandwidth of 1 GHz.

6.1.2 Josephson Effect Mixer

A Josephson junction can be operated as an efficient mixer with a very small value of P_{LO}. The Josephson mixer therefore resembles the large S-value mixer discussed above. The details of its operation, however, are entirely different. If P_{LO} at a frequency $\omega_{LO}/2$ is coupled to a Josephson junction, constant voltage steps with zero differential resistance appear which are separated by multiples of the voltage $V = \hbar\omega_{LO}/2e$. The steps are zero frequency beats between the AC Josephson frequency and the nth harmonic of ω_{LO}. The most useful type of Josephson mixer is biased with a constant current to a region between the n = 0 and n = 1 steps. In order to do this, it is necessary to use a Josephson junction which has no hysteresis on the DC I-V curve. The RF impedance of a Josephson junction biased in this way is real and nonlinear. It can serve as an efficient heterodyne down-converter for small RF signals.

The operation of a Josephson mixer can be most simply understood in the following manner. A local oscillator current is impressed on the diode such that the zero voltage current is diminished by approximately two. Under this condition the n = 0 current step I_o varies linearly with the RF current at the rate ω_{RF}. If the total RF current is $I_{RF} = I_S + I_{LO}$ and the junction is current biased at a point midway between the n = 0 and n = 1 steps, the junction voltage is modulated at ω_{RF} by an amount proportional to $R_D(dI_o/dI_{RF})^2$. The conversion efficiency L_c^{-1} is thus proportional to $R_D(dI_o/dI_{RF})^2$.

The detailed performance of this mixer has been calculated on the basis of the RSJ model. At values of the normalized frequency $\Omega_{RF} = \hbar\omega_{RF}/2eI_cR \ll 1$, the conversion efficiency into a single sideband can be considerably greater than unity. The nonlinearity is of high order so that efficient harmonic mixing is possible.

If the frequency at which the Josephson mixer is operated corresponds to $\Omega > 1$, the conversion loss increases as Ω^2. Even for $\Omega \gg 1$, the Josephson mixer retains an extraordinary capability as a harmonic mixer. Down conversion from 891 GHz with an $\sim$1 GHz local oscillator has been observed [Blaney and Knight, 1973]. The performance of Josephson effect fundamental mixers has been evaluated at least semi-quantitatively [Taur, et al., 1974a,b,c; Edrich, et al., 1977; Blaney and Knight, 1974] at 36, 300, and 891 GHz, respectively, using Nb point contact junctions with less than the maximum theoretical values of RI_c. In most of this work $\Omega = 1$ corresponded to $\lesssim$300 GHz. The most complete results are at 36 GHz where the measured conversion

efficiency and the noise are in good agreement with analog computer calculations based on the RSJ model including thermal (Johnson) noise in the shunt resistance. Based on this model, it is possible to predict the performance of Josephson effect mixers which use Nb junctions with the full theoretical value of $I_c R$ so that $\Omega = 1$ at $\sim$ 1 THz. The mixer contribution to the system noise temperature should be

$$T_m \approx (0.05 - 0.1)\nu T \qquad (6.3)$$

where ν is the frequency in GHz and T is the ambient temperature in Kelvin [Richards, et al., 1975]. The quantum noise limit of a heterodyne receiver $T = h\nu/k \approx 0.05\nu$ (GHz) should be reached for $T \lesssim 1$ K.

There is a practical lower limit to the mixer noise temperature T_m/T which can now be reached for small Ω. The predicted proportionality $T_m \propto \nu T$ occurs only if the RF source impedance is optimized. The optimum source impedance is much less than R for $\Omega \ll 1$. This low source impedance effectively shorts out the junction noise so as to give $T_m < T$ at low Ω. Since it is difficult to transform the impedance of a free space wave below a few ohms, optimum coupling is hard to achieve for $\Omega \lesssim 0.3$. Consequently, the experimental values of T_m/T are constant at ≈ 30 throughout the millimeter region. A series array of junctions could in principle solve this problem and allow the predicted values of T_m to be achieved [Richards, et al., 1975]. This prediction has not yet been verified experimentally.

Although the performance of the Josephson mixer cannot be understood in terms of a curvature parameter S, it shares some features of large S-value mixers, including a low saturation power level. The mixer is badly saturated when $P_s = 10^{-2} I_c^2 R \approx 10^{-10}$ W compared with a local oscillator power of $P_{LO} \approx I_c^2 R$. It seems plausible that the saturation level would be increased by the use of a high impedance series array of junctions since the power per junction would be decreased.

In summary, the Josephson effect mixer is a highly nonlinear low noise device which can show conversion gain. Values of $T_m \gtrsim 50$ K have been demonstrated at millimeter wavelengths and quantum noise limited operation is predicted theoretically.

6.2 Video Detectors

6.2.1 Super-Schottky Video Detector

Because of its high S-value at low temperature, the super-Schottky is an extremely quiet video detector [McColl, et al., 1976, 1977]. In this application, the voltage over which S is constant is important only to the saturation level of the signal. Experiments at 9 GHz have shown an NEP of 5.4×10^{-16} W/$\sqrt{\text{Hz}}$ at a temperature of 1.06 K. This is the best microwave video NEP yet reported. Parasitic loss contributes more than a factor 2 to this NEP and would be increasingly important at higher frequencies as is the case for the mixer application.

6.2.2 Josephson Effect Video Detector

The zero voltage current of a Josephson junction decreases as I_{RF}^2 for $I_{RF} \ll I_c$. Consequently, if no local oscillator power is applied, a non-hysteretic junction, which is current biased in the resistive region, will act as a square law detector for small signals. As with the mixer, the complexity of the Josephson effect makes this device quite different from the classical resistive detector [Kanter and Vernon, 1972]. For signal frequencies ω_S which are low compared with the Josephson frequency set by the bias voltage $\omega_J = 2eV_{bias}/\hbar$, there is classical video detection which is proportional to d^2V_o/dI_o^2. There is a dispersive enhancement and a change of phase when $\omega_S = \omega_J$, and the response is proportional to $R_D = dV_o/dI_o$ for $\omega_S > \omega_J$. An analysis of this device based on the RSJ model is in reasonable agreement with experiments at various millimeter and submillimeter wavelengths. An NEP of 5×10^{-15} W/$\sqrt{\text{Hz}}$ has been measured with a Nb point contact at 90 GHz [Kanter and Vernon, 1971]. A value of 5×10^{-16} W/$\sqrt{\text{Hz}}$ is expected [Ohta, et al., 1974] for an ideal Nb junction at 150 GHz. This value should scale as Ω at higher frequencies. It is difficult to match low impedance junctions to free space waves, similar to the problem with Josephson mixers. The properties of high impedance junctions ($R > 50$ Ohms) are degraded by the effects of ambient temperature thermal noise. As a consequence, series arrays of junctions may also be useful in impedance matching video detectors to free space or microwave circuitry.

6.3 Superconducting Bolometer

Thermal (bolometric) detectors have historically been the most sensitive wide band receivers of submillimeter wave radiation. These consist of a radiation

absorbing element, a thermometer, and a thermal link to the heat sink. To keep thermal noise and heat capacity to a minimum, the best bolometers are operated at pumped ^{4}He (or even ^{3}He) temperatures. The best submillimeter wave bolometers available [Clarke, et al., 1975b] use a $\sim 200\Omega/\square$ metal film on a transparent dielectric substrate as an absorbing element, and a superconducting Al film operated near its critical temperature of 1.3 K as the thermometer. The reported sensitivity of such bolometers is NEP = 2×10^{-15} W/$\sqrt{\text{Hz}}$, with areas of 0.16 cm^2 and response times of 20 ms. This NEP can, in principle, be reduced by a factor of 3 by decreasing the substrate thickness or increasing its Debye temperature, and a factor in excess of 10 by operating at ^{3}He temperatures. The numbers achieved represent a major recent improvement in performance at submillimeter wavelengths compared to that previously available from semiconductor bolometers. The primary reason for the improvement is increased radiation absorption efficiency.

6.4 Parametric Amplifiers

Under a variety of conditions, Josephson junctions exhibit a nonlinear inductive reactance. If this reactance is varied by a suitable pump source, parametric gain can be obtained. Gain is generally observed only if some care is taken to control dissipation at parasitic (unwanted) combination frequencies. If the junction resistance is made large compared with the parasitic termination impedance, then the idler is said to be shorted out. In this case no power is dissipated at the parasitic frequency. Since junction impedances rarely exceed 20 , this condition is difficult to meet at microwave frequencies. Alternatively the circuit impedances can be made large compared with the junction resistance. Although this termination is frequently used, it does not entirely prevent dissipation at the parasitic frequency since currents can still flow and dissipate power in the quasiparticle shunt conductance internal to the junction.

Two classes of Josephson parametric amplifiers have been demonstrated; those which can be pumped externally with a microwave/millimeter wave oscillator, or internally by means of the Josephson self oscillation.

6.4.1 Externally Pumped Paramp

The best performance of an externally pumped Josephson effect parametric amplifier has been obtained with a doubly degenerate negative resistance

amplifier which is operated with no current and voltage bias. The physical symmetry of an unbiased junction requires that the nonlinear inductance depend only on even powers of the current. The ampifier is therefore operated with $2\omega_p = \omega_s + \omega_i$ and $\omega_p \approx \omega_s \approx \omega_i$. The lowest parasitic frequencies are near $3\omega_p$ and $5\omega_p$.

Amplifiers of this type have been operated at 10 and 33 GHz using a series arrays of Dayem bridges [Parrish and Chiao, 1974; Chiao and Parrish, 1975, Feldman, et al., 1975] at 9 GHz using a series array of tunnel junctions [Claassen, private communication], and at 36 GHz with a single point contact [Taur and Richards, 1977]. Gain in excess of 10 dB is generally obtained if the bandwidth is sufficiently narrow to avoid saturation on external noise [Feldman, 1977]. Since the saturation power is predicted to increase with the number of junctions employed, the gain bandwidth parameter $G^{\frac{1}{2}}\Delta\omega/\omega$ should be larger for the array paramps. Values of 12-16 dB gain with 10 percent bandwidths have been observed at 10 and 33 GHz using arrays of $\sim$100 bridges. The dynamic range of these amplifiers is still relatively small but, if it is limited by external noise, it can in principle be increased by increasing the number of junctions employed.

The noise measured in this type of paramp has generally been dominated by noise from the (room temperature) circulator and the heterodyne receiver which follows it. Consequently, it has only been possible in most cases to set an upper limit to the noise expected from an amplifier operated with a cooled circulator. These upper limits typically correspond to $T_N \approx$ 20-50 K.

Depending on how the idlers are terminated, the maximum normalized frequency at which such an amplifier can be operated is $\Omega = 0.3$ to 0.5. Hysteresis on the DC I-V curve does not directly affect this device since it disappears under the operating conditions in which the zero voltage current is suppressed essentially to zero by the pump.

Attempts have been made to operate an externally pumped Josephson paramp in the singly degenerate mode in which $\omega_s \approx \omega_i \approx \omega_p/2$. Parametric oscillations, but not gain, have been seen in tunnel junctions and point contacts [Taur and Richards, 1977, Mygind, et al., 1976].

6.4.2 Internally Pumped Paramps

A Josephson junction can be voltage biased by passing a constant current through a shunt resistor which is small compared with the internal shunt resistance R of the junction. The voltage bias is effective up to a frequency set by R/L, where L is the inductance of the bias circuit, except for thermal fluctuations which frequency modulate the Josephson oscillations. The low inductance, voltage biased circuit is conventionally known as a resistive SQUID.

Gain has been observed [Kanter and Silver, 1971, Kanter, 1975a,b] at 30 MHz and 9 GHz in a point contact which was voltage biased as a degenerate parametric amplifier with $\omega_s + \omega_i = \omega_p = \omega_j$ and $\omega_s \approx \omega_i \approx \omega_p/2$. The contact was imbedded in a circuit which was resonant at $\omega_s \approx \omega_i$ and which short circuited other important combination frequencies. This amplifier closely resembles a conventional varactor paramp with a single important idler frequency. It is difficult to provide the required circuit properties for this amplifier at low microwave frequencies because of the $\sim 10\Omega$ impedance of typical point contacts. However, impedance matching becomes easier above 35 GHz. Series arrays of junctions might alleviate this problem, but would have to be operated in a synchronized voltage biased mode which has not yet been achieved at microwave frequencies.

A promising multi-idler internally pumped amplifier for very high frequency appplications has been demonstrated independently by two groups [Kanter, 1975a,b, Vystavkin, et al., 1977]. Although the devices appear qualitatively similar, the descriptions of them are quite different. One was analyzed as a resistive SQUID without reference to the I-V curve of the contact, and the other was analyzed in terms of the step induced in the measured I-V curve by a cavity which was resonant at ω_s. In both cases $\omega_p < \omega_s$ and the important idler frequencies are at $(\omega_s - \omega_p)$ and at $(2\omega_p - \omega_s)$. The convenional theory for a two idler paramp can be used to compute the gain-bandwidth parameter. The measured value of $G^{\frac{1}{2}}\Delta\omega/\omega$ was only 4×10^{-3}, limited by coupling problems for the low impedance junctions employed [Kanter, 1975a, b]. The maximum theoretical values are $\lesssim 0.4$ for normalized frequency $\Omega \approx 1$ and varies as $(2\Omega)^2$ for $\Omega > 1$. It therefore appears promising for operation at frequencies well above 100 GHz. The noise temperature of an amplifier operated at 10 GHz reaches a minimum value of ≈ 42 T for $\Omega = 1$. The relatively large noise in the two idler paramp can be understood in terms of the parametric upconversion of ambient temperature noise from the low frequency idler at $(\omega_s - \omega_p)$ to the signal frequency ω_s.

6.4.3 Parametric Upconverter

Another mode of parametric amplifier useful at low microwave frequencies is the parametric upconverter. This can be understood as a two idler amplifier or as a SQUID. In fact the RF SQUID is an externally pumped parametric upconverter; the DC SQUID is a self pumped parametric upconverter. In this mode $\omega_s << \omega_p$ and the two idlers at $(\omega_p - \omega_s)$ and $(\omega_p + \omega_s)$ are used as the output frequencies. Theoretical gain is the frequency ratio $(\omega_p \pm \omega_s)/\omega_s$ and the device now resembles a three terminal amplifier without use of a circulator. Theoretically this is the lowest noise amplifier with $T_N = T/G$.

In the only reported experiments [Kanter, 1975a,b] 115 MHz was upconverted by an external pump to 9 GHz with gain of 14 dB and $T_N \leq 3.6T$. This device was not optimized. It had a low saturation level and the noise was believed to be dominated by the amplifier following it.

The parametric upconverter can in principle be coupled with a low noise downconverter such as the super-Schottky to provide low noise single frequency amplification. This combination has been proposed as a low noise IF amplifier for a heterodyne receiver based on the super-Schottky heterodyne mixer [Silver, 1975]. In principle the gain of this proposed IF amplifier is GL_c, where G is the upconversion gain of the paramp and L_c is the conversion loss of the super-Schottky mixer. The noise temperature will be

$$T_N = (T + T_M)/G \, . \tag{6.4}$$

With $T_M < 10$ Kelvin as reported [McColl, et al., 1976, 1977] it is possible to obtain $T_N \lesssim 1K$.

6.5 Comparison of Receiver Technologies

Here we compare (adjusted) measurements and predictions for receiver front ends employing SCE with those of competing technologies. Present systems having noise temperatures below 300 K for operating frequencies above about 15 GHz are cryogenically

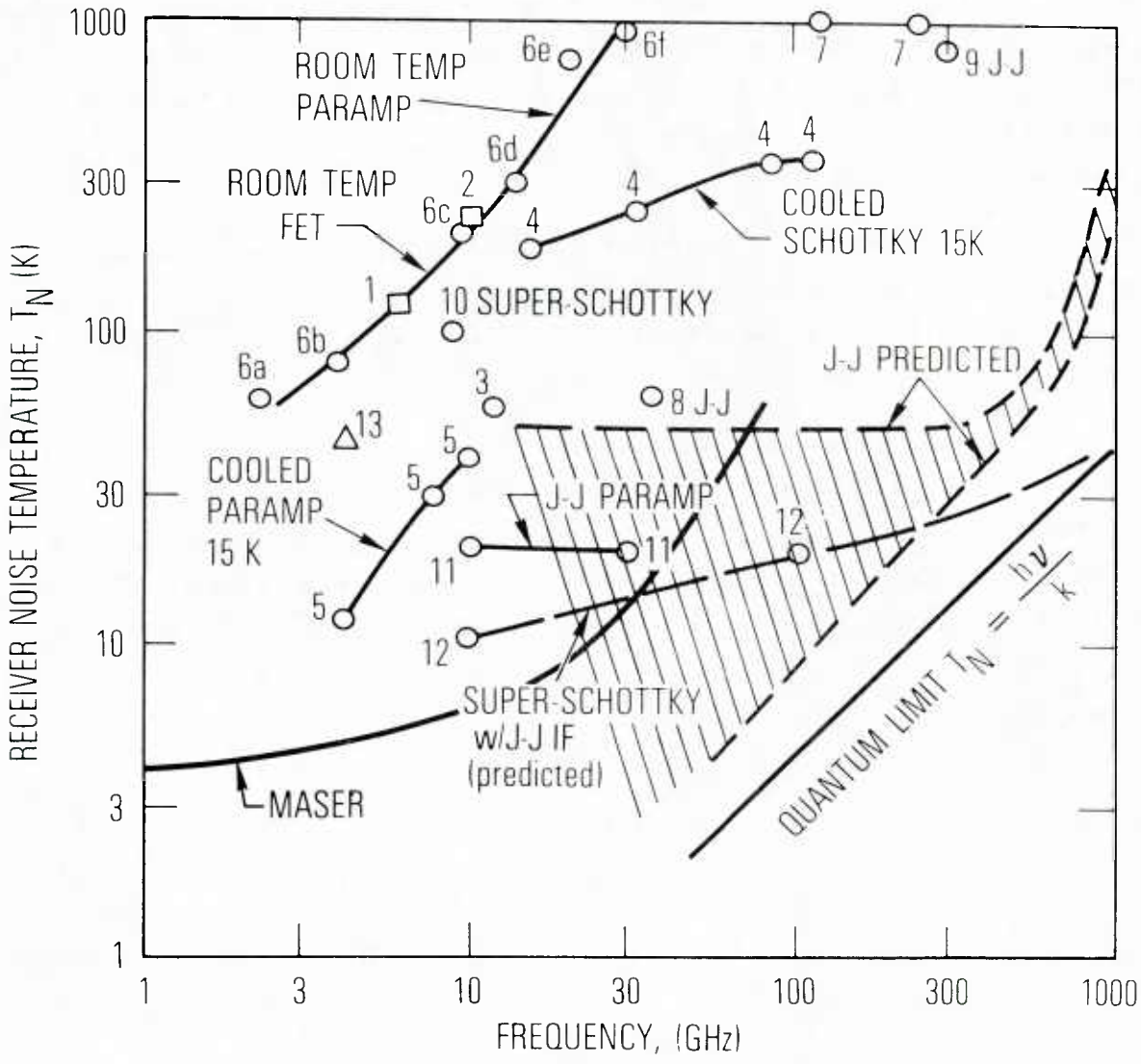

Figure 6.1

Comparison of low noise microwave/millimeter wave coherent receivers. Devices are identified in Table 6-1.

cooled. Thus, where receiver temperatures significantly below ambient temperatures are required, the use of superconductive devices does not impose a large penalty with regard to the refrigeration requirements.

The competing devices considered in this comparison are varactor parametric amplifiers and field-effect transistor (FET) amplifiers. As seen in Figure 6.1, the current noise temperature data for these two devices lie on the same curve, which passes through 200 K at 10 GHz and reaches 300 K at about 13 GHz. For mixer (heterodyne) front ends we assume an IF amplifier noise temperature of 15 K unless otherwise noted.

While the noise temperatures of room temperature GaAs FETs are not expected to improve to less than 120 K (as the gate length decreases to 0.25 micrometers), the use of other III-V binary, ternary, or quaternary materials may bring the effective noise temperature as low as 80 K at 10 GHz and 400 K at 30 GHz.

Next we consider cooled nonsuperconducting devices. Cooling the varactor parametric amplifier to about 15-20 K will reduce T_N by about a factor of five from the room temperature value. The FET noise is reduced by about the same factor when it is cooled. From an extrapolation of the cooled paramp and FET data to appreciably higher frequencies one expects T_N will reach 300 K at about 50 GHz. The noise temperature of the cooled Schottky diode (15 K) followed by a 15 K IF parametric amplifier also reaches T_N = 300 K at about 50 GHz and 350 K at 115 GHz. In the 115-240 GHz range cooled InSb bolometric mixers with a 15 K IF parametric amplifier give $T_N \approx$ 1000K, although this mixer has a very narrow bandwidth. Masers give noise temperatures below 10 K in the low GHz region although again bandwidth and tunability can be a problem above 10 GHz. Above 35 GHz maser noise temperature is expected to increase. However, masers are very competitive with cooled parametric amplifiers as low noise IF amplifiers.

The superconducting devices useful for coherent receivers are of two kinds, the Josephson junction and super-Schottky diodes discussed above. The Josephson junction can serve as either a mixer or parametric amplifier. Assuming the best reported Josephson mixers were to be combined with a 15 K IF parametric amplifier, the noise temperature at 36 GHz would be 65 K. A 30 GHz Josephson paramp had a reported T_N = 20 K. At 300 GHz a Josephson mixer with 20 K IF paramp produced $T_N \approx$ 850 K. The super-Schottky diode has only been used for mixing at 10 GHz thus far; with a 15 K IF parametric amplifier the SSB T_N would have been 100 K.

TABLE 6-1

Reference Data for Figure 6.1

(Number designates corresponding point(s) on Figure 6.1)

1.	Avantek 300 K GaAs FET with 9 dB gain
2.	Varian 300 K GaInAs FET with 11 dB gain
3.	Hewlett-Packard 90 K GaAs FET with 8 dB gain
4.	Weinreb and Kerr [1973], Kerr [1975]
5.	Scientific Communications, Inc. Model LR 150
6a.-6d.	Scientific Communications, Inc. Models ST-221A, SCP-292B, SCP-289, SCP-282, respectively.
6e.-6f.	Scientific Communications, Inc.
7.	Cooled InSb bolometer (T = 4.2 K), T. G. Phillips and K. B. Jefferts (quoted by A. A. Penzias [1974])
8.	Taur, et al. [1974d]
9.	Josephson Junction with T_{IF} = 20 K, Edrich, et al. [1977]
10.	McColl, et al., [1977]
11.	Chiao and Parrish [1976]
12.	Silver [1975] combined with results of McColl, et al. [1977]
13.	LNR Communications, Inc. Model NC4-40

One can expect SCE systems to demonstrate the greatest improvement for the following reasons: The margin between performance and theoretical expectation is greatest for SCE. This is true for both frequency limitations and noise performance. Furthermore, the more conventional devices and systems have received greater efforts to date and benefited from more extensive engineering refinements. SCE is just emerging from the scientific effect stage and most reported results can be considered comparable to cat whisker technology. The elementary devices, Josephson and super-Schottky diodes, are only now being developed to the point where major attention can be usefully directed to microwave circuit optimization. For example, the Josephson junction which gave the results at 36 GHz was not an optimized device. Depending on ability to achieve matching, the T_N with a 15 K IF amplifier should lie in the cross-hatched region in Fig. 6.1. The top of the cross-hatched region corresponds to what appears to be achievable now. The Josephson junction can have a high conversion efficiency (with gain even possible) so the noise contribution of the IF amplifier is less important than with other devices.

There is significant potential to extend the super-Schottky diode to 100 GHz and beyond with low conversion loss in order to minimize the effect of the IF amplifier noise. The (proposed) development of a low noise Joesphson IF amplifier would project a receiver noise temperature below 20 K at 100 GHz.

A major difficulty with Josephson junctions, both mixers and paramps, is the poor dynamic range. Some researchers believe this can be alleviated by the use of arrays to improve the impedance match and coherently add the saturation levels for each device without sacrifice in noise performance. This requires experimental verification.

In terms of sensitivity SCE receivers have a clear advantage at frequencies above 20 GHz and extending to near 1000 GHz.

6.6 Radiometric Sensing Systems

An important class of millimeter wave sensors are radiometers. These are distinguished from receivers by the nature of the signal--coherent intelligence of well defined bandwidth and format for receivers, and incoherent, thermal noise of extensive

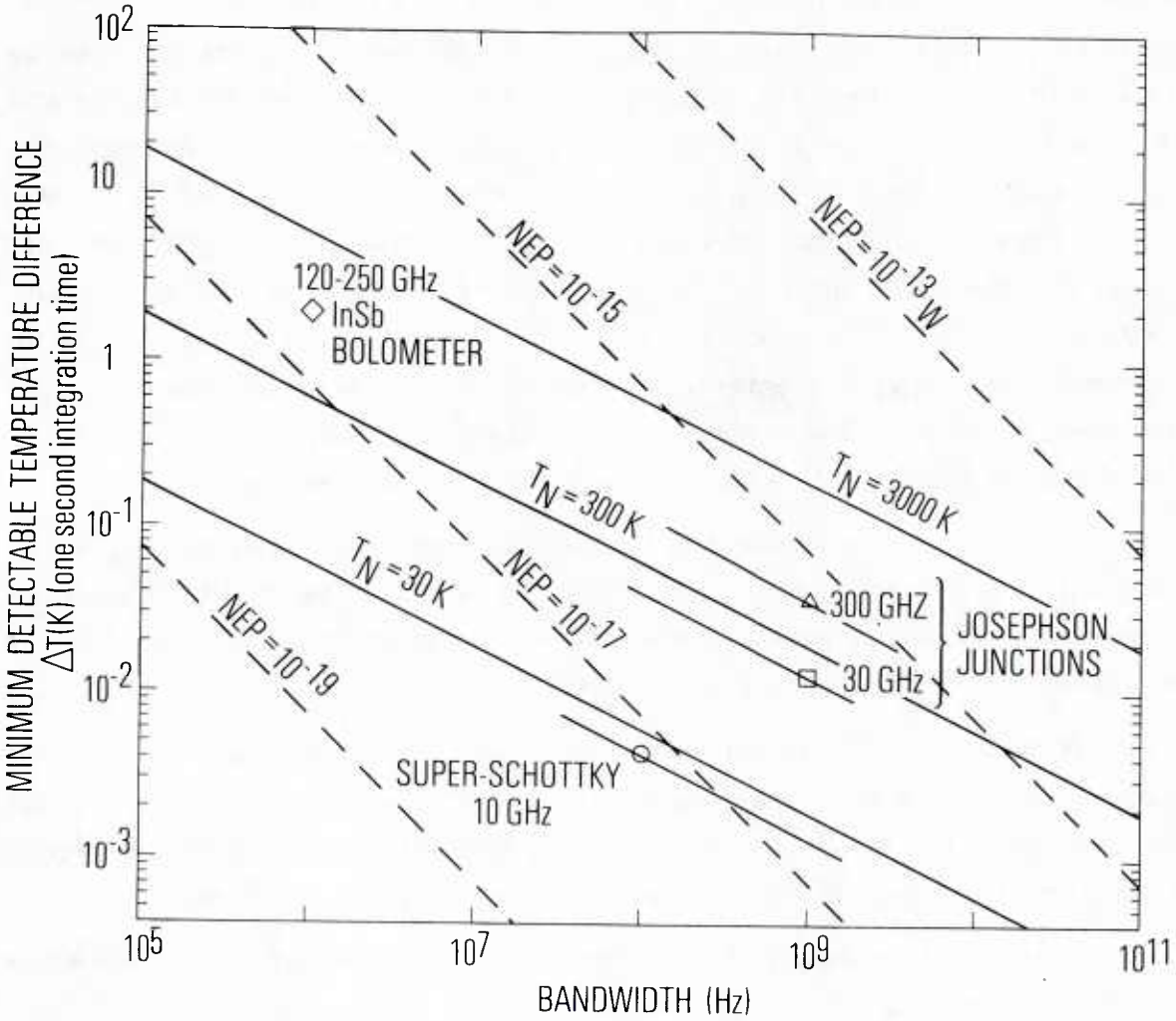

Figure 6.2

Sensitivity of millimeter wave radiometers.

bandwidth for radiometers. In radiometric applications one can use either coherent or incoherent detection. Figure 6.2 permits one to compare the system performance of the two techniques assuming diffraction limited angular resolution of the input aperture. The figure-of-merit for a radiometer is the minimum detectable temperature difference

$$\Delta T = \frac{T_N}{(B\tau)^{\frac{1}{2}}} \tag{6.5}$$

where T_N is the noise temperature of the radiometer, B is the detected signal bandwidth, and τ is the post-detection integration time. This factor is also related to the noise equivalent power by

$$\Delta T = \frac{NEP}{2kB\tau^{\frac{1}{2}}} \quad . \tag{6.6}$$

Cryogenic thermal detectors with NEPs near 10^{-15} watts/$\sqrt{\text{Hz}}$ have recently been demonstrated and should be usable throughout the mm and far IR regions. As recently as 1974, 10^{-13} W/$\sqrt{\text{Hz}}$ was assumed to represent the state-of-the-art [Penzias, 1974]. Most of this improvement has been realized by using thin metal films to obtain improved coupling of the radiation to the detectors. This is an active research area and devices with NEPs of the order of 10^{-17} W/$\sqrt{\text{Hz}}$ are predicted for the next decade.

For systems operating with optical coupling techniques one can readily choose to operate with less angular resolution when viewing spatially broad sources. Using larger detectors, with an associated degradation in resolution, an NEP improved by the square root of the total detector area would be expected. To obtain this with coherent detectors one would have to use an array of individual detectors with addition of their video signals. The present technologies appear compatible with such array fabrication. Arrays of detectors with individual data processing could also be useful in imaging applications.

In general incoherent detectors are favored for use at high frequencies in applications where wide bandwidths can be used. Conversely, coherent detectors promise improved performance at lower frequencies and smaller bandwidths.

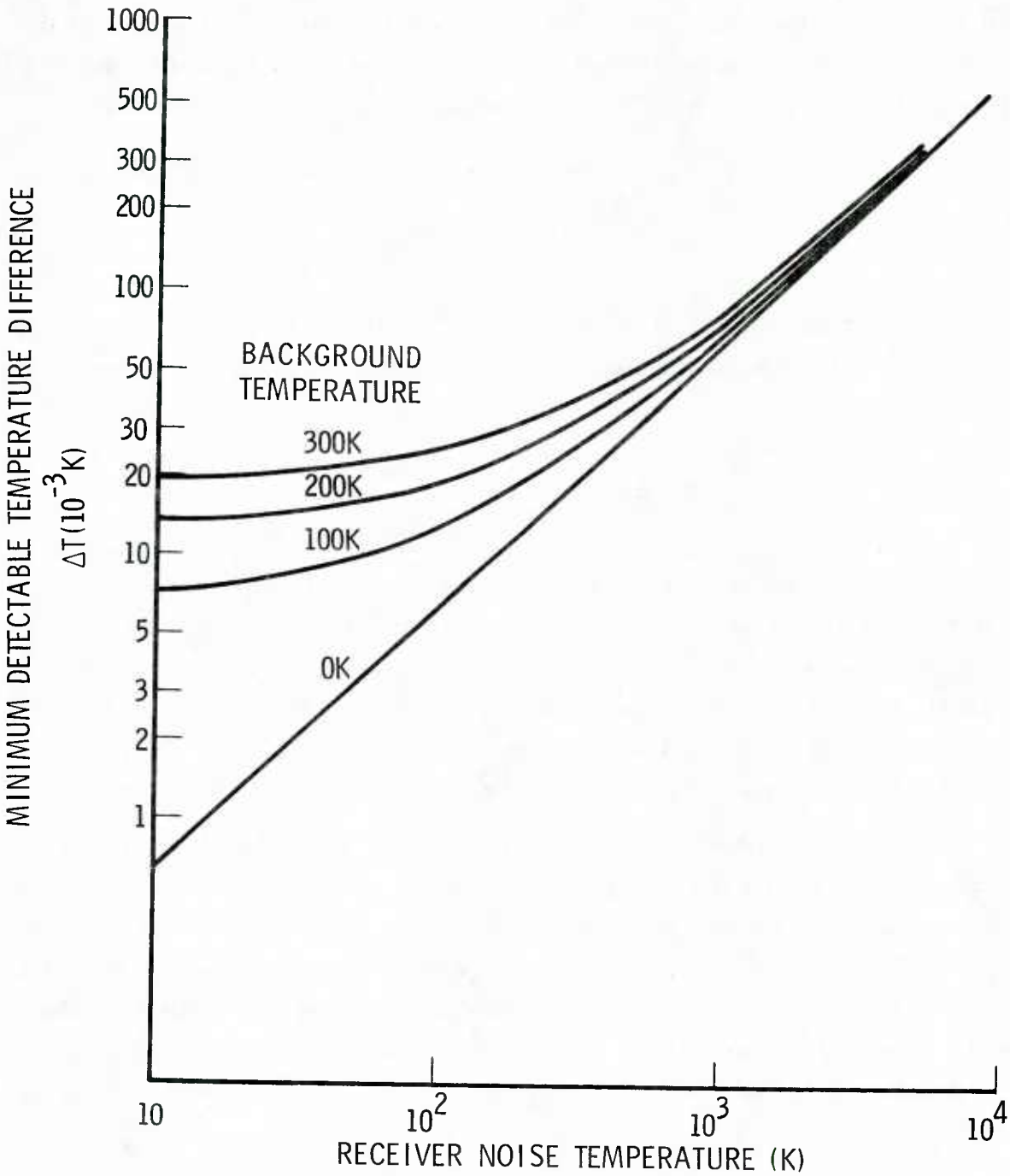

Figure 6.3

RMS noise ΔT for 1 sec integration time as a function of receiver noise temperature for different background temperatures. A 1 GHz bandwidth was assumed.

The use of Figure 6.2 and the interrelation between detector characteristics and systems performance are illustrated by the following brief discussion. First we consider the characteristics of a radiometer looking down on the earth from a satellite or high flying aircraft. Assuming that the background is 300 K thermal radiation, we can see from Figure 6.2 that an incoherent detector with an NEP = 10^{-15} W/$\sqrt{\text{Hz}}$ will be background limited at bandwidths greater than 10 GHz. Such detector bandwidths are readily achieved with incoherent detectors at frequencies above 100 GHz. However, for applications such as measuring atmospheric spectral lines, system bandwidths near 100 MHz and channel bandwidths less than 1 MHz are of interest. For 100 MHz a coherent detector with a receiver noise temperature below 100 K would be background limited with $\Delta T = 0.1$ K. By comparison, the 10^{-15} watts/$\sqrt{\text{Hz}}$ incoherent detector would give $\Delta T = 1$ K, and an NEP = 10^{-17} W/$\sqrt{\text{Hz}}$ would be required to give $\Delta T = 0.1$ K.

Imaging of the earth and oceans from satellite or aircraft by radiometric techniques in nearly all weather drives one to long wavelength systems to minimize obscuration by clouds, fog, smoke, etc. However, spatial resolution for passive imaging is determined by the angular resolution of the antenna; hence we are forced to consider millimeter waves such as 35 and 90 GHz. The system planner must make appropriate tradeoffs between spatial resolution, scan rates and coverage, contrast ratios, and sensitivity. The antenna temperatures of various targets have been measured at several millimeter wavelengths and are reported in Table 6-2. Antenna temperature is a direct measure of the energy received in the antenna from the source and includes the source temperature, emissivity, propagation losses, and antenna beam filling factor. The measured antenna temperature of the ocean varies from 105 K at 14 GHz to 207 K at 90 GHz. The temperature resolution is ΔT and depends on the post detection integration time τ as shown in Eq. (6.5). For a fixed ΔT and B, the time required to record one data point, or the size of a resolution cell in a scanning system, is proportional to T_N^2. One can see from Fig. 6.3 that it is reasonable to set the radiometer noise temperature T_N at about 1/3 of the background noise temperature.

In a terrestrial environment the background is approximately 300 K (200 K over water). Radiometers with $T_N \leq 100$ K at X-band and above will require cryogenic cooling, e.g., masers and paramps. If cryogenic cooling is accepted, SCE technology is a very competitive candidate; above 60 GHz it is the only player in the field which could

TABLE 6-2

ANTENNA TEMPERATURES OF SELECTED TARGETS[+]
(Temperature in kelvin)

Targets	Frequency		
	14 GHz	19 GHz	90 GHz
Vegetation	237 ± 16 N = 12	239 ± 11 N = 12	279.5 ± 3.5 N = 396
Concrete (Runway)	———	———	266 ± 4 N = 288
Docks	190 ± 11 N = 4	189 ± 5 N = 4	259 ± 7 N = 303
Ocean Water	105 ± 6 N = 14	114 ± 3 N = 16	207 ± 6 N = 242
Ships at Sea	———	———	159 ± 13* N = 255
Ships at Dock	80 N = 1	< 100 N = 1	168 ± 12** N = 168
C-54 Aircraft (on Runway)	———	———	225 ± 9 N = 18

+ King, et al. 1976
N = number of samples
1σ = ± values

* 4 ships, 425 ft to 708 ft lengths
** 5 ships, 250 ft to 750 ft lengths

achieve these noise temperatures and the large bandwidths desired in radiometric systems. In addition the prime power required for both the microwave pump sources and refrigeration are lower for the SCE system, and in particular for the microwave source as the frequency of operation increases beyond 35 GHz.

7. TUNABLE MICROWAVE SOURCES

7.1 General Characteristics

Tunable sources are needed for local oscillators in receivers and for the genesis of transmitter carrier frequencies. Among the functional parameters describing these units are:

1. Tuning speed/set-on time
2. Tuning bandwidth
3. Settling time
4. Post-tuning drift (extrinsic stability)
5. FM noise/residual FM
6. Modulation sensitivity
7. Output level
8. Noise background level
9. Efficiency

Conventional tunable RF sources use the principle of a resonant LC tank circuit to determine the oscillator frequency. Output frequency is proportional to $(LC)^{-\frac{1}{2}}$. Since the capacitance of a varactor is inversely proportional to the natural logarithm of the applied voltage, a voltage controlled oscillator (VCO) becomes possible. This general technique is representative of nearly all of the development in the field to date. A notable exception is the Josephson junction oscillator for which the output frequency is directly proportional to voltage (f = 483.594 GHz/mV).

7.2 Josephson Juction Microwave Oscillator

One of the earliest projected applications for Josephson junctions was a tunable oscillator from microwaves to the far infrared. This was based directly on Josephson's two relations,

$$j = j_c \sin \phi \qquad (7.1)$$

and

$$V = \Phi_o \frac{d\phi}{dt} . \tag{7.2}$$

These relations are expected to be valid up to voltages given by Eq. (3.3), or to frequencies associated with the superconducting energy gap. The amplitude of this oscillator is expected to be the critical current, I_c. Unfortunately, this promise has yet to be fulfilled. Some of the problems and characteristics are given below.

Because of its extremely nonlinear nature the behavior of a Josephson junction is extremely dependent on the circuit in which it is imbedded. Generally, the poor impedance match between the junction represented by Fig. 3.1 and most circuits exaggerates this effect. Furthermore, since the Josephson relations couple the junction voltages at DC ($V = V_o$), the fundamental frequency of interest ($f_o = V_o/\Phi_o$), and harmonics of f_o, the impedances at <u>all</u> these frequencies are important. Thus in the "current bias mode", the DC circuit impedance is much greater than R but the impedance at f_o must be comparable to the junction impedance in order to couple out appreciable energy. The resulting junction impedance is nonlinear making it difficult to preselect the voltage across the junction. In the "voltage bias mode", the DC circuit impedance is much less than R and the voltage can be preselected. The line width limit of the Josephson oscillator is [Silver and Zimmerman, 1975]

$$\Delta f = \frac{4\pi R_o kT}{\Phi_o^2} \tag{7.3}$$

where R_o is the effective shunt resistance of the junction, including the imbedding circuit. At $T = 4K$, $\Delta f = 16.2 \times 10^7 R_o$ hertz, where $R_o \approx R$ for current biased junctions and $R_o \lesssim 10^{-3} R$ for voltage biased junctions.

The signal power in the junction has a maximum value $I_c V$, where V is the microwave voltage. For a Josephson junction $V \approx \Phi_o f$ and $P \lesssim I_c \Phi_o f$. For $I_c \sim 10^{-3}$A, $P \lesssim 2 \times 10^{-18} f$, which projects to 10^{-8}W at 10 GHz. Measured powers delivered to an external load typically are 10^{-2} of the predicted maximum value.

The Josephson oscillator is unique in the following properties:

(1) frequency is precisely linear in frequency
(2) power increases linearly with frequency
(3) linewidth (particularly in voltage biased mode) is constant and hence Δ f/f increases linearly with frequency
(4) intrinsic frequency stability is independent of temperature.

The principal inadequacy is the low power. Here again researchers propose to use coherently oscillating arrays of junctions to increase the output power. The advantageous performance of such arrays is yet to be demonstrated.

7.3 Tuning Speed

In order to set the correct frequency of an oscillator, a linear voltage-to-frequency relationship must first be established for all but JJ oscillators. Linearization of conventional microwave oscillators is almost always accomplished in a piecewise linear approximation through the use of operational amplifiers and feedback circuitry which creates stepwise gain discontinuities. Typical varactor voltage swings of up to 40 volts are required for octave tuning ranges. This large voltage swing places severe constraints on the operational amplifier to the extent that tuning speed is now generally limited to 0.5×10^{-6} seconds per octave. For EHF spectrum devices this can be greater than 40 GHz/microsecond. This can be improved at the expense of additional nonlinearity. It is improbable that silicon technology operational amplifiers will ever improve this tuning speed by more than a factor of 3. In contrast, the Josephson junction has no limitations on tuning speed beyond the driving circuitry, requires small voltage excursions, and is perfectly linear.

7.4 Tuning Bandwidth

Tuning bandwidth for conventional tunable sources is limited by two factors, the active semiconductor device itself, and by the varactor and associated circuitry. The use of Gunn devices with varactor diodes now permits octave tuning bandwidths which may be extendable to a decade at the expense of set-on accuracy. IMPATT devices and

varactors are currently limited to 35% tunable bandwidth and are not expected to ever reach the octave range. In contrast, the JJ devices have no theoretical limits from DC to the characteristic frequency (~1000 GHz). In practice, large tunnel junctions with self resonant internal structures have kept tunable bandwidths from exceeding the octave range. However, point contact junctions and some arrays of proximity bridges have been tuned from audio to EHF frequencies.

7.5 Settling Time

Settling time for the conventional varactor tuned oscillator is largely dependent upon the various time constants of the associated linearizing circuitry and to a lesser extent on the thermal characteristics of the active device. Minimum settling time is obtained at the expense of maximum modulation bandwidth. Typical settling time (to within 1% of final frequency) is 1.5 microseconds for an across-the-band change of frequency. Doubling the modulation bandwidth typically increases settling time by a factor of three. In contrast, a JJ device is limited only by the characteristics of the input signal and the coupling network.

7.6 Post-Tuning Drift

Once a linearized VCO approaches its intended frequency, thermal time constants of critical components cause a shift of output frequency. This shift is determined mostly by the base-emitter currents creating the breakpoint positions of the piecewise linearizing process. One millisecond thermal time constants are typical. Similar time constants accrue from the varactor and the active semiconductor device. In contrast, the JJ should have no post-tuning drift.

7.7 FM Noise

Without a linearizer (i.e., best case), conventional VCO FM noise 25 kHz from the carrier frequency is typically 30 dB down, increasing logarithmically toward the carrier frequency. The addition of a linearizer generally increases the noise level by 10 dB. This is typical for a 4-8 GHz Gunn-varactor device. Impact-varactor and FET-varactor (preliminary results) are worse. In contrast, the theoretical linewidth of a JJ voltage-biased oscillator is $4.05 \times 10^{7} R_o T$ Hz at any carrier frequency, where R_o is the source resistance and T the temperature. R_o can be as low as $10^{-6}\Omega$ in the voltage-biased mode. In the current bias mode the JJ linewidth increases as R becomes the

junction shunt resistance. In all fairness it must be stated that JJ sources will require cooled FET amplifiers which add noise powers of

$$P_N = 4kTB \approx 3.3 \times 10^{-21} B \text{ watts} , \qquad (7.4)$$

where B is bandwidth in hertz.

7.8 Modulation Sensitivity

Because of the nonlinear modulation input impedance of varactors and the step discontinuities of associated linearizing circuitry, conventional VCO modulation sensitivity of 5 GHz/microsecond/volt can be achieved with less than 0.5% nonlinearity for octave units and less than 0.1% nonlinearity for 10% bandwidth units. The nonlinearity can be expected to be improved by a factor of 3 within 5 years, but tuning speed can only be improved at the expense of set-on accuracy and overshoot. In contrast, JJ tuning sensitivity is 483.594 MHz/microvolt with no theoretical limit on speed.

7.9 Output Level

Power output levels of bipolar transistor-varactor VCOs can be several volts into 50 ohms at frequencies below 1 GHz. Gunn diode-varactor VCOs operating in the 3-35 GHz spectrum generally exhibit output powers in the few hundreds of mW range while IMPATT-varactor VCOs exhibit several watts at 3 GHz and 10 mW at 225 GHz. FET-varactor VCOs exhibit power levels similar to Gunn devices. A single Josephson junction, in contrast is a low power device. The maximum power available is $I_c \Phi_o f$, which is $2 \times 10^{-19} f$ for a critical current of 100 μA. Thus at 10 GHz the theoretical limit is 10^{-9} W. Values approaching 10% of theoretical have been achieved, but 1% is more typical. With an array of 1000 such devices output power is still below a microwatt. Clearly an FET amplifier is needed in conjunction with the JJ oscillator. Although IMPATT-varactor and Gunn-varactor VCOs are an established art, 3 dB improvements in output power within 5 years are envisioned. FET-varactor VCOs are embryonic and 7 dB power output improvements are envisioned within 5 years. We can expect to achieve $\sim$50% of the available power in a single junction by optimizing the impedance matching network with a further increase from multiple junctions arrays within 5 years.

7.10 Noise Background Level

Conventional VCOs exhibit a noise floor 70 dB below the carrier at 5 MHz from the carrier. For a 200 mW device, the noise power floor is

$$T_N = 10^{-7} P_c / 4kB \qquad (7.5)$$

At 10 kHz from the carrier, noise power is 20 dB below the carrier and $T_N \sim 3.6 \times 10^{14}$K. In contrast, the noise power floor of the JJ VCO is essentially the operating temperature. If one uses a cooled FET following the JJ, this will be increased to about 60 K.

7.11 Efficiency

IMPATT-varactor VCOs typically exhibit power efficiencies up to 35% in the lower SHF spectrum, diminishing to a few percent in the middle of the EHF spectrum. Gunn-varactor VCOs are generally lower by a factor of two. FET-varactors should be capable of 30% efficiency through 30 GHz. JJ VCOs are typically $\lesssim$1% efficient, but there is no theoretical reason why this efficiency cannot be significantly improved--to $\sim$50%.

7.12 Summary

JJ VCOs exhibit tuning sensitivities 10^5 times greater than those of conventional VCOs. This ratio is not expected to change to any significant extent. The JJ phase noise and phase noise floor is also better than conventional devices by factors of 10^6 or more. Josephson junctions are significantly better than conventional VCOs in all respects except for power and efficiency. We can expect further improvement in power output, but only to the microwatt level. Their poor efficiency at this power level is not a major consideration since the major power consumption and production will have to be accomplished with FET amplifiers or other non-SCE devices. However the low phase noise and low noise floor present advantages for covert systems.

8. SUPERCONDUCTING-CAVITY CONTROLLED OSCILLATORS

8.1 Measures of Frequency Stability

The existence of very high Q ($\sim 10^{11}$) superconducting microwave-frequency resonators makes possible signal sources of very high spectral purity and frequency stability. Before describing what has been and may be achieved with such sources, it seems useful to define suitable measures of frequency stability.

Despite the long history of interest in the stability and purity of RF sources, only recently have well defined measures of frequency stability been proposed for universal use. The following is a selection of pertinent material from Barnes, et al. [1971].

Consider an instantaneous voltage signal

$$V(t) = \left[V_o + \varepsilon(t)\right] \sin\left[2\pi\nu_o t + \phi(t)\right] . \tag{8.1}$$

V_o and ν_o are the nominal amplitude and frequency, and $\varepsilon(t)$ and $\phi(t)$ are fluctuating quantities, assumed small. The signal phase is

$$\Phi(t) \equiv 2\pi\nu_o t + \phi(t) \tag{8.2}$$

and the instantaneous frequency is defined by

$$\nu(t) \equiv \frac{1}{2\pi}\frac{d\Phi(t)}{dt} = \nu_o + \frac{1}{2\pi}\frac{d\phi(t)}{dt} . \tag{8.3}$$

For present purposes the spectral density $S_g(f)$ of any pure real function $g(t)$ represents the one-sided Fourier amplitude at positive Fourier frequency f of the "power" $g^2(t)$, normalized so that

$$\langle g^2(t)\rangle = \int_0^\infty S_g(f)df, \tag{8.4}$$

where the brackets represent an infinite time average.

The voltage spectral density or RF spectrum $S_V(f)$, although widely used, is not a good primary measure of frequency stability because amplitude fluctuations $\epsilon(t)$ contribute to $S_V(f)$ along with phase fluctuations $\phi(t)$, and because in many cases where $\epsilon(t)$ is negligible, $S_V(f)$ is nevertheless not uniquely related to frequency fluctuations.

Define y(t), the instantaneous fractional frequency deviation from the nominal frequency ν_o,

$$y(t) \equiv \frac{\nu(t) - \nu_o}{\nu_o} = \frac{1}{2\pi\nu_o} \frac{d\phi(t)}{dt} . \tag{8.5}$$

A useful measure of frequency stability is then the spectral density of y(t), $S_y(f)$. One may also use the spectral density of the phase fluctuations $\phi(t)$, $S_\phi(f)$. These two spectral densities are related by

$$S_y(f) = \left(\frac{f}{\nu_o}\right)^2 S_\phi(f) . \tag{8.6}$$

In practice these frequency-domain measures of frequency stability are most readily determined in the high-frequency region of the spectrum.

Consider now the quantity

$$\bar{y}_k \equiv \frac{1}{\tau} \int_{t_k}^{t_k+\tau} y(t)dt = \frac{\phi(t_k+\tau) - \phi(t_k)}{2\pi\nu_o\tau} . \tag{8.7}$$

If one imagines a repetitive determination of $\bar{y}$ at intervals $T > \tau$, i.e., over periods of duration τ beginning at times $t_{k+1} = t_k + T$, $k = 0,1,2,3,\ldots N$, then one might define a second measure of frequency stability as the N-sample variance

$$\left\langle \sigma_y^2(N,T,\tau) \right\rangle = \left\langle \frac{1}{N-1} \sum_{n=1}^{N} \left(\bar{y}_n - \frac{1}{N} \sum_{k=1}^{N} \bar{y}_k\right)^2 \right\rangle \tag{8.8}$$

where again the brackets denote an infinite time average. Unfortunately, in practice many noise sources have very substantial fractions of the total noise power in the very low

Fourier frequency region (sometimes $<$ one cycle per year $\cong 3 \times 10^{-8}$ Hz). For such sources, any attempt to implement Eq. (8.8) experimentally is likely to yield results which depend more on the experimenter's stamina than on any meaningful characteristic of the system being studied. Therefore, the proposed second measure of frequency stability is the special case of Eq. (8.8) corresponding to N=2 (two samples) and T=τ (no dead time between samples),

$$\left\langle \sigma_y^2 \ (2,\tau,\tau) \right\rangle \equiv \sigma_y^2(\tau) \ = (1/2)\left\langle (\bar{y}_{k+1} - \bar{y}_k)^2 \right\rangle \ . \tag{8.9}$$

This is the Allan variance. It is the time-domain measure of frequency stability most suitable for long times and low frequencies. In practice, the unattainable infinite time average of Equation (8.9) is replaced by the estimate

$$\sigma_y^2(\tau) \cong \frac{1}{2m} \sum_{k=1}^{m} (\bar{y}_{k+1} - \bar{y}_k)^2 \ . \tag{8.10}$$

One may define a similar variance for the phase, but this appears not to be commonly used.

These frequency-domain and time-domain measures of frequency stability are, of course, related. Barnes, et al. [1971] give a formula by which $\left\langle \sigma_y^2(N,T,\tau) \right\rangle$ may be calculated, given $S_y(f)$. No simple prescription for the reverse translation is available in the general case. For a power-law spectral density of the form $S_y(f) = h_\alpha f^\alpha$ (h_α = a constant), $\left\langle \sigma_y^2(N,T,\tau) \right\rangle$ is convergent without any high or low frequency cutoffs on $S_y(f)$ for $-3 < \alpha < 1$ (note the absence of equality signs here). For $\alpha \geq 1$, a high-frequency cutoff is necessary for convergence.

A widely useful model consists of five independent noise processes $y_n(t)$, n = -2, -1, 0, 1, 2, so that

$$y(t) \ = \sum_{n=-2}^{2} y_n(t) \ . \tag{8.11}$$

Associated with each noise process is a power-law spectral density

$$S_{yn}(f) = \begin{cases} h_n f^n & ; \ 0 \leq f \leq f_n \\ 0 & ; \ f > f_n \end{cases} . \qquad (8.12)$$

As noted above, the high-frequency cutoff frequency is not essential for $n = -2$, -1, and 0. Each $y_n(t)$ contributes independently to $S_y(f)$ and to $\langle\sigma_y^2(N, T, \tau)\rangle$ or $\sigma_y^2(\tau)$. Barnes, et al. [1971] contains a large tabulation of relations from which the useful set given in Table 8-1 may be extracted. Ordinarily not all five types of noise contained in the model will actually appear in a given system.

Note that the dependence of $\sigma_y^2(\tau)$ on the cutoff frequency of the spectral density for the last two types of noise listed in Table 8-1 means that any experimental measurement of $\sigma_y^2(\tau)$ must include a specification of the bandwidth of the measuring system used.

A final point concerns long-term frequency drift. A system may display drift due to systematic sources. Such drift is deterministic and, strictly speaking, not subject to statistical analysis. Nevertheless, straightforward application of Equation (8.10) will yield a drift-associated "Allan variance." If the drift is linear at rate c_1, $y(t) = c_1 t$, this pseudo-Allan-variance is

$$\sigma_y^2(\tau) = \frac{c_1^2 \tau^2}{2} . \qquad (8.13)$$

8.2 Devices

The state-of-the-art of superconducting-cavity controlled oscillators is represented by an ensemble of three oscillators developed by J. P. Turneaure and S. R. Stein at Stanford [Stein and Turneaure, 1972, 1973, 1974, 1975, Stein 1974]. These use three niobium cavities with loaded quality factors Q_L ranging from 1.1×10^9 to 1.2×10^{10} (the unloaded Q's range from 2.5×10^9 to 4.7×10^{10}) to control the frequencies of Gunn-effect oscillators at nominal frequency and power of 8.6 GHz and 50 mW. These

Table 8-1

Five Principal Independent Noise Processes

Noise Type	$S_{yn}(f)\left[Hz^{-1}\right]$	$S_{\phi n}(f)\left[rad^2 Hz^{-1}\right]$	$\sigma_y^2(\tau)$
Random walk frequency	$h_{-2}f^{-2}$	$h_{-2}\nu_o^2 f^{-4}$	$\frac{(2\pi)^2}{6}h_{-2}\tau$
Flicker or 1/f frequency	$h_{-1}f^{-1}$	$h_{-1}\nu_o^2 f^{-3}$	$2 \ln 2 \, h_{-1}$
White frequency (random walk phase)	h_o	$h_o\nu_o^2 f^{-2}$	$\frac{h_o}{2}\tau^{-1}$
Flicker or 1/f phase	$h_1 f$	$h_1\nu_o^2 f^{-1}$	$\frac{h_1\tau^{-2}}{(2\pi)^2}\left\{3\left[2+\ln(2\pi f_h\tau)\right] \atop -\ln 2\right\}$
White phase	$h_2 f^2$	$h_2\nu_o^2$	$\frac{3h_2 f_h \tau^{-2}}{(2\pi)^2}$

"passive" frequency sources we called SCSOs, for Superconducting-Cavity Stabilized Oscillator. Studies of the frequency stability of these SCSOs have been made by intercomparing them (short-term fluctuations) and by comparing them with an ensemble of cesium frequency standards (long-term fluctuations and drift). It should be noted that the Cs standard's frequency is based on an atomic frequency, in fact the frequency which defines the second. The Cs standard therefore has both precision and accuracy. The SCSO's frequency is based on a physical artifact so that the SCSO has precision but no accuracy. The frequency stability of the SCSO is summarized in Fig. 8.1 (Allan variance) and Fig. 8.2 (spectral density of the phase).

Consider first the curve labeled "8.6 GHz SCSO (ACHIEVED)" in Fig. 8.1. This curve represents the performance actually achieved to date. For sampling times between about 10 sec and 5×10^3 sec there is a τ-independent "floor" in the Allan variance due to flicker or 1/f noise in the frequency. The floor shown at 6×10^{-16} has not been lowered since measurements taken in 1974 [Stein and Turneaure, 1975]. However, there is experimental evidence that this flicker noise floor is inversely proportional to the cavity Q and indirect evidence that the noise floor of the highest Q SCSO is about 3×10^{-16} [Turneaure, private communication]. The unloaded Q's of all three SCSOs will be increased to $\sim 1 \times 10^{11}$ and this is expected to push the flicker noise floor down to the 1×10^{-16} level shown on the curve labeled "8.6 GHz SCSO (EXPECTED)."

At sampling times above about 5×10^3 sec the Allan variance is dominated by a long-term drift which will be discussed below. The (ACHIEVED) curve corresponds to a recently achieved [Turneaure, private communication] typical drift rate of 1.5×10^{-14}/day. The smallest drift rate observed to date for one of the SCSOs is 0.5×10^{-14}/day. The τ-proportional part of the (EXPECTED) curve follows from Turneaure's belief that a drift rate of 1×10^{-15}/day is "quite likely."

The τ^{-1} proportional part of $\sigma_y(\tau)$ is associated with the white phase noise part of $S_\phi(f)$ (see Fig. 8.2). $S_\phi(f)$ also contains a number of relatively narrow intense peaks which result from mechanical vibration modes of the system. A narrow peak in $S_\phi(f)$ also makes a contribution to $\sigma_y(\tau)$ which is proportional to τ^{-1}. Reduction of vibration is believed to have accounted for a twenty-fold reduction in this part of $\sigma_y(\tau)$ achieved between 1974 and 1975. It is believed by Turneaure that the vibration peaks in $S_\phi(f)$ can be further reduced, lowering $\sigma_y(\tau)$ in the low-τ region to the $1 \times 10^{-15}\tau^{-1}$ level shown on the (EXPECTED) curve. The curve labeled "8.6 GHz SCSO

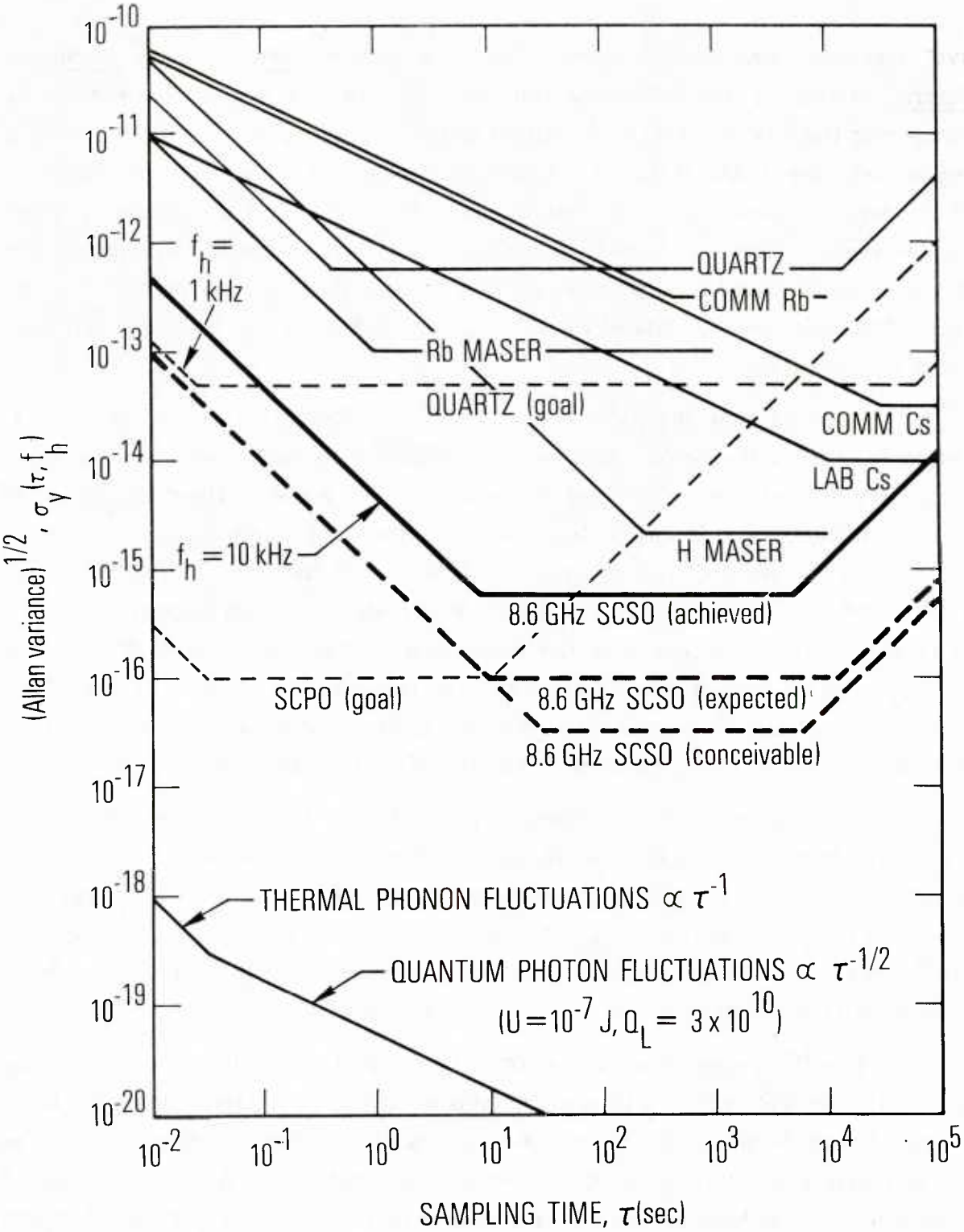

Figure 8.1

Comparative stability of various frequency standards and SC cavity oscillators a measured by the Allan variance.

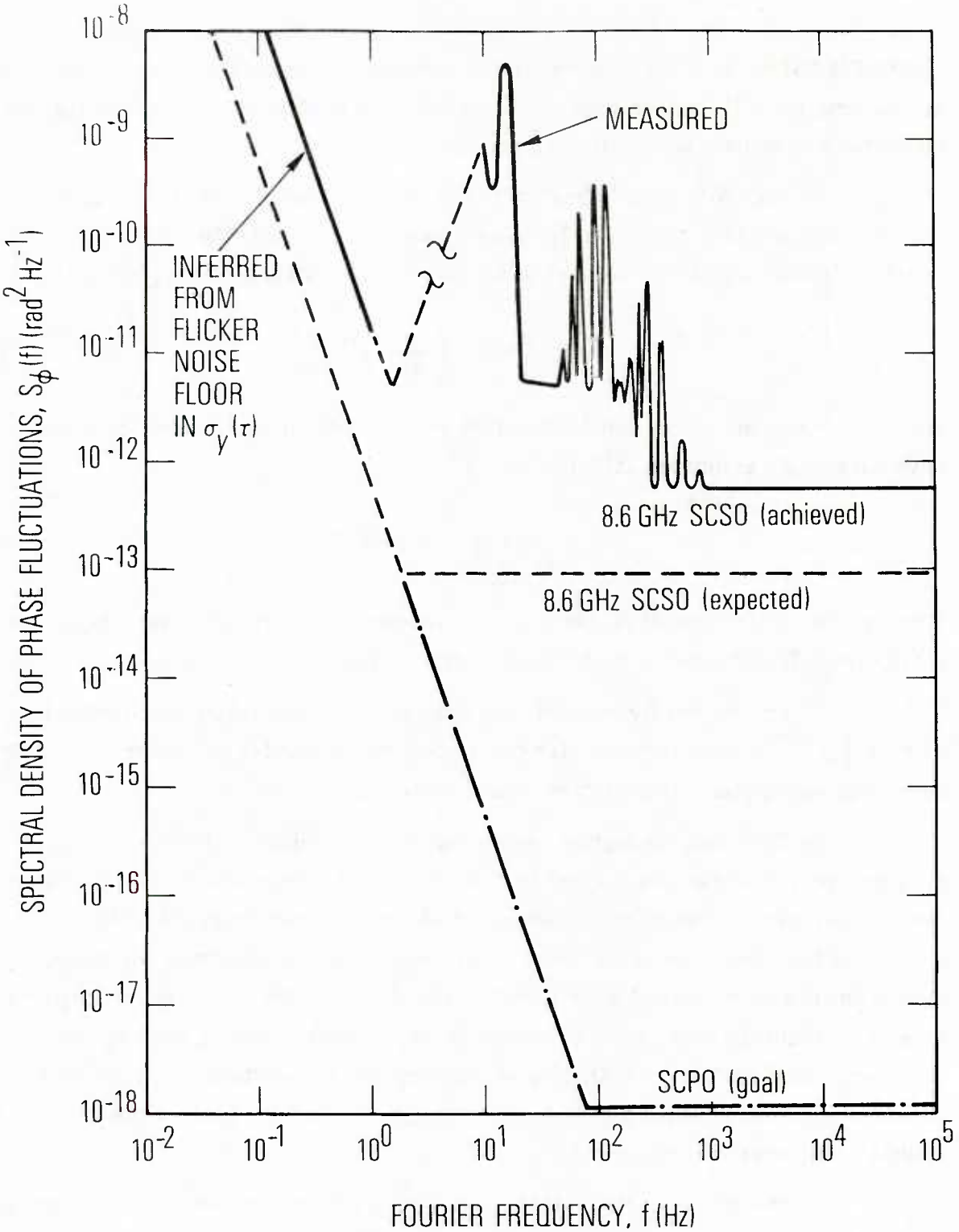

Figure 8.2

Spectral density of phase fluctuations for SC cavity stabilized oscillator.

(CONCEIVABLE)" is a more speculative projection by Turneaure of what may be possible in the long term if further improvements occur in ability to split the cavity resonance, understanding of long-term drift sources, etc.

Fig. 8.1 also indicates the nature of two fundamental limits on SCSO performance and of competitive frequency sources. At the bottom are limits imposed by quantum fluctuations in the number of photons in the cavity, given by [Stein, 1974]

$$\sigma_y(\tau) \cong \left(\frac{\pi}{Q_L U}\right)\tau^{-\frac{1}{2}} \tag{8.14}$$

and by dimensional noise due to quantum fluctuations in the number of phonons in the cavity material, estimated at [Stein, 1974]

$$\sigma_y(\tau) \cong 1 \times 10^{-20}\tau^{-1} \tag{8.15}$$

Clearly the performance of present and projected superconducting cavity controlled oscillators falls far short of these fundamental limits.

The curves for competitive sources have been taken uncritically from Fig. 1 of Stein [1974], except for those for quartz oscillators and for the superconducting cavity parametric oscillator. These latter require some explanation.

The superconducting cavity parametric oscillator (SCPO) is being developed by a group at NBS Boulder headed by S.R. Stein. This development is motivated by the need for a source of extremely high spectral purity (short-term stability) which can be multiplied into the infrared and even visible regions of the spectrum for direct frequency measurements of stabilized laser signals. The design of the SCPO is being optimized for minimum frequency noise in short sample times, at the expense of the long-term stability. The curve labeled "SCPO (GOAL)", which includes a long-term drift rising out of the flicker-noise floor at about 10 sec sample time, illustrates the current design goals for the SCPO [Stein, private communication].

The curve labeled QUARTZ in Fig. 8.1 is intended to represent performance currently achieved with quartz oscillators and is a composite of data from several sources. The small-sampling-time region is from Bedard [private communication], the flicker-noise floor is from Stein [1974], and the long-term drift region corresponds to a drift of 5×10^{-12}/day quoted as typical good performance by F. Walls [private communication].

The curve labeled QUARTZ (GOAL) is meant to represent the probable result of current work at NBS and elsewhere which is aimed at pushing the performance of quartz oscillators up to the limits imposed by the properties of the quartz crystals themselves rather than the associated electronics. In the small τ region, the indicated $\sigma_y(\tau) = 2 \times 10^{-15}\tau^{-1}$ has not yet been achieved, but "appears possible" [Turneaure and Stein, 1976]. A flicker noise floor of 8×10^{-14} has been observed at NBS, and the indicated level of 5×10^{-14} seems a reasonable goal with better crystals; a level of 1×10^{-14} is "more than can be expected". The long-term drift part of the curve corresponds to a drift of 1×10^{-12}/week which may be expected within two years using SC-cut crystals [Turneaure and Stein, 1976].

The previous paragraph describes the parameters of quartz oscillators operating at room temperature. There is a Soviet report of quartz oscillator Q's of 10^9 at cryogenic temperatures. A typical room temperature Q is 2.5×10^6. Operation at cryogenic temperatures might reduce many of the noise sources which limit the performance of quartz oscillators for the same reasons as it enhances the performance of superconducting cavity controlled oscillators. It is interesting to speculate how the performance of a quartz oscillator optimized for operation at helium temperatures might compare with the performance of a SCSO operating at the same temperature.

Figure 8.2 shows the spectral density of phase fluctuations corresponding to the SCSO and SCPO curves of Fig. 8.1. In the region 10-10^3 Hz there are peaks due to mechanical vibration modes of the system. The observed high frequency floor of $S_\phi(f)$ at 7×10^{-13} rad^2 Hz^{-1} corresponds to $\sigma_y(\tau) = 2.7 \times 10^{-15}\tau^{-1}$. Comparing this with the achieved level of $\sigma_y(\tau) = 5 \times 10^{-15}\tau^{-1}$, we see that about half of the observed small-τ $\sigma_y(\tau)$ may be due to these vibration peaks. The belief that they can be largely eliminated appears to account, at least in part, for the expected $\sigma_y(\tau) = 1 \times 10^{-15}\tau^{-1}$.

Since the cavity frequency is directly dependent on the size and shape of the cavity, there are many environmental factors which can cause frequency offsets or noise. These include:

1. Temperature changes alter the physical dimensions of the cavity via thermal expansion and the electrical dimensions via the temperature dependence of the surface resistance. The rates for the present SCSO are

$$\frac{1}{\nu_o}\frac{d\nu_o}{dT} = \begin{cases} 1 \times 10^{-9} K^{-1} & \text{at 1.4 K} \\ 1 \times 10^{-10} K^{-1} & \text{at 1.1 K} \end{cases} . \qquad (8.16)$$

The temperature is currently stabilized to about 10^{-5}K. This could be improved by an order or magnitude if necessary.

2. The frequency varies linearly with stored energy U due to electromagnetic radiation pressure and residual nonlinearity of the surface reactance. The rate is

$$\frac{1}{\nu_o}\frac{d\nu_o}{dU} \cong 2.5 \times 10^{-4} \text{ per joule} . \qquad (8.17)$$

The resulting fractional frequency offset is typically [Turneaure and Stein, 1976]

$$\frac{\delta\nu_o}{\nu_o} \cong (-2 \pm 1) \times 10^{-12} . \qquad (8.18)$$

3. Strain in the cavity or in nearby parts of the system due to the gravitational field or other accelerations may change the size or shape of the cavity. The estimated rate is:

$$\frac{1}{\nu_o}\frac{d\nu_o}{dg} \cong (10^{-8} - 10^{-9})\, g^{-1} . \qquad (8.19)$$

This effect also is manifested in a dependence of the cavity frequency on tilt of the mounting plate from which it is suspended, with a rate

$$\frac{1}{\nu_o}\frac{d\nu_o}{d\theta} \cong 1 \times 10^{-14} (\text{arc sec})^{-1} . \qquad (8.20)$$

4. Penetrating radiation may cause radiation-damage-induced changes in the volume of the cavity material.

5. Slow creep of the cavity material due to steady stress, or stress relaxation induced by mechanical vibration may change the cavity size or shape. There is some indication that reduction of mechanical vibration in the present SCSOs, intended primarily to reduce $\sigma_y(\tau)$ for small τ, has also decreased the long-term drift rate, suggesting that vibration induced stress relaxation does occur.

8.3 Future Directions

A great many questions must be answered before the SCSO can be properly evaluated for military application such as the GPS clock (see Section 16.2). These can only be answered by further research and development of the SCSO, with particular attention to the factors which limit its long-term stability. As noted above, there is evidence that the long-term drift of the SCSO is due at least in part to vibration-induced stress relaxation. The choice of Nb as the material for the present SCSO cavities was dictated in part by the fact that the necessary technology had already been developed and was in hand. Other materials, however, may be less subject to the mechanical vibration associated problems which appear to be the major limitation of the present SCSO in both the short term and long term. For example, single crystal silicon and sapphire of very high perfection are available, and should be subject to less stress relaxation. Silicon, in particular, can be obtained essentially dislocation-free. Another feature of these materials is that they have substantially smaller thermal-expansion coefficients than Nb at helium temperatures. It should be possible to construct high-Q cavities from sapphire or silicon by coating the material with a superconducting film. This could be Nb, but other materials should be considered as well. (Work reported at the 1976 Applied Superconductivity Conference suggests that Nb_3Sn may be a better superconductor for high-Q cavities than Nb.)

The mechanical structure of the cavity and its mounting should be optimized to minimize mechanical vibration and stress due to gravity or to other accelerations. This would be especially important in the space application where mechanical noise from on-board electromechanical devices and accelerations due to orientation and stabilization thrusters might be present. Also the possible use of SCE elements in the electronic circuitry could produce significant improvement in performance.

Research and development of the SCSO should be continued, with particular attention to those factors which limit its long term frequency stability. This R&D should include investigation of alternative materials and designs. Consideration should be given to the initiation of development of a prototype SCSO system suitable for satellite use, as a vehicle for study of the problems which would arise in such an application.

9. ANALOG INSTRUMENTATION

In this section we describe superconducting technology which can be applied to analog instrumentation for the precise and accurate measurement of basic electromagnetic quantities.

9.1 RF Standards

The response of an RF biased SQUID to a magnetic flux with amplitude Φ alternating at frequency ω_s is proportional to $J_1(2\pi\Phi/\Phi_o)$, where J_1 is the ordinary Bessel function of order 1. The Bessel function periodicity in the response is readily observable even when the SQUID readout system is unable to follow the signal oscillation itself. If the system signal-to-noise ratio is high enough to permit precise location of the response nulls corresponding to the zeroes of the Bessel function, the flux amplitude can be accurately determined in terms of the fundamental physical constant Φ_o. By comparing the flux produced by an RF current at frequency ω_s with the flux produced by an accurately measured DC or low frequency current, an accurate determination of the RF current can be made.

The potential of RF standards and calibration and measurement instrumentation based on SQUIDs is being explored at the National Bureau of Standards, Boulder [Kamper, et al. 1973, 1974] and at the National Physical Laboratory, Teddington, England. The advantages of such instruments include:

(1) RF Flux is measured in units of Φ_o, so that such instruments in effect automatically incorporate a primary standard.

(2) Inherent broad band operation.

(3) Sensitivity.

(4) Linearity.

(5) Relatively low cost.

The current state-of-the-art, projected performance, and the capability of competing technology may be summarized as follows:

9.1.1 RF Attenuation

RF attenuation has been measured up to about 100 MHz using an RF SQUID biased at 1 GHz. At 30 MHz, attenuation measurements made with such a SQUID agree to within 0.002 dB rms with the 30 MHz national standard of attenuation. The latter is a carefully made and maintained physical object, with estimated systematic errors which are considerably larger than 0.002 dB. The SQUID instrument thus may well be more accurate than the national standard, as expected, but there is no way to prove it. In the present instrument the Bessel function zeroes can be reset with a precision of 10^{-3} of the zero separation. However, estimated systematic errors are at the level of several milli-dB. It should be possible to reduce these significantly and provide an absolute accuracy of RF attenuation measurement better than 0.001 dB.

The dynamic range of the present instrument is 60 dB, corresponding to a range of 900 Bessel function zeroes or flux quanta per signal period, at maximum amplitude. If necessary, this dynamic range can be increased.

9.1.2 RF power

For RF power measurement, sensitivity becomes the most important factor once an accuracy level of $\pm$ 0.1 dB is achieved. At this level conventional instrumentation is limited to powers above -35 dBm. Using a SQUID an accuracy of $\pm$ 0.1 dB can be maintained down to power levels of -140 dBm. Such sensitivity coupled with accuracy is a significant advantage in evaluating the performance of sensitive receivers.

The above data are derived from NBS experience with a SQUID biased at 1 GHz. It appears that such a SQUID will function properly up to signal frequencies of about 0.1 times the bias frequency. The National Physical Laboratory is currently investigating the use of a SQUID biased at 10 GHz, which should operate at signal frequencies up to 1 GHz. NBS is considering a double junction DC-biased SQUID which is self-pumped at the Josephson frequency and should be usable at signal frequencies up to $\sim$100 GHz.

9.2 Direct Current Comparator

If a current is made to flow in a wire surrounded by a superconducting tube, flux conservation requires that a current of exactly the same magnitude but opposite in

direction be induced on the inner surface of the tube, and a current of exactly the same magnitude and the same direction on the outer surface of the tube. The distribution of the current on the outer surface of the tube is independent of the location of the source wire inside the tube. This current will of course create a magnetic field outside the tube. If another current flows in another wire inside the tube in a direcion opposite to the first, the induced field outside the tube will be zero if and only if the two currents are exactly equal in magnitude. This provides the basis for precision comparison of direct currents, for establishment of accurate current ratios, and hence of accurate resistance ratios. A ratio precision of 1×10^{-10} is readily available. Using a SQUID magnetometer to detect the field null outside the tube, a resolution of 1.5×10^{-9} ampere-turns has been achieved. If needed, this precision and sensitivity could be somewhat improved. Applications include the calibration of precision resistive ratio dividers, e.g., for the Josephson voltage standard (see below), and the comparision of high resistance resistors where self-heating effects are a problem.

The best available conventional instrument is the so-called Custers current comparator. This is an AC device which depends on precision-wound ratio transformers and is commercially available. Its precision and sensitivity are two-to-three orders of magnitude worse than the superconducting current comparator.

9.3 Josephson Voltage Standard

For completeness, we note that since 1973 the U.S. legal volt V_{NBS} has been defined through the relation

$$\frac{2e}{h} = 4.83593420 \times 10^{14}\ \mathrm{Hz}/V_{NBS}$$

DC voltages can be determined in terms of V_{NBS} and the AC Josephson effect with an accuracy of $1\text{-}2 \times 10^{-8}$. Voltage comparisons using electrochemical standard cells have accuracies at least an order of magnitude less.

10. PASSIVE MICROWAVE/MILLIMETER WAVE COMPONENTS

One advantage of superconductivity in microwave/millimeter wave systems arises from its best known property, low electrical loss. As the operating frequency of electronic systems is increased through the microwave and millimeter wave region, electrical losses in the various circuit elements and transmission lines increase, contributing to significant degradation in system performance in two important ways. First, in signal generating and transmitting systems, loss wastes transmitter power and must be compensated for by higher power or reduced margins. Frequently this lowers lifetime and reliability. Second, in receiving and signal processing systems, loss both reduces available signal power and increases system noise. Furthermore, the available power from microwave sources tends to decrease as f^{-2}, exaggerating the problem in millimeter wave systems.

The attenuation of conventional waveguides at 300 K ranges from about 0.01 dB/ft for brass waveguide at 3 GHz to 0.2 dB/ft for brass guide at 36 GHz, and is approximately 0.6 dB/ft for silver waveguide operating in the 90 to 100 GHz region. This increase in attenuation in air-filled waveguide is associated with the increase of surface resistance of normal conductors which varies $f^{\frac{1}{2}}$. Cooling metals to cryogenic temperatures (but in the normal state) may reduce their surface resistances by one or two orders of magnitude (Fig. 10.1). However, when materials are cooled below their superconducting transition temperatures, there is a very dramatic decrease in ohmic losses. It is well known that at DC the resistance of a superconductor is at least 15 orders of magnitude smaller than that of copper at 300 K. However, at radio frequencies and above ohmic losses are measurable. At temperatures well below T_c and for frequencies much less than the gap frequency, surface (conductivity) losses vary as f^2. (See Eq. (2.6) and Fig. 10.1.) For example, at 1 GHz losses in a superconductor are about four orders of magnitude less than in copper at 300 K. With increasing frequency, the ratio of the surface losses in a normal metal to that of a superconductor become progressively smaller, such that above the gap frequency they are essentially equal. From inspection of the curves in Figure 10.1, the ratio at 36 GHz should be of the order of 200. Danielson [1973] obtained a value of surface resistance of 2×10^{-4} ohms for lead at 4.2 K using a TE_{011} cylindrical cavity and a ratio of 400 between a copper and lead cavity, both values in good agreement with Figure 10.1. Thus, in 100 GHz niobium waveguide attenuation should be reduced by approximately 10^2, to about 0.01 dB/ft. Further reduction in surface losses may be

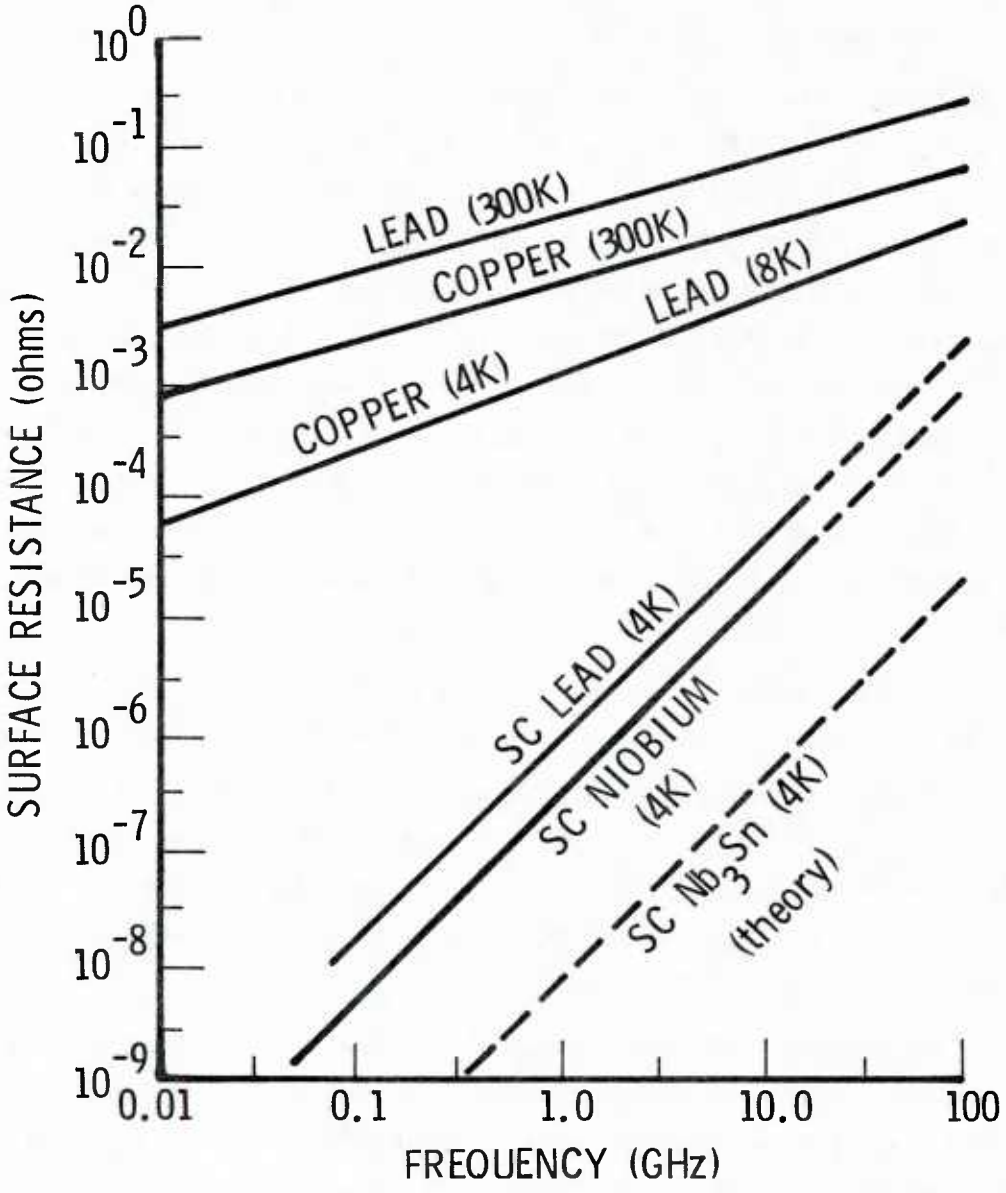

Figure 10.1

The microwave surface resistance of superconducting lead, niobium, and niobium-tin (Nb_3Sn) at 4 K. The solid lines represent experimental data, while the dashed lines are linear extrapolations. For comparison, the values for normal copper and lead are given at cryogenic and room temperature. [Hartwig and Passow, 1975].

realized with the use of Nb_3Sn which has a theoretical value of surface resistance at 4 K which is about a factor of 100 smaller than that of niobium. Initial studies at 3 and 10 GHz have given experimental values of surface resistance within a factor of 2 of the theoretical value. However, the preparation and surface condition problems involved with this material must be studied in greater detail before it can be considered for microwave and millimeter transmission lines.

The present trend toward microwave integrated circuits requires the use of thick film stripline and microstrip. For this type of circuit element, loss in the dielectric material on which the film is deposited must also be considered as well as the radiation losses resulting from the "open" nature of these components. The latter can be controlled by the use of either ground planes or shield cans. Information on dielectric losses, usually measured in terms of a "loss tangent", of materials at low temperature and microwave frequencies are scarce, but the reported values [Hartwig and Passow, 1965] of the loss tangent for materials such as teflon, quartz, alumina, lucalox, etc. tend to be in the range of 10^{-6} to 10^{-4}; the lowest reported value is that of single crystal sapphire (Al_2O_3) which is about 2×10^{-7}. Since liquid helium is likely to be in the vicinity of such components, we note that Hartwig and Grissom [1975] have reported that the loss tangent for liquid helium is less than 10^{-10}, and thus can be neglected in most devices.

The effect of these dielectric losses on simple configurations such as cavities and other resonant structures can be calculated in a fairly straightforward manner. In this case a dielectric loss factor can be defined as $(Q_{diel})^{-1} = \alpha \tan \delta$, where α is the filling factor (usually of the order of unity when the cavity is filled with the dielectric under consideration). Thus a superconducting cavity that is dielectrically loaded with single crystal sapphire will have a limiting Q of the order of 10^7 while an air-filled or liquid helium filled cavity will have Q's approaching 10^{10}.

There is very little published literature on superconducting stripline and/or microstrip filters and resonators. DiNardo, et al.[1971] have made microstrip resonators using lead deposited on lucalox. The loss tangent for lucalox is reported to be 1.4×10^{-6} at 4 K for frequencies near 10 GHz. A ring microstrip resonator at 14.3 GHz exhibited an unloaded Q of 2×10^5 at 4 K, consistent with a dielectric loss limited situation. Cooling to 1.8 K raised the unloaded Q value to 5×10^5.

It is not easy to make a general statement about the reduction in attenuation that might be realized with the use of superconducting materials in the fabrication of microstrip and/or stripline transmission lines. However, it is possible to estimate the improvement that might be obtained in the case of a specific configuration. For example, a 50 ohm stripline line fabricated with gold metallization on alumina (loss tangent of alumina is 6×10^{-4}) and operating at 10 GHz and 300 K has an attenuation of 5 dB/meter associated with surface resistance losses and 1.5 dB/meter from dielectric losses [Spielman, NRL, private communication]. Assuming that gold and copper have equal microwave surface losses, changing the metalization from gold to a superconductor can reduce surface losses by a factor of 10^3. Thus the superconducting loss will be of the order of 0.005 dB/meter. Using single crystal sapphire instead of alumina for the dielectric substrate material (loss tangent is 2×10^{-7}), the dielectric losses could be further decreased by a factor of 3×10^3 and thus would be of the order of 0.001 dB/meter. Hence, for this particular 10 GHz stripline configuration, attenuation losses can be reduced by a factor of 10^3 by fabricating the device from superconductor on single crystal sapphire and operating at 4 K as compared to a room temperature circuit made with gold metalization on alumina.

It is more difficult to estimate the improvement in stripline performance at 100 GHz that might be achieved using superconductor metalization. The surface resistance of niobium is about a factor of 80 smaller than that of copper (see Fig. 10.1). Assuming that there are materials with adequately small values of dielectric loss tangents at 100 GHz and 4 K, it will be possible to fabricate superconducting 50 ohm striplines that have attenuation losses 80 times smaller than a room temperature line with identical geometry.

10.1 Directions for Future Work

The very limited information on superconductive passive circuit elements operating at frequencies above 10 GHz indicates that reduction in attenuation of the order of 10^2 or greater should be achievable when compared to equivalent room temperature devices. Cooling to cryogenic temperatures just to reduce such losses is frequently not justified. However, when the active elements in the subsystem are also superconducting, such as Josephson and super-Schottky diodes, then the use of passive superconducting circuit elements clearly becomes desirable and will further improve the performance of the overall (sub)system.

Since thick film microstrip circuit technology and theory are well established disciplines, the development of superconductive thick film circuits elements can be fairly straightforward. However more data should be obtained about the dielectic loss tangent of commonly used substrate materials at frequencies above 10 GHz and at cryogenic temperatures. In addition, more exotic materials such as single crystal sapphire, dislocation-free silicon with intrinsic resistivity, etc. should be surveyed in order to establish the lower limit for values of loss tangent at microwave frequencies and cryogenic temperatures. It is desirable to fabricate superconducting thick film circuit elements using either lead or niobium metalization and eventually Nb_3Sn metalization. The secondary goal of this program should be to develop techniques in thick film technology to match the very low impedance of Josephson devices to conventional circuit elements.

11. REFRIGERATION

One of the most commonly raised issues, indeed the most frequently voiced objection to the use of superconducting electronics, is the requirement for cryogenic cooling. Because this is a vital support function and imposes a psychological as well as physical handicap on the acceptance and use of SCE it was included in this Study and is discussed here. This section is not intended to be a complete study of cryogenic cooling, but rather a review of the relevant status and an indicator of possible approaches to solution.

11.1 Thermodynamics

Elementary thermodynamics tells us that in order to refrigerate it is necessary to have a source of usable energy, either work W or heat Q_1 at an elevated temperature T_1, a heat sink at "ambient" temperature T_0, plus a mechanism for using the energy source to pump heat Q_2 out of a cold space at T_2 and dump it into the ambient sink. For present purposes it is useful to recall that the best possible performance (Carnot efficiency) of a refrigerator driven by work is

$$W/Q_2 = (T_0 - T_2)/T_2 \tag{11.1}$$

Ambient temperature T_0 is generally around 300 K (perhaps lower in interplanetary space), so W/Q_2 is unity if the cold space is at 150 K and about 100 if it is at 3 K. Small refrigerators are seldom more than 10% efficient, so that the actual ratios are of the order of 10 at 150 K and 1000 at 3 K [Strobridge, 1973]. For a refrigerator driven by heat Q_1 from a hot source at T_1, the best possible performance is given by

$$\frac{Q_1}{Q_2} = \frac{(T_0 - T_2)\,T_1}{(T_1 - T_0)\,T_2} \quad . \tag{11.2}$$

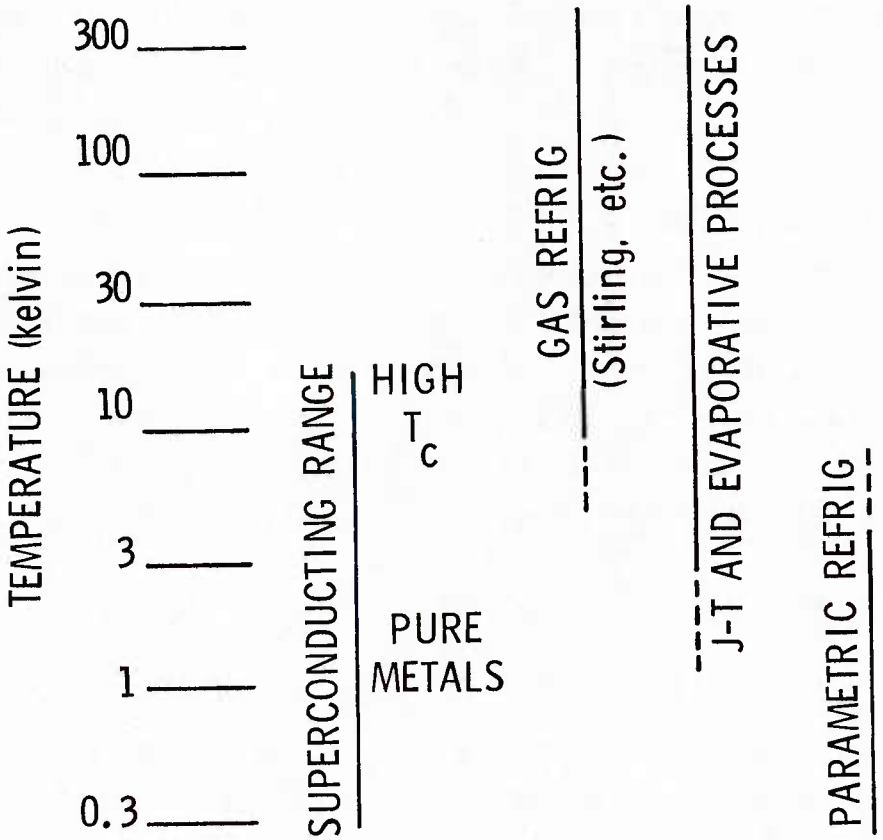

Figure 11.1

Temperature regions for current refrigeration methods. Lines show performance range of various processes relative to superconductivity. Dashed lines indicate marginal performance. Figure is a rough guide only. For example, a paramagnetic Stirling machine has been proposed to operate as high as 300 K. Other useful processes are: Peltier, paraelectricity, absorption, desorption, dilution, vortex tube, etc.

For example, if T_1 is 600 K and T_0 is 300 K, it requires at least 2 watts of heat from the hot source to pump 1 watt of heat out of a cold space at 150 K, or to pump 10 mW out of a cold space at 3 K. Again, real machines are inefficient, so these figures must be multiplied by an order of magnitude or more.

Many small SCE applications require only milliwatts or less of refrigeration at 4 K, so that even with inefficient refrigerators the power requirements may be quite modest. Unfortunately, thermodynamics provides no clue as to how best to design a refrigerator mechanism. A great many distinct mechanisms have been investigated, some of which bear no obvious relation to each other and are difficult even to classify, which leads to the suspicion that there may be useful effects as yet undiscovered.

Figure 11.1 schematically classifies current refrigeration between 300 K and SC temperatures. All current systems spanning this range refrigerate by expanding a conceptually-perfect gas, usually helium or hydrogen, against an external constraint such as a piston, or by expanding a real gas against its own inter-molecular forces (the Joule-Thompson process), or by a combination of both (as in the Collins machine).

Very few low-temperature (2-20K) refrigerators are in use at this time for operating SCE. A few have been used for operating masers at 4 K (the ADL "cryodyne"). Since our experience is heavily weighted toward evaporative cooling with liquid helium, our natural conservatism favors continuing this practice. On the other hand, there is a widespread recognition that if SCE is sufficiently useful to warrant the cryogenic investment, then the balance must shift toward self-contained closed-cycle refrigeration. A crude analogy may be the fact that no one now considers going back to an ice box in preference to an electric refrigerator no matter how infrequently one may need to add ice. Parenthetically, the household refrigerator is probably the most durable trouble free appliance currently available.

11.2 Evaporative Cooling and Closed-Cycle Refrigerators

The current state-of-the-art of cryogeneration for SC is primarily based on the use of helium in two distinctly different types of systems. The first, and by far the most widely used, is evaporative cooling using liquid helium which has been liquefied in some large central facility. The temperature can be controlled over a range of $\sim$1 to 5 K

by controlling the vapor pressure over the liquid. A variation of this technique is to continuously transfer liquid helium to the SCE package at a servo-controlled rate just sufficient to maintain the temperature at the required value. Controlled transfer is often used where temperatures above 5 K must be maintained.

The second system uses helium or other gases as working fluids in a refrigeration cycle involving compression with heat rejection at ambient temperature, and expansion with heat absorption at low temperature. Such systems are also used to liquify helium which may then be used for evaporative cooling of SCE. In a broad sense evaporative cooling is just one step in the complete refrigeration system. However from the viewpoint of a practical SCE user, the two sytems are distinctly different. The variations of compression-expansion machines are too numerous to mention even in outline. We briefly survey the most common types of machines, but it is unlikely that these machines are optimum with respect to any but a very restricted set of parameters.

An appropriate third category of cryogeneration systems is all those not included in the above description, e.g., para-electric, paramagnetic, and thermoelectric cooling. Then there are techniques and components which may be associated with gas refrigeration but which are sufficiently unique or promising to deserve separate mention, for example: the vortex tube, the absorption refrigerator, the "fluidyne" and similar engines, helical and spiral compressors, the hydrogen desorption compressor, and others.

A refrigerator design depends on how it is driven. For example if one operates an expansion engine on a cylinder of compressed gas the hot and the cold ends of the refrigerator are physically disconnected and remotely located from each other. This sort of operation may be quite practical for intermittent operation of SCE requiring very little refrigeration. For continuous operation a refrigerator should be a compact closed system consisting of a compressor and expander, a heat exchanger, and interconnection. Such refrigerators require a mechanical energy source such as an electric motor or a gasoline engine. However a vast reduction in mechanical complexity can be effected by utilizing the primary energy source (i.e., heat) to perform the compression and expansion in a much more direct way without all the mechanical paraphenalia of a conventional engine-driven refrigerator. Such a system is called Vuilleumier (VM) and has only two essential moving parts, neither of which are subject to large forces like those on a piston.

The essence of this discourse is that while a great number of refrigeration ideas, processes, components, and systems have been developed, there remains a great opportunity for innovation in producing a good refrigeration system for SCE. Such a device should span the gap betwen 300 K and SC temperatures and be portable, low-interference, versatile, reliable, and efficient.

The refrigeration capacity required by SCE may be estimated from experience with liquid helium evaporative coolers. The cryostat of Dinger et al. [1976] at NRL evaporates 1.8 liters/day from a dewar of 180 liter capacity (hold time of 102 days) and refrigerates several liters of SCE. The power input is about 60 mW; the rest of the refrigeration capacity of the helium gas as it warms to room temperature (about 4.2 W) is used to intercept heat conduction and radiation from the environment which would otherwise evaporate the contents in a rather short time.

These numbers indicate that rather small refrigeration capacity is required even for quite large volumes. In fact one has the flexibility to optimize the refrigeration capacity vs temperature. With evaporative cooling the refrigeration capacity vs temperature is fixed by the nature of the fluid and clearly cannot be optimized. Also a cryogenerator does not require a large liquid reservoir. The conclusion, therefore, is that the refrigeration requirements estimated from liquid helium cryostat performance may be quite conservative when applied to refrigerators.

If a helium dewar design could be scaled, the radiation heat input would be proportional to the surface area or the 2/3 power of the volume, and heat conduction would be proportional to the linear dimensions or the 1/3 power of the volume. Thus, if the NRL 180 liter dewar were scaled down by a factor of 64 to a volume of 2.8 liters, the evaporation rate should be between 0.11 and 0.45 liters/day depending upon the relative importance of conduction and radiation. Although small helium dewars have evaporation rates greater than 1/2 liter/day, these figures are of interest in connection with the design of efficient small refrigerators to cool volumes of a liter or so. An evaporation rate of 1 liter/day indicates a power input of about 35 mW at 4.2 K and a total heat input of about 2.5 W if the helium leaves the dewar at 300 K.

It is instructive to scale upward to see what is required for hold times of a year or more. If the volume is 8 times as large, 1440 liters, the evaporation rate should

increase by a factor of 2 to 4. The most optimistic estimate would, therefore, be a hold time of 400 days. Another factor of 8, or 11000 liters, would give an optimistic estimate of 4 years.

The issue of whether to use a liquid helium cryostat or a closed-cycle refrigerator is a complex one involving cost, availability of helium, duty cycle of use, reliability, requirements for angular flexibility, portability, shock resistance, user psychology, and possibly even such things as whether the instrument can be transported on passenger airplanes (liquid helium-filled vessels are presently prohibited). The present cost of liquid helium is $3 to $5 per liter, so the cost of operating a cryostat on a semi-continuous basis is of the order of thousands of dollars per year; the cost will probably go up as the supply of natural gas decreases. On the other hand one commercially-made small 4 K cryogenerator costs about $8000, but this price could drop by a large factor if most users stopped using liquid helium and used the cryogenerator instead. For example, the price of liquid helium dropped by a factor of 10 (in real money) between 1950 and 1970 as the market went from low volume to high volume.

A few users have experimented with a combined system by using a liquid helium cryostat for their SCE and a cryogenerator to cool a radiation shield and thereby reduce the evaporation rate to a low value. Such a system may in principle greatly reduce the operating budget for liquid helium, and this seems to be its main justification.

11.2.1 Stirling Machine

In this section we review the status of one promising type of machine, of which variations have been extensively developed for small-scale cryogeneration since 1960. This is the Stirling machine, which was invented in 1816 and then was practically ignored until after 1950. A readily available elementary review of Stirling refrigerators was written by J. Kohler [1965].

A Stirling machine has only two essential moving parts, a piston and a displacer, and no valves. It is probably the most efficient small gas refrigerator known for cryogenics and has been highly developed by N. V. Philips, Eindhoven. Commercial devices are now capable of reaching temperatures of 6 K with a few hundred watts input power, from which it is easy to obtain liquid helium temperatures with a J-T expansion stage on the lower end. An experimental low power non-magnetic Stirling

machine at NBS, Boulder has recently maintained 13 K for several thousand hours with approximately 10 W mechanical input power (which is projected to require 20 W input to an electric motor).

The Gifford-McMahon cryogenerator, which is made commerically by CTI and others, utilizes an essential element of the Stirling machine, the displacer, with a conventional valved compressor. It is less efficient than the Stirling machine but has the advantage for some purposes that the compressor can be mounted several meters away from the cold part.

Perhaps the most elegant of all gas refrigerators is the Vuilleumier machine. It may be described as two Stirling machines back-to-back, such that the two pistons can be omitted, and there are still only two essential moving parts. Heat is applied to one end of one displacer cylinder, and refrigeration is obtained at the end of the other displacer. Well engineered small VM machines developed by Hughes Aircraft have operated unattended approximately 10^4 hours with 2 kW heat input and have achieved temperatures below 6 K [Renyer, private communication]. Information on this and other developments can be found in Report AFFDL-TR-73-149, Vol. 1 (Proc. of the Cryogenic Cooler Conference, Dec. 1973).

All the above machines use crankshafts and connecting rods, or similar mechanisms, to drive the pistons and displacers so there are actually more than two moving parts. However, practical Stirling engines have in fact been reduced to two moving parts by using mechanical resonance and gas coupling to eliminate the crankshaft. There is no reason in principle why this idea could not be applied to Stirling refrigerators.

11.3 Peltier Cooling

Thermoelectric cooling using the Peltier effect is a recurring dream of cryogenic engineers. For an electrical couple in which one element is superconducting (so that its thermoelectric coefficients vanish), MacDonald, et al. [1959] showed that the maximum achievable temperature difference ΔT_{max} between hot and cold junctions is given by

$$\frac{\Delta T_{max}}{T_0} = \frac{S^2 T_0}{K\rho} \qquad (11.3)$$

where

T_0 = temperature of the cold junction,

S = absolute thermoelectric power of the non-superconducting member of the couple appropriately averaged over the temperature interval between the hot and cold junctions,

K = thermal conductivity, and

ρ = resistivity.

For a simple material which obeys the Wiedemann-Franz law,

$$L_o \equiv \frac{K\rho}{T} = \frac{\pi^2 k^2}{3e^2} = 2.44 \times 10^{-8}\ V^2 K^{-2}\ , \qquad (11.4)$$

this becomes

$$\frac{\Delta T_{max}}{T_0} = \frac{S^2}{L_o}\ . \qquad (11.5)$$

Although Peltier coolers are used near room temperature, the observed thermoelectric powers in the liquid helium region are $\lesssim 10\ \mu V K^{-1}$ and $\Delta T_{max}/T_0 \lesssim 4 \times 10^{-3}$. $K\rho/T$ for pure metals can be substantially smaller than L_o, but the low temperature thermoelectric powers are also small. $K\rho/T$ is generally greater than L_o for semi-conductors and low-conductive metals. Even if a material with much larger thermoelectric power were discovered, the large currents ($\sim$ amperes) required to drive a Peltier couple would be unacceptable in many applications. We therefore conclude that Peltier cooling is not a practical option for cooling cryoelectronic systems.

11.4 Heat Transfer to Liquid Helium

Although the total power dissipation in contemplated SCE systems is small, and the dissipation per element is small, there is a relatively high dissipation per unit area in certain proposed applications such as microwave oscillators and high speed latching computer logic. Hence it is relevant to inquire into the thermal transfer from the devices to the heat bath, liquid helium. Some pertinent parameters for ^{4}He are:

Normal boiling temperature at 1 atm pressure	T_o	=	4.2 K
Temperature of He_I - He_{II} transition on liquid-vapor coexistence curve	T_λ	=	2.18 K
Critical point temperature	T_c	=	5.20 K
Critical point pressure	P_c	=	2.26 atm
Melting pressure at T = 0 (essentially constant for $T < 2K$)	P_m	=	25 atm

There are two regimes of interest in considering heat transfer from a solid to liquid ^{4}He.

11.4.1 $T_{He} > T_\lambda$ (He_I)

The thermal conductivity of ^{4}He in the vicinity of T_o is about 2×10^{-4} W cm^{-1}K^{-1} and only weakly dependent on temperature and pressure. (This is approximately the value expected for an ideal classical gas with the specific heat and viscosity of He_I.) In a non-circulating helium bath at atmospheric pressure heat transfer from a heated solid at temperature T_s to liquid He_I at temperature T_{He} exhibits the following characteristics:

(a) For sufficiently small heat flux in an unconstricted geometry, cooling occurs by free convection. In this regime the heat flux J_q is approximately proportional to $\Delta T \equiv (T_s - T_{He})$ and the heat transfer coefficient is [Grassman and Karagounis, 1958]

$$\frac{J_q}{\Delta T} \approx 0.2\,(T_{He} - 2.2)\,\text{W cm}^{-2}\text{K}^{-1}. \qquad (11.6)$$

(b) At some threshold heat flux, nucleate boiling begins at the solid surface. ΔT at the threshold is [Grassman and Karagounis, 1958]

$$\Delta T_t \approx 0.5\,(4.2 - T_{He}) \qquad (11.7)$$

and the threshold heat flux is thus

$$J_{qt} \approx 0.1\,(4.2 - T_{He})\,(T_{He} - 2.2)\,. \qquad (11.8)$$

These approximate expressions for $J_q/\Delta T$ and ΔT_t should not be taken too seriously near T_λ and 4.2 K. It is probably fair to say [M. Jones (NBS), private communication] that the heat flux at the threshold of nucleate boiling is typically 0.05 - 0.1 W cm^{-2} in the range $T_\lambda < T < 4.2$ K, but may be as low as 0.01 W cm^{-2}. Note that a threshold heat flux of 0.05 W cm^{-2}, if due to non-convective thermal conductivity, would require a temperature gradient of 250 K cm^{-1} in the He. If vapor bubble motion is unconstrained, nucleate boiling enhances heat transfer. However, it is accompanied by temperature fluctuations and mechanical effects which are undesirable in an electronic system.

(c) At very high heat fluxes, a transition to film boiling occurs and a continuous film of ^{4}He vapor forms at the solid surface. This sharply reduces heat transfer and the system becomes thermally unstable.

11.4.2 $T_{He} \lesssim T_\lambda$ (He_{II})

Heat transport in He_{II} at fluxes up to several W cm^{-2} requires a negligibly small temperature gradient. The flux is a highly nonlinear function of the gradient and there are strong temperature and geometry dependences in the problem.

This complex situation is often summarized by stating that the effective thermal conductivity of He_{II} in unconstricted geometries is infinite for all intents and purposes (10^3 times the room temperature thermal conductivity of copper is an often quoted figure).

What this means is that heat transfer from a solid to superfluid He_{II} is limited not by heat transport in the liquid but by the Kapitza or thermal boundary resistance at the solid-liquid interface. Such a thermal boundary resistance occurs at any interface between two different media. An obvious source is the acoustic or phonon mismatch between the media, and this mechanism does satisfactorily account for the boundary resistance between two solids or between a solid and a non-quantum liquid. Phonon energy transport from a solid into liquid helium however, is much more efficient than would be predicted by the acoustic mismatch theory; although the acoustic mismatch is huge, effective interface phonon tranmissivities approaching unity are observed [Challis, 1974].

For present purposes we will pass over this unresolved problem in low temperature physics and recount the pertinent phenomenological properties of the Kapitza resistance. When both the heat flux J_q and the temperature difference across the interface $\Delta T = (T_s - T_{He})$ are small, the Kapitza conductance may be defined as $h_k \equiv J_q/\Delta T$ where $h_k \approx AT^3$. The constant A depends on the solid material and its surface condition; for some materials values of A ranging over an order of magnitude have been observed. A depends slightly on whether the He is normal or superfluid. Typical values are:

	$A\ (W\ cm^{-2}K^{-4})$	
Pb	0.8	[maximum observed, Challis, 1974]
Sn	0.2	[Gittelman and Bozowski, 1962] .

At $T_s = 1.8$ K, the Kapitza conductance for Pb would thus range downward from about 5 $W\ cm^{-2}\ K^{-1}$.

If ΔT is not small compared with T_s and T_{He}, the phonon equivalent of Stefan's Law is more appropriate,

$$J_q = \frac{A}{4} (T_s^4 - T_{He}^4) \tag{11.9}$$

and the effective heat transfer coefficient is

$$J_q = \frac{A}{4} \frac{(T_s^4 - T_{He}^4)}{(T_s - T_{He})} = \frac{A}{4} (T_s^2 + T_{He}^2)(T_s + T_{He}). \tag{11.10}$$

The Kapitza resistance is, of course, still present when the helium is not superfluid. However, if we consider heat transfer at a nucleate boiling threshold flux of 0.1 W cm^{-2} at $\Delta T_t = 0.5$ K ($T_{He} = 3.2$ K, $T_s = 3.7$ K), then the temperature jump across a Pb-He_I interface might be as small as 2.5×10^{-3} K. Put another way, the Kapitza conductance is usually much larger than the effective heat transfer coefficient of freely convecting normal He, so that the thermal boundary resistance may be neglected.

11.4.3 Summary

In summary, the heat transfer characteristics to liquid helium are:

(a) Stable cooling of a heated solid in a static (non-circulating) bath of normal He_I with unconstricted geometry occurs by free convection for heat fluxes J_q less than 0.01 to 0.1 W cm^{-2} (0.05 W cm^{-2} is a useful typical value). The limit is set by the transition to nucleate boiling at the solid surface. The corresponding effective heat transfer coefficient $J_q/\Delta T$ is typically 0.2 W cm^{-2} K^{-1}.

(b) Stable cooling at effective heat transfer coefficients up to 1 W cm^{-2} K^{-1} may be obtained in force-circulated supercritical He.

(c) Cooling of a solid in superfluid He_{II} is limited by the Kapitza or thermal boundary resistance. The Kapitza conductance $h_k \equiv J_q/\Delta T \approx AT^3$, and depends strongly on the solid material and its surface condition. At T = 1.8 K, typical values of h_k lie in the range 0.5 - 5 W cm^{-2} K^{-1}.

Consider two application examples:

(1) A superconducting digital processor with 10^5 devices cm^{-2} operating in the latching mode with each device dissipating 1 μW when latched, and latched 10% of the time. This implies an average power dissipation of 10 mW cm^{-2}, which can be handled by free convection cooling in a static He_I bath at 4.2 K. If the device density is increased to 10^6 cm^{-2}, free convection cooling may not be adequate unless power dissipation is reduced, e.g., by use of the non-latching mode. If the dissipation cannot be maintained at the 10 mW cm^{-2} level, it can always be handled by operation in superfluid He_{II} or, perhaps, by operation in supercritical He under forced circulation.

(2) A high power superconducting cavity with surface resistance $R_s = 10^{-8}\Omega$, operating at a maximum field $B_{RF} \sim B_c = 1kG = 0.1T$. The power dissipation at the surface is

$$P \sim \tfrac{1}{2} R_s H^2 = \tfrac{1}{2} R_s \frac{B_c^2}{\mu_o^2} = 30 \text{ W m}^{-2} = 3 \text{ mW cm}^{-2}, \qquad (11.11)$$

within the acceptable limits for all cooling modes.

APPLICATION TO MILITARY SYSTEMS

12. INTRODUCTION

Superconductive electronics can be exploited in military electronic systems which require lower loss, greater sensitivity, and/or greater speed/bandwidth than can be usefully delivered by conventional technology. This occurs at very low frequencies, at upper microwave and millimeter wave frequencies, in high speed analog-digital converters and high speed digital processors, and in other selected areas. This portion of the report enumerates and discusses these opportunities and the potential payoff.

The applications at low frequencies are principally based on the SQUID, whose sensitivity, size, and bandwidth combine to outclass conventional devices. SCE technology is particularly applicable to magnetic anomaly detection and localization and to low frequency communications. Certain superconducting receiving antennas are also advantageous for low frequency systems.

The probable impact of SCE digital processors and analog-to-digital (A/D) converters is a result of the unique combination of high speed and low power dissipation which will permit high packing density for Josephson junction logic, memory, and A/D converters. This has potential application to large digital computers, radar signal processors, space systems, and electronic warfare.

Low noise, wideband receivers at millimeter wavelengths are based on the use of super-Schottky mixers and Josephson junction mixers and amplifiers as well as passive superconducting components. These will have application for intercept, space communications, electronic warfare, and radar. Radiometric sensors configured from these receivers can have important application in ocean surveillance and atmospheric sounding.

Microwave oscillators can be configured from SCE by using either high Q superconducting cavities or Josephson junctions. In the first case we have the possibility of extremely stable sources, possibly rivaling the atomic standards for use as clocks. In the second case one can achieve high stability and spectral purity for linear voltage controlled oscillators at microwave and millimeter wavelengths.

Before many of these applications can be realized, further R&D will be required. Recommendations for achieving these goals are given in the Executive Summary at the front of this report.

13. DOD IMPACT OF SC DIGITAL ELECTRONICS

The potential importance of superconducting digital electronics is a consequence of its unique combination of high speed at low power and high density. Below we briefly review several applications which span the gamut from weapons design to operational radars and space systems.

13.1 General Purpose Computing Needs

Computer modeling and simulation is a very important tool for addressing problems which are too difficult, expensive, or time consuming to solve experimentally, or whose parameters need to be established prior to an experimental verification. In some cases, such as nuclear weapons design or nuclear effects prediction, the experiments are not permitted. There also are classes of problems which can only be addressed by computation, and the length of time required and expense involved is presently unacceptable. In all these cases, a reliable computational capability equivalent to 100 CDC 7600's is required.

SCE systems under development already promise to duplicate the capability of an IBM 360 system in a volume of $(10\ cm)^3$, exclusive of bulk memory. We can therefore envision a computational capability 10^3 times that presently available; cryogenic minicomputers could be the equivalent of present computer centers and would be available for use in field or mobile systems.

13.2 Impact of Digital Techniques in Radar

Modern radar concepts include spread spectrum, frequency hopped, high speed digitally coded systems, and synthetic aperture. The state-of-the-art and cost effectiveness of digital processing will have a strong impact on practical implementation, especially when we include such features as adaptive clutter thresholding and high spatial resolution. For example, very long codes (50,000 to several million bits) running at several GHz clock speeds and requiring many doppler channels present a very formidable real time signal processing problem. A range of 200 miles, range resolution of 2 feet, and 32 doppler bins require 16.896 K data cells, each cell containing two 8-bit words for each radar pulse. If adaptive thresholding for each resolution cell and code change from pulse

to pulse are used, very high speeds are required for real time processing. Current technology requires parallel associative processors.

Pulse radar systems at X-band and above are implemented by mixing the carrier frequency down to a video frequency band where the information within the echo is digitized and processed. This technique requires wide dynamic range amplifiers and mixers which precede the digital processing section. The video band is normally determined by the A/D conversion rates of present technology. Digitizing is considered to be the most reliable, versatile, and fault tolerant scheme for handling the information contained in the radar pulse as well as for providing the protection and dynamic range called for in jamming situations. Josephson junction digital circuitry may provide the necessary performance and cost features to allow digitizing at the most effective level in the system. Because of high speed and low signal level required it may be feasible to A/D convert at the carrier frequency with only modest wideband gain preceding the converter. This would simplify the demodulation and allow straightforward digital processing to be immediately applied which, obviously, must also be done at high speeds. Because of the low device power, SCE circuit power will allow LSI implementation with its concomitant lower cost and simplicity.

13.3 Electronic Warfare

As radar systems become more sophisticated and use chirping of pulses, multiple pulses, jitter and phase modulation of CW emission, the difficulty of electronic countermeasures multiplies. The analysis and modification of the received signals in order to eventually deceive the attacker calls for very high speed processing to adapt rapidly to the varying environment. Greater versatility is provided if these systems are designed to operate with digital processing early in the sequence of steps. The A/D conversion process should be performed at the carrier frequency and thus demands a very high GHz rate digital technology.

A major area where SCE has no peer is fast switching with 3 or 4 orders of magnitude lower power dissipation than any alternate technology. Typically this switching time is 10-20 picoseconds with the possibility of either latching or nonlatching logic. At least one large industrial company is pursuing large scale SCE data processors operating at these rates. In any event, hyperfast electronics could lead to multi-GHz sampling rates

(A/D converters) which allow the possibility of realizing Fast Fourier Transforms (FFT) directly on RF pulses at 5 or 10 GHz. From a tactical Navy point of view, this would represent a quantum jump in performance. Specifically, considering the generalized intercept problem, it would allow accurate pulse finger printing and large scale electronic environment tracking. At this stage of exploratory development it is not known whether the cost per unit would ever allow mass deployment for electronic intercept systems. Although this could change in the future, present electronic intercept systems (0-18 GHz) should cost no more than $0.5 million/copy. But it is hard to perceive the picosecond FFT capability not costing 3 or 4 times more.

Actually it is in the radar rather than the ECM intercept field that the hyperfast data processing capability would be most useful. This is because the average data rate into a radar system is much higher and the raw number crunching capability can be used continuously. Some of the areas in radar which require large scale digital processing are as follows:

(1) Automatic detection
(2) Signal integration
(3) Automatic tracking
(4) Constant false alarm rate receivers
(5) MTI (moving target indication) and pulse doppler filtering
(6) Pulse compression
(7) Synthetic aperture radar
(8) Target classification
(9) Antenna beam forming
(10) Adaptive processing

It is clear that multi-GHz sampling and A/D converters along with expanded memory and processing will allow considerable improvement in some or all of these functions. Although unit costs for radar systems are substantially higher than intercept/countermeasure systems, we cannot project the added cost/unit compared with the improved performance.

13.4 Digital Processing in Space Systems

If both the technology and cryogenics technology can be developed to the point where long life (5-7 years) space qualified superconducting processors are available, a potential application exists in the space-borne processor area.

The lack of processing on a sensing platform implies that all of the data that has been gathered must be transmitted to the ground for processing. It is anticipated that the communication network required to support this type of system will have large data rates (Gigabits/sec). These information rates place stringent requirements on the communication sytem components and also force the designer to configure systems using higher transmission frequencies which are more susceptible to attenuation because of the atmosphere, clouds, and rain.

If one were to implement processing on the sensor platform to reduce the required communication system data rates by a factor of 10 to 100, this would significantly reduce the communication system complexities. Clearly, this would place the future communication requirements at a level where they could be met with present and near future technology. It would give the designer more flexibility in his choice of communication system parameters (i.e., frequency, power, antenna gain, etc.) and would also ease the spectral congestion constraints. It would also reduce the ground station operational requirements and make possible the reception of critical data in near real time at remote sites using a simpler receiving system terrestrial distribution network.

It appears that processors which could handle gigabit data rates are possible using superconducting technology. The implementation of this type of system in space would require ultrareliable, low power, small volume, small weight processors that are space qualified and have capabilities that are comparable to or exceed present day ground based computers. These requirements would dictate that the research funds should be allocated not only for device technology, but equally important, for cryogenic technology.

13.5 High Speed Mass Memory

A potential application exists for a high speed mass memory ($10^{11} - 10^{12}$ bits) which can serve as spaceborne data recorders. As a consequence of the power, weight. and size limitations, along with hands off reliability, consideration of potential

candidates has generally been reduced to CCDs and magnetic bubbles. However, the recent development of digital Josephson junction technology makes SCE a realistic candidate. It has all the attributes required: small bit size, very low power, and very high speed.

Single flux quantum memory cells can be fabricated by planar batch fabrication methods with cell sizes less than $(10 \text{ micron})^2$. This produces 10^6 bits/cm^2 of area. With 200 ten inch boards we can accomplish 10^{11} bits in less than 1 cu ft. Energy stored per bit is approximately 1 electron volt (1.6×10^{-19} joules); energy is dissipated only during read or write operations at the rate of $\sim 10^{-19}$ joules/bit. Hence 10^9 bits per sec could be individually written and read with 10^{-10} watts of power. However, the requirements of individual bit addressing would probably be unacceptable from a system point of view so that a shift register approach would be required. If all 10^{11} bits were in a single shift register, the power would be in excess of 10^{11} bits $\times 10^{-10}$ watts/bit or 10 watts. A compromise approach of connecting N bits in a single shift register would result in a dissipation of $N \times 10^{-10}$ watts per shift register plus power to sequentially address each of the shift registers. Total power dissipation could be less than 10 milliwatts. Refrigeration requirements should be less than 100 W prime power.

13.6 Adaptive Arrays

In communications and collection systems the driving parameter is signal-to-noise (or interferer) ratio. This performance can often be improved by using arrays of sensing elements and further enhanced if the element outputs are processed to provide spatial or temporal selection in favor of the signal of interest. For example, a null in the array response can be steered to reduce the contribution of an interferer or adjustments in the array can be made to separate out multiple modes of the same signal. The necessary operations call for the handling of multiple sensor information and, in general, the real time processing of these outputs at a high rate. High speed processing will make it possible to handle higher frequency signals, use more sensors, and adapt more rapidly to more widely varying environmental conditions.

14. NAVAL SYSTEMS APPLICATION OF SQUIDS

There are several applications for superconducting electronics in the frequency region from DC through the HF band: (1) for the detection and localization of magnetic anomalies; (2) as a compact low noise H-field receiving antenna for communications by submerged submarines on station; and (3) in the frequency band from HF down, as detecting elements in antenna arrays where beam forming (i.e., the placing of nulls to selectively reject interfering signals) is desired.

14.1 Magnetic Anomaly Detection and Localization

At the present time the detection and localization of magnetic anomalies is accomplished by using either component field flux-gate magnetometers or total field, scalar, optically pumped vapor magnetometers. Operations employing either of these total field instruments are quite often limited by geomagnetic background noise. The advent of the SQUID has made it feasible to build short baseline gradiometers with adequate sensitivity to detect magnetic anomalies at ranges comparable to that achieved by the AN-ASQ/81 during periods of low geomagnetic noise. Furthermore, the sensitivity that could ultimately be obtained for SQUIDs is several orders of magnitudes greater than the value presently achieved and thus further enhancement in detection range should be possible once experience has been gained in using presently available SQUID devices. (The AN-ASQ/81, an optically pumped helium vapor magnetometer, has a sensitivity which is about an order of magnitude above theoretical instrument noise. No other non-superconductive magnetometer has either a demonstrated or theoretical instrument noise approaching that of the SQUID system.)

The concept of using an array of magnetometers and gradiometers for localization of magnetic anomalies is being pursued by NCSL. The simultaneous output of five gradiometers, each measuring an appropriate field gradient component, and one magnetometer, which can be either a component or scalar instrument, can be suitably processed to provide information in real time about the range, azimuth, declination, orientation, and magnitude of the magnetic dipole moment of an anomaly.

14.2 Low Frequency Communication Systems

Another crucial requirement for the Navy is to communicate with its submarines on station. If signals are to penetrate into the ocean, the carrier frequency must be kept low since the electrical skin depth varies inversely with the square root of the frequency. However, the size of the optimum antenna increases as the carrier frequency is decreased and thus the selection of an operating frequency to communicate with submerged submarines must be a compromise between many factors including these two. For the proposed SANGUINE-SEAFARER system, the operating frequency is between 30 and 130 Hz. Even at this frequency the size of the transmitting antenna is large and this system has had difficulty finding a location that is satisfactory to both the Navy's requirements and environmentalist groups. If higher operating frequencies were selected, the size of the transmitting antenna would be more manageable but the receiving antenna will have to be positioned much closer to the surface of the ocean, thus increasing the submarine's vulnerability to detection.

The operational requirements of the SANGUINE-SEAFARER system are such that a magnetic sensitivity of 10^{-10} gauss/$\sqrt{\text{Hz}}$ is required. The E-field antenna with the required sensitivity is long and cumbersome and must be deployed far behind the submarine. However, the reception characteristics of such an antenna are very directional and the submarine must travel in a prescribed orientation relative to the transmitting antenna in order to receive the signal. This is a totally undesirable situation. A trailing wire H-field antenna, also of comparable length, was developed in order to relax this restriction on the submarine orientation in order to receive signals from the master transmitter. Unfortunately, the noise in this H-field antenna was about 15 dB above the required instrument noise level. Thus, alternatives had to be considered by the Navy for the receiving antenna for the submarine communication system.

The SQUID magnetometer easily satisfies the magnetic field sensitivity requirements of 10^{-10} gauss/$\sqrt{\text{Hz}}$ in this frequency band and will require a volume of 1 ft^3 exclusive of the cryogenic cooling apparatus. However, the very serious motion induced signals in the output of SQUID systems moving in the earth's magnetic field led NRL to propose a scalar system using three nominally orthogonal SQUID sensors and appropriate signal processing to obtain a rotationally invariant signal. This technique when properly implemented will provide an output independent of platform and antenna orientation.

A three axis SQUID system has been procured and tested by receiving weak signals both at the surface of the earth as well as several hundred feet below the surface of the ocean. An adaptive data processing system has been proposed and tested using simulated data. At the present time the interfacing of the SQUID triaxial system and a mini-computer is underway. Actual field testing of the assembled system mounted in a towed fish will probably have to wait for a final decision on the characteristics of the systems that the Navy will use for communication to submerged submarines on station.

The concept of the three axis scalar SQUID system has been carried sufficiently far to have demonstrated its merits for the reception of low frequency signals. If the ELF system should not become operational due to the protest of environmentalists, and a higher signal frequency is selected in the low kilohertz range, scalar SQUID systems with sensitivities approaching 10^{-12} gauss/$\sqrt{\text{Hz}}$ could be developed. Platform stability in the kilohertz region will be noticeably better than at lower frequencies since the signal frequency will be further removed from the dominant oscillation frequency of most towed bodies, which is of the order of one hertz. A minimal and possibly primitive processing procedure may be adequate for signal reception at kilohertz signal frequencies.

In summary, it is totally within the present day technology to build a small scalar H-field antenna capable of detecting signals of 10^{-10} gauss/$\sqrt{\text{Hz}}$ amplitude using SQUID sensors which can be moved through the earth's magnetic field without placing drastic requirements on the stability of a hydrodynamically but not actively stabilized platform. With some additional improvement in SQUID magnetic flux noise performance, optimization of field sensing coils and improved SQUID electronics, a scalar SQUID system with signal reception capabilities of the order of 10^{-12} gauss/$\sqrt{\text{Hz}}$ should be available in the near future. There is no competing conventional, (that is, nonsuperconducting) system which can provide this level of sensitivity at signal frequencies below 1 kilohertz. In addition, at frequencies below 100 hertz, the competing sytems tend to be physically large and unwieldy. Since the Navy does have interest in the detection of electromagnetic signals in this range, systems using SQUID sensors are obviously the direction that should be pursued.

14.3 Receiving Antenna Pattern Generation, VHF and Below

The ideal receiver in a multi-signal environment would use frequency and spatial filters to optimize detection of the desired signal and reject the background interference. The initial sensitivity is uniform over the full frequency band of interest and at all orientations. As a signal is detected a decision is made as to whether it is the desired signal or undesirable interference. Filtering and pattern null-forming are adaptively generated to discriminate against all unwanted signals. Such adaptation requires considerable information acquisiton, processing, decision-making, and control. If large dynamic ranges are involved it also requies high stability in the sensor (antenna) elements. Since shipboard electromagnetic interference and atmospheric noise are simply unwanted signals, and since such signals are frequently discrete, especially in azimuth, effective rejection requires reception sensitivities much higher than indicated by published statistical noise tables. For very closely spaced elements, $d \ll \lambda$, the sensitivity and stability requirements are even more stringent. Also in the closely spaced antenna case it becomes important to avoid high element efficiencies which lead to high mutual interactions and consequently instabilities and narrowband performance.

For high stability, wide bandwidth, and low noise sensor (antenna) elements the SQUID appears to offer significant advantages and additional exploration of opportunities should be undertaken. For detection, recognition, decision and control, as well as stability, digital methods are very attractive. The need for multiple processing involving numerous parallel logic paths suggests that digitizing of the received signals should be undertaken at the earliest stage that clock rates and dynamic range makes feasible. Early digitizing also removes instabilities and drift of analog components.

Digitizing limitations and digital processing speed and economics are very significant factors in achieving adaptive pattern forming. The possible impact of SCE on digital analysis will be discussed in the following chapter.

14.4 Electrically Small Aperiodic Antennas

When electrically small antennas (i.e., small with respect to the free space wavelength) are resonated, the resulting bandwidth and efficiency are usually low. It is

feasible however to construct wideband loops and dipoles, called aperiodic.* An aperiodic dipole (or monopole) is simply a short dipole connected to a voltage amplifier, where the amplifier input impedance is large compared to the dipole reactance. As long as this condition and the small length hold, the dipole-amplifier output is independent of frequency, i.e., aperiodic. Since GaAs FET amplifiers have high impedance and low noise, such antennas are practical for receiving as long as the amplifier noise does not degrade the overall noise temperature. For example with an amplifier noise figure of 10 dB the environmental noise is 10 dB higher than the amplifier noise at 25 MHz. Lower noise figure amplifiers will allow operation at higher frequencies.

The aperiodic loop is fed into a low impedance current amplifier. The open circuit voltage V is proportional to number of turns, diameter in wavelengths, and effective permeability, while the reactance X is proportional to turns squared, diameter in wavelengths, and effective permeability, all for a small loop. Since the output current is V/X, it is independent of diameter and permeability and varies as 1/N. So the aperiodic loop should have one turn. Unfortunately low impedance transistor amplifiers tend to have large noise figures, and so the upper usable frequency is well below the typical 25 MHz quoted above, and may well be 5 to 10 MHz. A SQUID amplifier offers low input impedance and low noise temperature, and, in fact, an external loop coupled Josephson junction is just an aperiodic loop with a low impedance amplifier. Such devices will offer significant advantages over conventional antennas in the HF band (3-30 MHz) and in that part of the VHF band (30-300 MHz) where it is impractical to use larger (quarter wave) antennas.

A problem with all small antennas, especially those using high impedance amplifiers is susceptibility to high voltage pulses caused by atmospherics, EMP, RFI, etc. This is related to the large noise bandwidth of an aperiodic antenna. Since the noise bandwidth is very much greater than the signal bandwidth, there tends to be a problem obtaining enough dynamic range. This applies to the SQUID (JJ amplifier connected to an aperiodic loop) and may be particularly serious because of the inherently small dynamic range.

---

*The term "frequency independent" is more appropriate, but already has a well defined usage in antenna practice.

15. MICROWAVE/MILLIMETER WAVE RECEIVERS

It is abundantly clear the SCE will lead to sensitive receivers at microwave and millimeter wave frequencies. It is also evident that superconducting receivers will not be generally employed "across the board." Two factors mitigate against their widespread use: at frequencies below 20 GHz conventional technology is very good and far more convenient to use than SCE because of the absence of cryogenic cooling, and in many applications the background environmental noise reduces or eliminates the advantage of a low noise receiver. Nevertheless, important areas of advantage can be identified. These include systems at frequencies of 35 GHz and above and special applications requiring very wide bandwidths below 35 GHz.

A general requirement which will warrant the use of SCE receivers below 35 GHz is that the receiver should be looking at a relatively cold background. For terrestrial applications this contrains one to "look angles" greater than 10^{o} above the horizon ($< 80^{o}$ below zenith) as shown by Fig. 15.1. For airborne or space-borne systems the receiver should not be pointed below the earth's limb. At frequencies above about 35 GHz, the background requirement is not quite so severe since conventional receivers are not expected to achieve 300 K noise temperatures.

15.1 Intercept Receivers

Because of the low noise and wide bandwidth that are inherent in superconducting devices, valid applications exist in the communication intercept area above 20 GHz.

If one configures a system at 35 GHz where the sensor is constrained to an elevation angle above 10^{o}, then the anticipated ambient noise level is consistent with a temperature $\lesssim 70$ K; at an elevation angle above 30^{o} the ambient noise level is consistent with a temperature $\lesssim 30$ K.

State-of-the-art parametric amplifier performance at 35 GHz is in the 100-200 K region (Fig. 6.1), although it is not clear that this noise temperature can be maintained over the desired GHz bandwidths. Superconducting receivers have a potential to achieve waveguide bandwidths with lower noise temperatures. At higher frequencies, such as 90-100 GHz, the potential advantage of SCE becomes greater. The application of SCE receivers to electronic intercept offers significant opportunities for improvement over conventional technology. This is discussed further in Section 18 on electronic warfare.

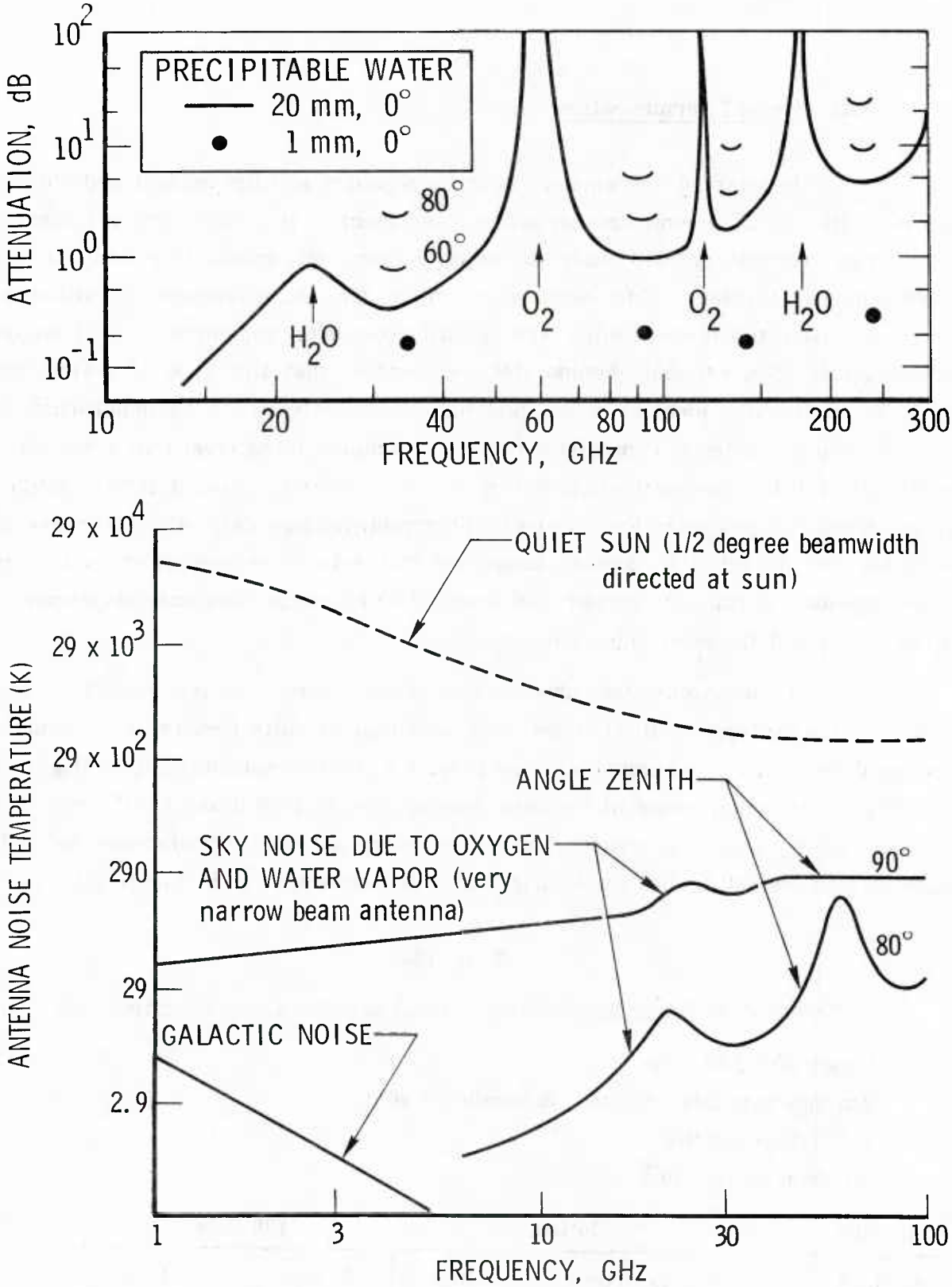

Figure 15.1

(Top) graph of total atmospheric attenuation as a function of frequency, look angle, and precipitable water vapor. (Bottom) antenna noise temperature as a function of frequency.

15.2 Space Communication

Because of the ambient noise background and the present and anticipated state-of-the-art of communication sytem componentry, it is not expected that superconducting technology will have a large impact on ground-to-ground microwave communication sytems. One area where there may be advantage in utilizing this technology is satellite-to-satellite and satellite-to-ground communication at millimeter wavelengths. The rationale behind this judgment is that this type of system can be designed so that the ambient noise level that competes with the communication link is that of deep space and is appreciably below the ambient noise level that a terrestrial or earth-to-satellite communication system has to overcome. Also it is anticipated that future satellite communication systems will incorporate large data rates ($>$1 gigabit/sec). SCE has the potential to provide broadband low noise receivers which could operate advantageously in this environment and would diminish the performance requirements for other portions of the communication system.

To determine the advantage of using superconductive technology for this purpose, it is instructive to consider some potential satellite-to-satelite communication link requirements. As an example, if we project a receiver capable of operating in the 50 to 100 GHz frequency range with a noise temperature of 1000 K and a SCE receiver could achieve 100 K, then the power required to close a typical synchronous satellite-to-satellite communication link for a variety of conditions are given in Table 15-1.

Table 15-1

Transmitter Power Required for Typical Satellite Communication Link

Range $\approx$35,000 miles

Antenna gain (both transmit & receive) = 60 dB

5 dB margin on link

Bit Error Rate = 10^{-6}

Frequency	50 GHz		100 GHz	
Date Rate	.5 Gbps	1 Gbps	.5 Gbps	1 Gbps
Conventional Receiver T_R = 1000 K	3 W	6 W	12 W	24 W
SCE Receiver T_R = 100 K	0.3 W	0.6 W	1.2 W	2.4 W

The key tradeoffs to be made are between bandwidth, transmitter power (and prime power and weight required for a satellite), and refrigeration weight and prime power for a SCE receiver. One can expect to meet the requirements of this conventional system in the 5-10 year period. On the other hand, the superconducting receiver has minimal heat load and a reliable refrigerator should require less than 50 W of prime power on a space paltform. This leaves open the clear possibility of data rates in excess of 10 Gbps. Furthermore, in a satellite-to-ground millimeter wave link the cryogenic receiving system is on the ground while the transmitter power reduction of a factor of ten will result in a saving of spacecraft power, weight, and increased reliability.

15.3 Radar

General purpose radar systems operate in an environment which makes superconducting receivers appear unnecessary because of background noise and propagation effects (see Fig. 15.1). The problem of space object identification is one which requires high sensitivity and high resolution.

The principal candidates to replace or supplement microwave radar imaging are millimeter and laser radar imaging systems. It is not our purpose here to argue relative merits of these frequencies, but to point out an opportunity for significant system improvement at 94 GHz.

The radar signal-to-noise ratio is given by

$$\frac{S}{N} \approx \frac{P_T G_T G_R \lambda^2 \alpha^2}{32 \pi^3 k T_s R^4} \tag{15.1}$$

where

G_T = gain of transmitting aperture

G_R = gain of receiving aperture

λ = wavelength

P_T	=	transmitter power
R	=	slant range to target
α	=	atmospheric attenuation
B	=	bandwidth of receiver
T_s	=	receiving system noise temperature
σ	=	radar-cross-section of the target.

Radars at 94 GHz are severly limited by the available transmitter power. (A 1 kW tube was developed by Hughes and demonstrated at Aerospace Corp. in 1970.) Because of the low power, illumination of satellites or other targets at slant ranges beyond 100 miles requires long pulse radars and target image information is derived from a wideband chirp technique. By pulse compression techniques a 1 GHz chirp can be converted to 0.5 foot range resolution and similar cross-range accuracy can be derived from relative doppler shifts at 94 GHz. A recent DARPA funded program of this type had a baseline design of 10 dB S/N for a 1 m^2 target at 1200 miles range. This design objective was a 7 dB noise figure receiver (T_R = 1100 K) to be developed with a 1 kW transmitter on a 15 foot antenna at sea level. However, the number of targets of interest within the projected radar range was small and various concepts to expand the range were considered. Four possible areas can be considered: larger antenna gain, greater transmitter power, lower receiving system noise temperature, and reduction in atmospheric loss and noise.

Because of the rapid R^4 space loss, a factor of 10 (10 dB) improvement in any of the factors (except α) results in only a 1.8 increase in range. A change to a bistatic antenna arrangement would allow elimination of the duplexer and its loss, and use of a superconducting low noise receiver described earlier would allow T_S to be reduced to approximately 100 K (1.25 dB). These would effect nearly twice the range and make further improvements in performance more attractive. By making the second antenna 10 dB higher gain and reducing the atmospheric loss by choosing a new site, slant ranges of 11,000 miles against a 1 m^2 target would be possible. This would probably include nearly all non-geosynchronous satellites. Development and installation of the superconducting low noise receiver would probably be the lowest cost factor in the improvement program.

15.4 Ocean Surveillance and Atmospheric Sounding

A number of DOD applications require or can utilize passive radiometric or thermal detection in the microwave to sub mm wave spectral region. These can be categorized according to the radiometric temperature of the background against which the target must be identified. Superconducting low noise radiometers can be used to advantage in several instances because they offer operational advantages over conventional state-of-the-art radiometers. Systems applications which can be identified are ocean surveillance, terrain mapping, atmospheric sounding from meteorological satellites, and detection and monitoring of minor atmospheric constituents such as ozone.

In the first two cases, frequencies at millimeter wave atmospheric windows such as the 85-115 GHz band, are attractive because of resolution achieved with small apertures and near all weather operation [King, et al., 1976]. The sensitivity is degraded in fog and clouds, but under better conditions radiometer temperatures $\lesssim 100$ K are clearly advantageous as seen from Fig. 6.3. We note that the antenna temperatures of most targets are below 290 K at 90 GHz.

The problem in atmospheric sounding is to determine the global atmospheric temperature and moisture profile for weather prediction by measuring the emission spectral power density on such strong lines as the 60 GHz 0_2 band and the 180 GHz H_2O band from orbiting satellites. Minor atmospheric constituents have important environmental consequences. They also can provide information about atmospheric temperature and dynamics. Millimeter wave spectroscopic detection is a powerful method of detecting these constituents and determining the atmospheric profiles [Shimabukuro, et al., in press]. The accuracy with which such profiles can be determined, including spatial resolution at fixed ΔT, is significantly degraded by poor radiometer performance. At 60 GHz and above, the projected performance of SCE radiometers is more than an order of magnitude greater than conventional technology.

16. MICROWAVE OSCILLATORS

16.1 Local Oscillators

Communications frequencies are rapidly moving up to the 35 and 94 GHz frequency ranges. In order to use these bands, superheterodyne local oscillators are called for which maintain both frequency stability and spectral purity. Adequate frequency stability is provided by quartz oscillators operated at 5 MHz and multiplied up to the necessary frequency. However, this multiplication accentuates the sideband noise power spectrum and thereby degrades the S/N ratio of the system. The use of SCE local oscillators can provide both the frequency stability and low phase noise spectrum, although amplification will be required to drive conventional mixers. Furthermore, if the receivers use SCE front end devices such as super-Schottky or Josephson mixers, the required LO power is greatly reduced and can be achieved without the use of noisier conventional amplifiers.

The superconducting cavity stablized oscillator (SCSO) performance already achieved (see Section 8) makes it unequaled by any other oscillator for frequency stability at sampling times up to about 10^4 sec. It should therefore be considered wherever an application requires the utmost in short-term stability. The design goal of the superconducting cavity parametric oscillator exceeds that of the SCSO by several orders of magnitude, again for sampling times below about one second.

The phase noise in a good FM receiver in 1 Hz bandwidth is currently typically -80 dB at 20 kHz from the local oscillator frequency and -106 dB at 500 kHz from the local oscillator frequency. A performance 10-20 dB better than this would be desirable. This can be achieved with the SCSO as it now stands.

16.2 Stable Clock

The requirements for the clock in satellite based navigational systems such as the Global Positioning System (GPS) include good short-term stability, phase noise of -86 dB Hz^{-1}, and a long-term stability corresponding to a $\sigma_y(\tau) \lesssim 10^{-14}$ over a period between clock updates of 10 days (8.64×10^5 sec.). In principle, both the cesium beam and

hydrogen maser clocks have the required long-term stability since their frequencies are derived from atomic transition frequencies. We note in Figure 8.1, however, that the flicker noise floor of commercial Cs clocks is inadequate and that for laboratory Cs clocks is marginal. The H maser flicker floor appears to be acceptable. However, the wavelength of this primary standard (21 cm) results in a very large clock which cannot be reduced in size because of this fundamental limit. Superconducting cavities which can be used to directly stabilize oscillators at microwave frequencies (3 cm wavelength) have demonstrated short term stability beyond that required by such DOD navigational systems as GPS/NAVSTAR. Furthermore, the SCSO at its projected performance level would meet the long-term stability requirements while at the same time having considerably less low frequency phase noise than the H maser. The SCSO should therefore be seriously considered as an alternative to the H maser for the GPS clock.

17. ANTENNAS AND OTHER PASSIVE COMPONENTS

17.1 Multiple-Beams and Scanning Antenna Feeds

Electronically scanned phased arrays and multiple beam antennas are used for radar, navigation, direction finding, and satellite communications, to mention a few important applications. Almost all of these antennas have a feed structure that connects from a receiver or transmitter port (sometimes multiple ports) to either a set of array elements or to a set of horns feeding a reflector or lens. Feed structures are usually composed of power splitters (hybrid junctions) and phasers, and may be implemented in coaxial cable, waveguide, or stripline. While some fixed single beam or limited scan feed networks have relatively low loss below 1 dB, a more typical range for either a scanning network, a mulitple beam network, or a wideband (corporate feed) network is 2-5 dB.

A typical example is the DSCS-3 receiver multiple beam antenna. (Since the DSCS-3 satellite is under development the following data are approximate but typical.) It consists of a waveguide lens excited by a hexagonal lattice of 61 feed horns. Each feed horn produces a spot beam on the earth from synchronous altitude; all feeds together cover the earth. The feed network through use of variable power dividers (VPD) allows any combination of beams to be produced from a single beam to earth coverage. The feed is basically a corporate feed with the VPD providing 2 outputs of adjustable phase and relative power division at each corporate level. Each path contains 6 VPD's in series, with a total of 61 VPD's. A single VPD consists of a ring hybrid with two 3 dB hybrids and two ferrite phasers in a ring connection. The phaser settings control the phase and amplitude of the VPD output. Typical losses are:

phaser	.4 dB
hybrid	.1 dB
VPD	.5 dB

6 VPD	3.0 dB
misc. guide & flanges	1.0 dB
Total Loss	4.0 dB

This 4 dB insertion loss is not excessively large for such a feed network; it represents very careful design and phaser development.

Superconductive technology might help in two ways, reducing losses and allowing low loss implementation in strip line. There is little doubt that most of the 1.6 dB of the copper loss can be eliminated through the use of superconductivity. However, the larger loss component, 2.4 dB in the example above, is ferrite phaser loss. There is some evidence that microwave circulator loss does not decrease significantly, and may actually increase at low temperatures [Comstock and Fay, 1965; Roth, et al., 1966; Edrich and West, 1970]. This certainly is an area of concern if microwave superconducting technology is to have the maximum impact.

As the frequency increases, dielectric losses in stripline or microstrip tend to predominate, and especially above 10 GHz. An antenna feed network could be implemented in either type of superconducting stripline at cryogenic temperatures; for some materials the dielectric loss decreases markedly with lower temperature. With careful surface finishing of the superconducting metal the resistive loss can be negligible. The remaining question is whether phasers could be developed to have low loss (less than .05 dB) at helium temperatures. The paucity of data indicates a definite need for active experimentation in this field.

17.2 VLF Transmitting Antenna Using Super-Coil

VLF transmitting antennas are typically large vertical monopoles with top loading wires, all supported by steel towers and guys. Since the net reactance is capacitive, a tuning coil or helix is placed at the feed point to tune the antenna. Typically these coils are solenoids wound of litz wire; the wire may be several inches in diameter, and the coils may be 10 ft or more in diameter. Q's are in the 2000 range, and overall antenna efficiencies are in the 50-80% range, depending on frequency.

A superconducting coil would reduce a major loss component, so a calculation is made of a typical station to evaluate the advantages of a super-coil. The Lualualei (Hawaii) antenna as recently modified is used as an example [Watt, 1967]. Parameters are:

$C_{antenna}$	=	0.041×10^{-6} F
$L_{antenna}$	=	0.11 mH
$R_{radiation}$	=	0.108 ohm
R_{loss}	=	0.033 ohm
f	=	23.4 kHz
$X_{antenna}$	=	-150 ohm
I	=	2230 Amp.

The approximate helix parameters are:

diameter	=	10 ft
length	=	12.5 ft
turns	=	24
L	=	1.02 mH
R_{coil}	=	0.06 ohms
Q_{coil}	=	2500

The antenna efficiency is approximately 54%, the overall Q is 746, and the bandwidth is 31 Hz. Much work has been done on superconducting cables for power lines and for electrical machinery. The best loss data that were readily available on composite supercables came from measurements on various three phase cables by Beall [1975]. The best of these showed a power loss of 30 W per three phase mile at 10^4 amps, with the conductor diameter chosen to give a surface field of 1000 gauss. If the loss scales with current, assuming a constant surface field, the loss for 2230 amp is 0.731 mW/ft at 60 Hz. AC cable losses appear to scale with frequency, independent of cable type, to first order as long as the cable is well designed. Murphy et al. [1975] give frequency dependence to 20 kHz; at 60 Hz the loss is approximately 2×10^7 while at 24 kHz it is 4×10^9. Only relative numbers are of interest; the increase with frequency is a factor of 200. Thus the very approximate loss at 24 kHz with 1000 gauss surface field is 14.6 mW/ft. And so the coil, which has 754 feet of wire, has a power loss of 110 W. The coil Q is

$$Q = \frac{\omega LI^2}{P_{diss}} = 6.8 \times 10^6 .$$

The coil resistance is 22 micro-ohms. If this Q could be realized in practice, the antenna efficiency would increase to 77%, a 23% increase. Overall the Q is 1064 and the bandwidth equals 22 Hz. In addition to the coil heat load, the dewar penetration heat load must be estimated. A 3000 amp DC penetration for 2 conductors has a typical 6W loss. For AC cables the number will be larger; assume a tripled loss, 18 W. The total helium heat load is now 128W. A typical refrigerator efficiency at this level is 25% of Carnot, or .0025. This gives a power line cooling load of 51 kW. The transmitter power is 1 MW, so that the saving of coil power is 230 kW RF, or roughly 460 kW line power, The net power line saving is 409 kW; at 8¢/kWh the power saving is $200K/year. In addition, the radiated power has increased by 23%.

Frequency shift keying could be handled by tap switching either on the supercoil or on a small normal inductance.

There are, of course, problems. Even with a Q of 2500 it is necessary to shield the helix inside a metal lined room. With a Q over a million, minute stray couplings can easily reduce Q by a factor of 10. If this were to happen, the helium heat load would exceed the normal coil loss. On the other hand, with superconducting cable it is not necessary to use a large solenoid to get high Q. A toroidal shape can be used which reduces both size and external coupling effects. Even so the problem of realizing a $Q = 7 \times 10^6$ is quite serious. Since this represents hardware not yet realized, it would be in order to build a smaller SC coil to determine if such Q's could be used in practice. If so, then a supercoil would be attractive.

17.3 Super-Loop Antennas

Loop antennas are widely used for direction finding and for radio/TV receivers. Both loop efficiency and atmospheric noise vary as f^{-3} for small loops and for frequencies below roughly HF. Thus a given size of loop and receiver that is atmospheric noise dominated, at say 1 MHz, will continue to be atmospheric noise dominated at lower frequencies. However, the practical problem of resonating and impedance matching a loop becomes more difficult as the frequency decreases. There is little advantage in cooling a receiving loop to increase its efficiency. In fact cooling may increase the Q sufficiently to yield unacceptably small bandwidth. When the loop is immersed in a lossy medium (sea or earth) both signal and noise are attenuated by refraction and skin losses.

Now the problem becomes that of providing sufficient effective length to yield a usable signal level at the amplifier. In this application the high efficiency of a superconducting loop (super-loop) may be advantageous. Such a loop could be tuned or aperiodic (see Section 14.4). If tuned, the super-loop will have very narrow bandwidth due to small radiation resistance (varying as diameter/wavelength to fourth power). Implicit here is a small diameter because only low frequencies penetrate lossy media significantly. The aperiodic loop is a more useful choice. Thus for receiving, the super-loop is only advantageous when used below the surface of the earth or sea.

Loops are seldom used for transmitting: resonant size loops have a multilobe pattern, while electrically small loops have efficiency that varies as diameter/wavelength to fourth power. In contrast small dipole efficiency varies as length/wavelength squared. Note that ferrite cored super-loops are not attractive as the efficiency is now controlled by the ferrite loss. Although the loop efficiency could be greatly increased using a super-loop, the bandwidth is likely to be a difficulty as the room temperature Q is controlled by the copper loss. Equally important is the comparison with a short dipole; the dipole can occupy the entire volume that the loop plus dewar occupies. This tradeoff is difficult to make as there are many size and geometry variables. A more direct tradeoff is between a super-loop and a room temperature dipole (or whip) with a super-coil for tuning. The dipole and super-coil is clearly better as the efficiencies are both close to unity but the super-coil requires a much smaller cooled volume. The super-coil is evaluated in Section 17.2. In summary the super-loop for transmitting has no advantage.

17.4 Passive Millimeter Wave Components

The use of superconducting materials to fabricate microwave circuit elements, especially for use above 30 GHz, seems to be a very attractive option for improving performance of millimeter wave systems.

Many passive components can be made from superconducting material. These include waveguides, coaxial cables, strip lines, couplers, hybrids, diplexers, filters, and cavities. We should seriously consider the use of these elements in combination with either active SCE devices, such as Josephson and super Schottky diodes, or conventional devices.

Above 18 GHz, and in particular in the 35 and 94 GHz windows, almost all systems use waveguides for interconnection. Waveguide, however, is lossy and difficult to fabricate when many components are closely packed. For example, waveguide at 94 GHz has approximately 0.6 dB/ft loss. Use of these higher frequencies is limited in part by the prohibitively high losses of strip lines at 30 GHz and above. Superconducting strip line and microstrip offer a potentially significant improvement, both in reducing loss and in denser packaging. In a superconducting transmission line, whether coaxial or strip, the major losses are due to electrostrictive processes in the dielectric. Dielectric loss is reduced for some dielectrics at low temperatures but little data seem to be available. Special geometries offer promise of lower loss. For example, inverted microstrip, where the metallic conductor is located as usual above a metallic plane, but with the dielectric sheet above the strip, greatly reduces dielectric loss. Such a line might be fabricated by starting with a suitable low loss dielectric substrate that has a metal surface, then etching away all except the desired strip pattern. Now the substrate is precisely spaced against a metal plane.

Such a special microstrip would probably offer good performance from 18 to 100 GHz when cooled to cryogenic temperatures. It would be useful to develop low loss transmission line techniques for these frequencies and then to compare cryogenic and superconducting performance.

18. ELECTRONIC WARFARE

Electronic warfare systems are the most recent to be universally deployed on naval ships and airborne platforms. The evolution of electronic warfare systems follows that of radar, and many electronic techniques are common to both. The principal missions of any electronic warfare sytem are:

(1) Intercept any and all radar emission illuminating the ship/plane and concurrently determine the direction from which this radiation comes (i.e., instantaneous frequency and direction finding of all external radar emissions).

(2) Register all incoherent radar/video parameters for emitter identification, either instantaneously or at some later date. Typically, these would be radar PRF, pulsewidth scan interval (search or track).

(3) In combat situations, use the intercept information to generate active (retransmit) radiation to deceive the incoming weapons platform in both range and angle. For good technical reasons, this third task is generally limited to X-band (old nomenclature), H, I, J band (new nomenclature). Numerically, this means a high power capability from 7-12 GHz at present; in the future this capability will have to be extended to 18 GHz and higher. High power is a special problem, and there is no good technical reason that SCE can make a significant contribution to high power technology.

Thus the principle applications of SCE appear to be directed at items (1) and (2) above, the all band intercept and signal processing problems. However SCE may also be important for the low power regeneration of the reradiated signal.

18.1 Electronic Intercept

Intercept systems have generally sliced up the radar spectrum into bandwidths, such as:

8 - 16 GHz (full octave bandwidth)

8 - 12.5 GHz (wave guide bandwidth)

8 - 12 GHz (semi-octave bandwidth).

Within each band, all of the rf electronics must have an instantaneous bandwidth as great as the above.

The current front-end configuration of intercept receivers takes the form of a low noise amplifier (e.g., TWTA, paramp, GaAs FET) whose instantaneous noise bandwidth is one of those listed above, and a narrowband tunable filter which can linearly tune in 10^{-3} - 10^{-6} sec anywhere in this band. This filter reduces the 4-8 GHz noise bandwidth to 20 - 30 MHz with a signal-to-noise improvement which is the ratio of the noise bandwidth of the amplifier to that of the filter. This improvement is gained at the expense of probability of intercept over the rest of the band, and possible inability to handle a chirped or frequency hopping radar that may change as much as .5 GHz on a pulse-to-pulse basis. In this regard it becomes clear that the ideal intercept system may be required to operate over a wide range of information rate, frequency, and dynamic range, all with a signal-to-noise ratio that varies from a threshold level to some finite value.

The rf hardware to accomplish these tasks is being rapidly replaced by the GaAs FET technology which appears to be cheaper, more reliable, and perform better than the current TWTA technology. The GaAs FET active modules have excellent characteristics for EW/intercept systems (wideband, large dynamic range, good noise figures, excellent reliability and lifetime, modest cost in large numbers). This technology has been demonstrated up to 12 GHz; theoretical predictions indicate that it should work, although with deteriorating performance, up to 35 GHz. There is no technical reason that SCE, or anything else, can really compete with this technology in this spectral region. However, in the EHF or millimeter wave region (from 30-300 GHz) the projected performance of SCE exceeds that expected for any competing technology. SCE appears capable of meeting all requirements for receiver front-ends with the possible exception of saturation level.

Presently deployed systems in the millimeter wave spectrum are very few and narrow band. There is a long term naval requirement that all capital ships contain

radiation intercept capability from DC to 120 GHz. Presently, this capability exists up to 12 or 18 GHz on most ships and development models on a selected few go up to 40 GHz. Virtually nothing exists from 40-120 GHz. Operational systems in this region are hampered because:

(1) Available transmitter power is extremely low.

(2) Outside of a few windows, atmospheric absorption by water vapor and oxygen severely affect the transmission path (see Figure 15.1).

(3) Millimeter waves are sensitive to particle scattering (rain, snow) in the transmission path precluding all weather use.

Millimeter waves take on added significance because (1) the smaller wavelength allows greater angular resolution and relatively more power on target for a given small aperture, and (2) 30 GHz to 120 GHz represents 90 GHz bandwidth to cover, which is 3 X the bandwidth of the presently covered range.

At these frequencies, it is a virtual certainty that intercepted power will be low and waveguide losses at the front end can ruin the system. For this reason, serious consideration should be given to low loss superconducting transmission lines in any ship deploying a millimeter wave intercept system. This is evident from consideration of the system noise temperature,

$$T_s = T_a + T_o (L_i - 1) + L_i T_R \qquad (18.1)$$

where

T_s = receiver system noise temperature

T_o = equilibrium temperature of transmission line

T_R = noise temperature of receiver

T_a = antenna noise temperature (elevation angle dependent, but $\leq$ 290 Kelvin)

L_i = loss preceding receiver (losses from antenna to receiver).

At millimeter wavelengths, loss in high quality commercial waveguide approaches ½ dB/foot at room temperature. A superconducting transmission line has the dual effect of reducing the loss and reducing the equilibrium temperature of the loss (see Section 10), and this term is as important as the effective noise temperture T_R of the receiver (whether conventional or SCE).

This system noise power, given by BkT_s where B is the total instantaneous bandwidth, must be compared with the received power in order to obtain the working signal-to-noise ratio for the intercept system. The received power is

$$P_{rec} = \frac{P_t G_t G_r \lambda^2 L}{(4\pi)^2 R^2} \tag{18.2}$$

where

P_t = transmitter power (watts)

G_t = transmitter antenna gain

G_r = receiver antenna gain

R = range (meters)

λ = wavelength (meters)

L = transmission path loss (includes all losses from active element in transmitter to active element in receiver.)

Now let us compare the received power at constant range between a 10 GHz and a 100 GHz intercept. Thus the ratio of the received powers is

$$\frac{P_{rec\ 100\ GHz}}{P_{rec\ \ 10\ GHz}} = \frac{(P_t G_t G_r \lambda^2 L)_{\ 100\ GHz}}{(P_t G_t G_r \lambda^2 L)_{\ 10\ GHz}} \ . \tag{18.2}$$

If we require the intercept antenna to receive all pulses isotropically, G_r will be approximately 0dB in each case. For a fixed transmitter aperture, $G_t \propto 1/\lambda^2$. Hence the ratio of Eq. (18.2) reduces to

$$\frac{P_{rec\ 100\ GHz}}{P_{rec\ \ 10\ GHz}} = \frac{(P_tL)_{\ 100\ GHz}}{(P_tL)_{\ 10\ GHz}} . \qquad (18.3)$$

Typically transmitter power varies as λ^2. Even though 100 GHz is in an atmospheric window (Fig. 15.1) we can expect the horizontal transmission losses to be 10X as great at 100 GHz as at 10 GHz. Thus

$$\frac{P_{rec\ 100\ GHz}}{P_{rec\ \ 10\ GHz}} = 10^{-3} \text{ or } -30 \text{ dB} . \qquad (18.4)$$

The principal advantage of millimeter waves is the increase in antenna gain as λ decreases. Thus 30 dB gain can be realized for a 3 cm diameter aperture at 100 GHz.

If we assume at 100 GHz

P_t = 10 kW

G_t = 30 dB

R = 10 km

G_r = 0 dB

then

$$P_{rec\ 100\ GHz} \approx 6 \times 10^{-9}\ L \text{ watts.} \qquad (18.5)$$

Including the atmospheric losses at sea level for a horizontal path, we would typically have

$$P_{rec\ 100\ GHz} \approx 10^{-6} \text{ mW} . \qquad (18.6)$$

At 1 km the maximum signal would increase by 20 dB. Asumming a 40 dB dynamic range the signal threshold would be 10^{-11} watts. Assuming a perfect receiver, T_s = 290 K (Eq. 18.1) and the total thermal noise is kT_sB. Comparing this noise with the threshold signal we have available a bandwidth

$$B = 10^{-11}/kT_s \approx 2.5 \text{ GHz} \ . \qquad (18.7)$$

With a 13 dB signal-to-noise ratio this number would have to be reduced again by a factor of 20. This would bring the instantaneous bandwidths down to 100 MHz as a useful channel quantization or an instantaneous tuning bandwidth. Any front end loss or receiver noise figure would further reduce this number. For a 90 GHz RF bandwidth this leads to 900 tuning steps or channels. 100 MHz frequency resolution at 100 GHz appears comparable to 10 MHz resolution at 10 GHz. Of course in a full system the 100 MHz channel width would taper to 10 MHz at X-band. Coincidentally, a –40 to –80 dBm dynamic range is scaled down in absolute power approximately 30-40 dB from existing X-band IFM intercept systems.

18.2 Implementation of Multi-Octave Millimeter Wave Intercept Systems

From Eq. (18.1) and the discussion above, it is highly desirable to reduce the intrinsically lossy components associated with the physical length from intercept antenna to receiver. Presumably this can be done via cryogenically cooled waveguide, strip line, or its equivalent. Certainly, it is desirable to have the receiver in close proximity to the antenna, but this may be physically impossible in a ship mast installation.

The equivalent of YIG varactor frequency channel tuning appears to be non-existent at these frequencies. Likewise broad band low noise traveling wave tubes are non-existent and GaAs FET technology appears to have a theoretical limit of amplification of around 40 GHz.

SCE receiver front ends using either Josephson junctions or super-Schottky diode mixers are expected to achieve low noise temperatures $\lesssim 50$ K (Figure 6.1).

On the surface, it appears that there are two general approaches to the octave or semi-octave emitter intercept problem. One could approach this from the laboratory technology of direct amplification (say parametric amplification) followed by direct detection. At these frequencies the entire cryogenic complex would have to be located at the antenna installation. While demonstrated superconducting parametric amplifiers have excellent noise figures and bandwidth, they suffer from extremely poor dynamic range properties, i.e., roughly 10-13 dB pinned to the noise floor. Attempts are being made to improve this via the Josephson arrays, but the theory and techniques of

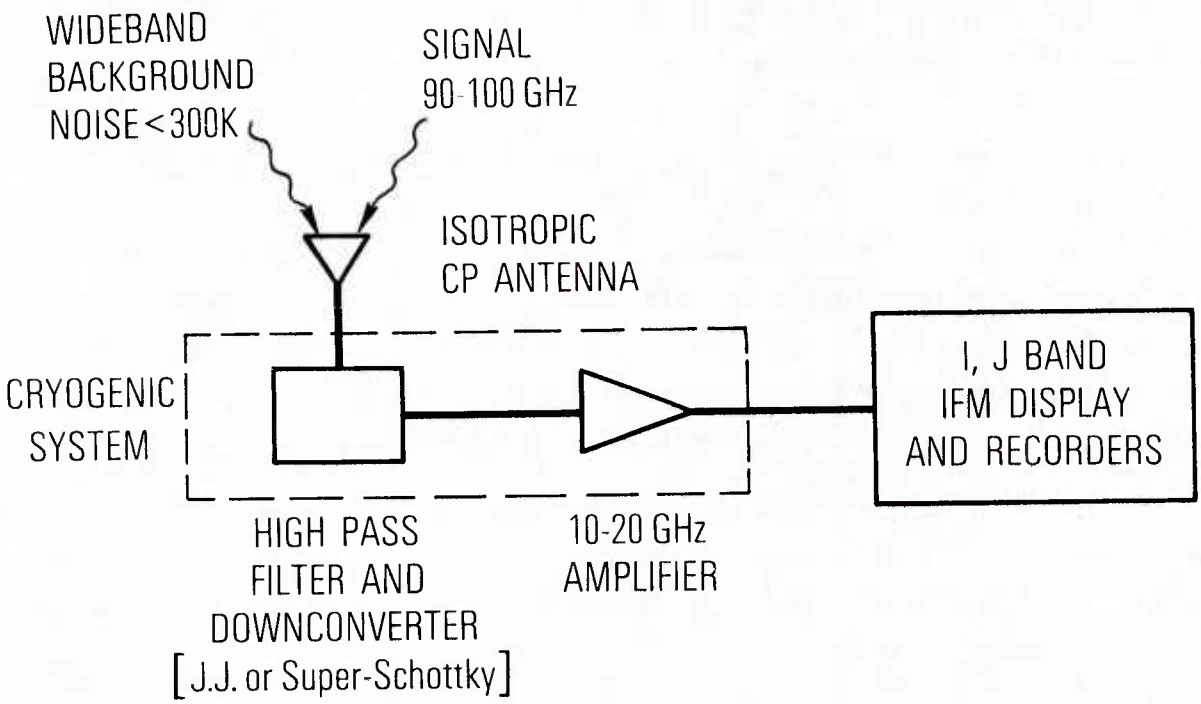

Figure 18.1

Skeletal circuit of millimeter wave intercept receivers.

array coupling have not yet been developed. Certainly array phase locking and impedance matching is highly desirable for practical microwave devices and this type of work should be vigorously pursued. A swept-frequency amplifier would give a low probability of intercept and the extremely wide noise background would probably saturate the amplifier considerably since there is no tracking filter scanning with the frequency, yielding unacceptable false alarm rates in the working dynamic range.

The second approach would be a down converter to a video frequency with sub-channeling. It is clear from Section 6 that down conversion can be done either with Josephson junctions or super-Schottky diodes, but it is by no means clear that a satisfactory linear dynamic range can be achieved. Again it is quite possible that a working field unit will require array technology, an area which is not completely understood. In any event, a 10% bandwidth at 100 GHz downconverted to 10-20 GHz could be handled by GaAs FET technology and video intercept IFM circuits. This would have the added advantage of allowing finite waveguide runs to a non-cryogenic environment (see Figure 18.1).

This figure represents a skeletal circuit, and one could argue that parallel channel frequency multiplexing (in the 10-20 GHz IF) could be used with synchronous SCE detectors terminating each channel, with noise collapsing tunable filters. Such an approach needs to be examined further with respect to the economics (cost/channel) vs what it buys in IFM sensitivity and will not be discussed here.

Summarizing then, it appears that a most significant development in intercept capabilities at millimeter wave frequencies is a broad band very low noise receiver including input waveguides. In terms of near term applications this should initially concentrate on 30 GHz, but the longer term goal should be at 100 GHz.

18.3 Spread Spectrum/Frequency Agile Intercepts

Spread spectrum, and/or frequency agile radars considerably complicate the intercept/countermeasure problem. Basically, the use of these broad band signals forces the intercept system to use a much wider instantaneous noise bandwidth and degrades the intercept signal-to-noise ratio by the ratio of instantaneous noise bandwidths. Thus the receiver intercept system is forced to track in time the entire frequency bandwidth of the signal. Such a radar system is fairly simple to implement with linear VCO tuning units

controlling the radar frequency. For example, a radar which is randomly frequency agile over a 500 MHz bandwidth on a pulse to pulse basis forces the intercept system to work with a 500 MHz bandwidth to maintain 100% probability of intercept while the radar receiver can retune on a pulse to pulse basis maintaining its 5-10 MHz information bandwidth. Hence the operational intercept noise bandwidth and the working S/N ratio is deteriorated by 17-20 dB. This can have serious implications against accurate RF frequency measurements.

Execution of active countermeasures against such signals (frequency agile with/without chirp) is seriously affected, as the instantaneous frequency must be presumed and delayed in a proper pattern. With the advent of gigabit A/D converters and concomitant digital memory, it will be possible to construct a completely digital deception repeater system including independent RGPO/RGPI loops and quasi instantaneous RF frequency synthesis.

Thus like the areas mentioned in the digital processing of radar, multi gigabit A/D converters could lead to a quantum jump in performance in active repeater technology. The Josephson junction logic appears to be the only device capable of even considering such high speed sampling rates.

18.4 Active Countermeasures

There is a continuing effort to develop ultra broadband, ultra-linear discriminators for set-on active countermeasures from both fixed and expendable platforms. This type of device is particularly useful at X(I,J) band with semi-octave bandwidth. There is a possibility that this might be realizable by using a suitable configuration of Josephson junctions. Set-on accuracy of 5 GHz within 20 nanoseconds is desirable. Again, a realistic prototype may require the use of JJ arrays, which at present are not understood or developed.

REFERENCES

1. J. A. Barnes, A. R. Chi, L. S. Cutler, D. J. Healey, D. B. Leeson, T. E. McGunigal, J. A. Mullen, Jr., W. L. Smith, R. L. Sydnor, R.F.C. Vessot, and G.M.R. Winkler, "Characterization of Frequency Stability," IEEE Transactions on Instrumentation and Measurement, IM-20, 105 (1971).

2. W. T. Beall, "Development of Niobium-Copper-Invar-Composite Conductor for an AC Superconducting Power Transmission Cable," IEEE Transactions on Magnetics, MAG-11, 381 (1975).

3. T. G. Blaney and D.J.E. Knight, "Experiments Using a Superconducting Point-Contact Harmonic Mixer Near 1 THz," Journal of Physics, D6, 936 (1973).

4. T. G. Blaney and D.J.E. Knight, "Direct 825th Harmonic Mixing of a 1 GHz Source With an HCN Laser in a Josephson Junction," Journal of Physics, D7, 1882 (1974).

5. R. F. Broom, W. Jutzi and Th. O. Mohr, "A 1.4 Mil^2 Memory Cell with Josephson Junctions," IEEE Transactions on Magnetics, MAG-11, 755 (1975).

6. W. H. Campbell, "Geomagnetic Pulsations," in Physics of Geomagnetic Phenomena, p. 822. Edited by S. Matsushita and W. H. Campbell (Academic Press, N.Y.) (1967).

7. L. J. Challis, "Kapitza Resistance and Acoustic Transmission Across Boundaries at High Frequencies," Journal of Physics, C7, 481 (1974).

8. R. Y. Chiao and P. T. Parrish, "Observations of the SUPARAMP at 33 GHz," Journal of Applied Physics, 47, 2639 (1976).

9. J. Clarke, "Low Frequency Applications of Superconducting Quantum Interference Devices," Proceedings of IEEE, 61, 8 (1973).

10. J. Clarke, W. M. Goubau and M. B. Ketchen, "A Reliable DC SQUID Made With Tunnel Junctions," IEEE Transactions on Magnetics, MAG-11, 724 (1975a).

11. J. Clarke and G. Hawkins, "Flicker (1/f) Noise in Josephson Tunnel Junctions," Physical Review, B-14, 2826 (1976).

12. J. Clarke, G. I. Hoffer, P. L. Richards, and N. H. Yeh, "Superconducting Transition Edge Bolometer," Low Temperature Physics - LT14, p. 226 (North Holland/American Elsevier, Amsterdam/New York) (1975b).

13. D. Cohen, E. A. Edelsack, and J. E. Zimmerman, "Magnetocardiograms Taken Inside a Shielded Room with a Superconducting Point-Contact Magnetometer," Applied Physics Letters, 16, 278 (1970).

14. R. L. Comstock and C. E. Fay, "Performance and Ferrimagnetic Material Considerations in Cryogenic Microwave Devices," Journal of Applied Physics, 36, 1253 (1965).

15. M. Danielson, "Superconducting Lead Cavities at 35 GHz," Proceedings of IEEE, 61, 71 (1973).

16. A. Th. A. M. de Waele and R. de Bruyn Ouboter, "Quantum-Interference Phenomena in Point Contacts Between Two Superconductors," Physica, 41, 225 (1969a).

17. A. Th. A. M. de Waele and R. de Bruyn Ouboter, "On the Critical Current Through a Symmetrical Double Contact Between Two Superconductors as a Function of the Applied Magnetic Field," Physica, 42, 626 (1969b).

18. A. J. DiNardo, J. G. Smith and F. R. Arams, "Superconducting Microstrip High-Q Microwave Resonators," Journal of Applied Physics, 41, 186 (1971).

19. R. J. Dinger, J. R. Davis, and M. Nisenoff, "Long-Hold-Time Liquid-Helium Dewar For Cooling of a SQUID ELF Antenna," NRL Memorandum Report 3256, (1976).

20. J. Edrich and R. G. West, "Low-Loss Cryogenic L-Band Circulator," IEEE Transactions on Microwave Theory and Techniques, MTT-18, 743 (1970).

21. J. Edrich, D. B. Sullivan, and D. G. McDonald, "Results, Potentials, and Limitations of Josephson Mixer Receivers at MM and Long Sub MM Wavelengths," IEEE Transactions on Microwave Theory and Techniques, MTT-13, in press (1977).

22. M. J. Feldman, "The Thermally Saturated SUPARAMP," Journal of Applied Physics, 48, 1301 (1977).

23. M. J. Feldman, P. T. Parrish, and R. Y. Chiao, "Parametric Amplification by Unbiased Josephson Junctions," Journal of Applied Physics, 46, 4031 (1975).

24. N. V. Frederick, W. D. Stanley, J. E. Zimmerman, and R. J. Dinger, "An Application of Superconducting Quantum Interference Magnetometers to Geophysical Prospecting," IEEE Transactions on Geoscience Electronics, GE-12, 102 (1974).

25. J. I. Gittleman and S. Bozowski, "Some Aspects of the Kapitza Resistance," Physical Review, 128, 646 (1962).

26. P. Grassmann and A. Karagounis, "Heat Transfer to Boiling Helium in the Range of Nuclear and Film Boiling," Proceedings of Fifth International Conference on Low Temperature Physics and Chemistry, p. 41, (Univ. of Wisconsin Press, Madison) (1958).

27. W. H. Hartwig and D. Grissom, "Dielectric Dissipation Measurement Below 7.2^{o}K," Low Temperature Physics LT-9, p. 1243 (Plenum Press, N. Y.) (1965).

28. W. H. Hartwig and C. Passow, "RF Superconducting Devices " in Applied Superconductivity, Vol. II, p. 585, Edited by V. L. Newhouse (Academic Press, N. Y.) (1975).

29. C. L. Huang and T. Van Duzer, "Schottky Diodes and Other Devices on Thin Silicon Membranes," IEEE Transactions on Electron Devices, ED-23, 579 (1976).

30. L. D. Jackel, W. W. Webb, J. E. Lukens, and S. S. Pei, "Measurement of the Probability Distribution of Thermally Excited Fluxoid Transitions in a Superconducting Ring Closed by a Josephson Junction," Physical Review, B9, 115 (1974).

31. D. W. Jillie, J. E. Lukens, and Y. H. Kao, "Observation of Microwave Synchronization of Thin Film Microbridge Arrays," IEEE Transactions on Magnetics, MAG-11, 671 (1975).

32. D. W. Jillie, J. E. Lukens, Y. H. Kao and G. J. Dolan, "Observation of Voltage Locking and Other Interactions in Coupled Microbridge Josephson Junctions," Physics Letters, 55A, 381 (1976).

33. B. D. Josephson, "Supercurrents Through Barriers," Advances in Physics, 14, 419 (1965).

34. R. A. Kamper, M. B. Simmonds, C. A. Hoer, and R. Adair, "Measurement of rf Power and Attenuation Using Superconducting Quantum Interference Devices," NBS Technical Note 643 (1973).

35. R. A. Kamper, M. B. Simmonds, R. T. Adair, and C. A. Hoer, "Advances in the Measurement of rf Power and Attenuation Using SQUIDs," NBS Technical Note 661 (1974).

36. H. Kanter, "Parametric Amplification With Self-Pumped Josephson Junctions," IEEE Transactions on Magnetics, MAG-11, 789 (1975a).

37. H. Kanter, "Two Idler Parametric Amplification with Josephson Junctions," Journal of Applied Physics, 46, 4018 (1975b).

38. H. Kanter and A. H. Silver, "Self-Pumped Josephson Parametric Amplification," Applied Physics Letters, 19, 515 (1971).

39. H. Kanter and F. L. Vernon, Jr., "Noise Voltage in Josephson Junctions," Physics Letters, 32A, 155 (1971).

40. H. Kanter and F. L. Vernon, Jr., "High Frequency Response of Josephson Point Contacts," Journal of Applied Physics, 43, 3174 (1972).

41. A. R. Kerr, "Low-Noise Temperature and Cryogenic Mixers for 80-120 GHz," IEEE Transactions on Microwave Theory and Techniques, MTT-23, 781 (1975).

42. H. E. King, J. D. White, W. J. Wilson, T. T. Mori, J. P. Hollinger, B. E. Troy, J. E. Kenney, and J. T. McGoogan, "90 GHz Radiometric Imaging," Aerospace Corporation TR-0076(6230-40)-1 (1976).

43. J. Kohler, "The Stirling Refrigeration Cycle," Scientific American, 212, 119 (1965).

44. J. Kurkijarvi and W. W. Webb, "Thermal Fluctuation Noise in a Superconducting Flux Detector," Proceedings of Applied Superconductivity Conference, Annapolis, p. 581, IEEE Publ. No. 72 CHO 682-5-TABSC (IEEE, New York) (1972).

45. D. K. C. MacDonald, E. Mooser, W. B. Pearson, I. M. Templeton, and S. B. Woods, "On the Possibility of Thermoelectric Refrigeration at Very Low Temperatures," Philosophic Magazine 4, 433 (1959).

46. M. McColl, R. J. Pedersen, M. F. Bottjer, M. F. Millea, A. H. Silver, and F. L. Vernon, Jr., "The Super-Schottky Microwave Mixer," Applied Physics Letters, 28, 159 (1976).

47. M. McColl, M. F. Millea, A. H. Silver, M. F. Bottjer, R. J. Pedersen, and F. L. Vernon, Jr., "The Super-Schottky Microwave Mixer," IEEE Transactions on Magnetics, MAG-13, 221 (1977).

48. D. E. McCumber, "Effect of AC Impedance on DC Voltage-Current Characteristics of Superconductor Weak-Link Junctions," Journal of Applied Physics, 39, 3113 (1968).

49. D. G. McDonald, V. E. Kose, K. M. Evensen, J. S. Wells, and J. D. Cupp, "Harmonic Generation and Submillimeter Wave Mixing With the Josephson Effect," Applied Physics Letters, 15, 121 (1969).

50. D. G. McDonald, F. R. Petersen, J. D. Cupp, B. L. Danielson, and E. G. Johnson, "Josephson Junctions at 45 times the Energy-Gap Frequency," Applied Physics Letters, 24, 335 (1974).

51. J. H. Murphy, M. S. Walker, and W. J. Carr, Jr., "Alternating Field Losses in a Rectangular Multifilamentary NbTi Superconductor," IEEE Transactions on Magnetics, MAG-11,313 (1975).

52. J. Mygind, N. F. Pedersen, and O. H. Sorensen, "Direct Detection of the Parametrically Generated Half-Harmonic Voltage in a Josephson Tunnel Junction," Applied Physics Letters, 29, 317 (1976).

53. J. Niemeyer and V. Kose, "Observation of Large DC Supercurrents at Nonzero Voltages in Josephson Tunnel Junctions," Applied Physics Letters, 29, 380 (1976).

54. M. Octavio, W. J. Skocpol and M. Tinkham, "Improved Performance of Tin Variable-Thickness Superconducting Microbridges," IEEE Transactions on Magnetics, MAG-13, 739 (1977).

55. H. Ohta, M. J. Feldman, P. T. Parrish, and R. Y. Chiao, "Sensitivity of Josephson-Effect Millimeter-Wave Radiometer," Revue de Physique Appliquee, 9, 61 (1974).

56. D. W. Palmer and J. E. Mercereau, "Coherent Effects in Series Arrays of Proximity Effect Superconducting Bridges," IEEE Transactions on Magnetics, MAG-11, 667 (1975).

57. P. T. Parrish and R. Y. Chiao, "Amplification of Microwaves by Superconducting Microbridges in a Four-Wave Parametric Mode," Applied Physics Letters, 25, 627 (1974).

58. A. A. Penzias, "The Current State of Competing (Non Josephson Junction) Techniques," Revue de Physique Appliquee, 9, 7 (1974).

59. P. L. Richards, J. H. Claassen, and Y. Taur, "Josephson Effect MM-Wave Receivers," Low Temperature Physics - LT14, p. 238 (North Holland/American Elsevier, Amsterdam/New York) (1975).

60. D. H. Roth, W. W. Schedelbeek, and G. H. Schollmeier, "Investigation of Ferrimagnetic Materials at Low Temperatures and Some Applications in Low-Noise Receivers," IEEE Transactions on Magnetics, MAG-2, 256 (1966).

61. F. I. Shimabukuro, P. L. Smith, and W. J. Wilson, "Estimation of Daytime and Nighttime Distribution of Atmospheric Ozone From Ground Based MM-Wavelength Measurements," Journal of Applied Meteorology (in press).

62. A. H. Silver, "Superconducting Low Noise Receivers," IEEE Transactions on Magnetics, MAG-11, 794 (1975).

63. A. H. Silver and J. E. Zimmerman, "Quantum States and Transitions in Weakly Connected Superconducting Rings," Physical Review, 157, 317 (1967).

64. A. H. Silver and J. E. Zimmerman, "Josephson Weak Link Devices" in Applied Superconductivity, Vol. I, p. 1, Edited by V. L. Newhouse, (Academic Press, New York) (1975).

65. W. J. Skocpol, M. R. Beasley and M. Tinkham, "Self-Heating Hotspots in Superconducting Thin-Film Microbridges," Journal of Applied Physics, 45, 4054 (1974).

66. S. R. Stein, "The Superconducting-Cavity Stabilized Oscillator and an Experiment to Detect Time Variation of the Fundamental Constants," Ph.D. Dissertation, Stanford University (1974).

67. S. R. Stein and J. P. Turneaure, "Superconducting-Cavity Stabilized Oscillator of High Stability," Electronics Letters 8, 321 (1972).

68. S. R. Stein and J. P. Turneaure, "The Development of the Superconducting-Cavity Stabilized Oscillator," Proceedings of the 27th Annual Symposium on Frequency Control, p. 414 (Electronic Industries Association, Washington, D.C.) (1973).

69. S. R. Stein and J. P. Turneaure, "Superconducting-Cavity Stabilized Oscillators of 10^{-14} Stability," Low Temperature Physics - LT13, p. 535 (Plenum Press, N.Y.) (1974).

70. S. R. Stein and J. P. Turneaure, "Superconducting-Cavity Stabilized Oscillators with Improved Frequency Stability," Proceedings of IEEE Letters, 63, 1249 (1975).

71. W. C. Stewart, "Current-Voltage Characteristics of Josephson Junctions," Applied Physics Letters, 12, 277 (1968).

72. T. R. Strobridge, "Cryogenic Refrigerators - An Updated Survey," NBS Technical Note 655 (1973).

73. Y. Taur, J. H. Claassen, and P. L. Richards, "Conversion Gain and Noise in a Josephson Mixer," Revue de Physique Appliquee, 9, 263 (1974a).

74. Y. Taur, J. H. Claassen, and P. L. Richards, "Conversion Gain in a Josephson Effect Mixer," Applied Physics Letters, 24, 101 (1974b).

75. Y. Taur, J. H. Classen, and P. L. Richards, "Noise in Josephson Point Contacts With and Without RF Bias," Applied Physics Letters, 25, 759 (1974c).

76. Y. Taur, J. H. Claassen, and P. L. Richards, "Josephson Junctions As Heterodyne Detectors," IEEE Transactions on Microwave Theory and Techniques, MTT-22, 1005 (1974d).

77. Y. Taur and P. L. Richards, "A Josephson Effect Parametric Amplifier at 36 GHz," IEEE Transactions on Magnetics, MAG-13, 252 (1977).

78. M. Tinkham, "Tunneling Generation, Relaxation and Tunneling Detection of Hole-Electron Imbalance in Superconductors," Physical Review, B6, 1747 (1972).

79. M. Tinkham and J. Clarke, "Theory or Pair-Quasiparticle Potential Difference in Non-Equilibrium Superconductors," Physical Review Letters, 28, 1366 (1972).

80. M. Tinkham, M. Octavio, and W. J. Skocpol, "Heating Effects in High-Frequency Metallic Josephson Devices: Voltage Limit, Bolometric Mixing and Noise," Journal of Applied Physics, 48, 1311 (1977).

81. J. P. Turneaure and S. R. Stein, " An Experimental Limit on the Time Variation of the Fine Structure Constant," Proceedings of Fifth International Conference on Atomic Masses and Fundamental Constants, p. 636 (Plenum Press, N.Y.) (1976).

82. A. N. Vystavkin, V. N. Gubankov, L. S. Kuzmin, K. K. Likharev, V. V. Migulin, and V. K. Semenov, "One-Frequency Parametric Amplifier Using Self-Pumped Josephson Junction," IEEE Transactions on Magnetics, MAG-13, 233 (1977).

83. A. D. Watt, VLF Radio Engineering, Pergamon Press (1967).

84. S. Weinreb and A. R. Kerr, "Cryogenic Cooling of Mixers For Millimeter and Centimeter Wavelengths," IEEE Journal of Solid-State Circuits, SC-8, 58 (1973).

85. T. Wong, J.T.C. Yeh and D. N. Langenberg, "Quasiparticle-Injection-Induced Superconducting Weak Links, Physical Review Letters, 37, 150 (1976).

86. J. E. Zimmerman and A. H. Silver, "Macroscopic Quantum Interference Effects Through Superconducting Point Contacts," Physical Review 141, 367 (1966).

Appendix I

NAVY STUDY GROUP ON SUPERCONDUCTIVE ELECTRONICS

Full Time Participants

Dr. Fernand Bedard
National Security Agency
DIRNSA/R5
Fort Meade, MD 20755

Dr. Richard Brandt
Office of Naval Research
Branch Office
1030 East Green Street
Pasadena, CA 91106

Dr. James Carpenter
The Aerospace Corporation
P. O. Box 92957
Los Angeles, CA 90009

Mr. Edgar Edelsack
Code 427
Office of Naval Research
Alrington, VA 22217

Dr. Robert Hansen
R. C. Hansen, Inc.
P. O. Box 215
Tarzana, CA 91356

Mr. Verne Hildebrand
Naval Electronics Laboratory
Center (Code 2020)
271 Catalina Boulevard
San Diego, CA 92152

Prof. Donald Langenberg
Department of Physics
University of Pennslyvania
Philadelphia, PA 19174

Dr. Martin Nisenoff
Code 6435
Naval Research Laboratory
Washington, DC 20375

Prof. Paul Richards
Department of Physics
University of California
Berkeley, CA 94720

Dr. David Scott
4415 Great Oak Road
Rockville, MD 20853

Dr. Arnold Silver
The Aerospace Corporation
P. O. Box 92957
Los Angeles, CA 90009

Dr. Robert Terhune
Ford Scientific Laboratories
P. O. Box 2053
Dearborn, MI 48121

Prof. Michael Tinkham
Department of Physics
Harvard University
Cambridge, MA 02138

Prof. Theodore Van Duzer
Dept. of Electrical Engineering
University of California
Berkeley, CA 94720

Dr. Nancy Welker
Laboratory for Physical Sciences
4928 College Avenue
College Park, MD 20740

Mr. Max Yoder
Code 427
Office of Naval Research
Arlington, VA 22217

Dr. James Zimmerman
Cryogenics Division
National Bureau of Standards
Boulder, CO 80302

Technical Consultants

Dr. Kenneth Allen
Physics Division
Coastal Technology Department
Naval Coastal Systems Laboratory
Panama City, FL 32401

Prof. Raymond Chiao
Department of Physics
University of California
Berkeley, CA 94720

Prof. John Clarke
Department of Physics
University of California
Berkeley, CA 94720

Dr. Thomas Finnegan
National Bureau of Standards
Gaithersburg, MD 20234

Mr. James Franson
Department of Physics
California Institute of Technology
Pasadena, CA 91101

Prof. Robin Giffard
Department of Physics
Stanford University
Stanford, CA 94305

Dr. Dennis Herrell
IBM Research Center
Yorktown Heights, NY 10598

Prof. James Lukens
Department of Physics
State University of New York
at Stony Brook
Stony Brook, NY 11794

Dr. Malcolm McColl
The Aerospace Corporation
P. O. Box 92957
Los Angeles, CA 90009

Dr. Donald McDonald
Cryogenics Division
National Bureau of Standards
Boulder, CO 80302

Mr. David McIntyre
Chief, Computational Division
AFWL Mail Stop 53
Kirtland AFB, NM 87117

Mr. Elliot Ressler
Code 2031
Naval Air Development Center
Warminster, PA 18974

Dr. Merrill Skolnik
Code 5300
Naval Research Laboratory
Washington, DC 20375

Dr. John Turneaure
Department of Physics
Stanford University
Stanford, CA 94305

Dr. Frank Vernon
The Aerospace Corporation
P. O. Box 92957
Los Angeles, CA 90009

Dr. Virgil Wall
The Aerospace Corporation
P. O. Box 92957
Los Angeles, CA 90009

Appendix II

Agenda

System Opportunities (Classified)

Radar	M. Skolnik
Satellite Communications	V. Wall
HF Communications/Navigation	E. Ressler
Electronic Warfare	D. Scott
Data Processing	D. McIntyre
LF Communications	M. Nisenoff

Low Frequency Devices

LF Systems	M. Nisenoff
SQUIDs/LF Noise	J. Clarke
LF Amplifiers	R. Giffard
LF Signal Processing	K. Allen

Arrays and Coupled Junctions

Physics of Josephson Junctions	M. Tinkham
Arrays of Coupled Junctions	J. Lukens
Large Array Coherence	J. Franson
Impedance Matching	T. Finnegan

High Frequency Devices

Josephson Mixers	P. Richards
Super-Schottky Mixers	M. McColl
Superconducting Paramps	R. Chiao
SQUID Paramps	F. Vernon, Jr.
Cavities and Oscillators	J. Turneaure

Digital Devices

Superconductor/Semiconductor Junctions	T. Van Duzer
Superconducting Computers	N. Welker
Superconducting Computers	D. Herrell
A/D Converters	D. McDonald

Other Topics

Refrigeration	J. Zimmerman
Small Antennas	R. Hansen